ProQuest LLC.
789 East Eisenhower Parkway
P.O. Box 1346
Ann Arbor, MI 48106 - 1346

THE DEFORMATION CHARACTERISTICS OF CRYSTALLINE MERCURY AT 77°K AND 4.2°K

by

John Stuart Abell

A Thesis submitted to the
University of Surrey
for the degree of
Doctor of Philosophy
in the Faculty of Science

March 1969

ABSTRACT

The normal structure of mercury is unique in that it is the only metal having rhombehedral symmetry to possess a single lattice structure. This fact, together with the nearness of the structure to f.c.c., make its deformation behaviour particularly interesting. The present investigation describes the orientation dependence of the deformation characteristics of mercury at two different temperatures. The large standard stereographic triangle associated with the low symmetry structure of mercury occupies one sixth of the full stereogram. Theoretical considerations have shown that, within this one triangle, slip on three different variants of the observed mode is possible, the boundaries between the corresponding regions having two distinct characteristics. These predictions have been tested by experiments on single crystals at 77°K and the role of twinning and kinking in the deformation process assessed.

Single crystals tested in tension at 4.2°K have been found to undergo a stress-induced phase transformation. Evidence for this reaction is presented in the form of superconductivity and electrical resistance measurements and the martensitic nature of the transition established. Both the properties of the new phase and the nature of its production served to distinguish this transformation from the previously reported low temperature $\alpha - \beta$ transition. It has thus been labelled the γ phase.

Detailed metallographic observations determined the shear elements associated with this transformation as $\{\bar{1}13\}\langle\bar{1}\bar{1}0\rangle$, $g = 0.47$, the indices referring to the f.c.r. cell of α-mercury. The morphology of the transformed crystals has been interpreted in terms of the accommodation of the martensitic plates in the parent matrix and the crystallography of the habit plane and associated shear direction. A marked dependence of the occurrence of the transformation on the orientation of the crystal has been interpreted by regarding the shear process associated with the transformation as a conventional deformation mode. Further explanation of the results using various approaches such as lattice geometry and anisotropic elasticity theory has been attempted. The application of the current theories of martensite crystallography to this transformation based on a product crystal structure predicted using the pseudopotential theory of metals is also reported. Finally, an account of an experimental investigation, using an X-ray diffraction technique, to determine the actual product structure is presented.

ADDITIONAL MATERIAL SUBMITTED

Two papers are submitted with this thesis:

The Crystallography of the α to γ Martensitic Transformation in Crystalline Mercury, by J.S. Abell and A.G. Crocker

Scripta Metallurgica, Vol. 2, p. 419, 1968

The α to γ Martensite Transformation in Crystalline Mercury, by J.S. Abell and A.G. Crocker

Proceedings of an International Conference on The Mechanism of Phase Transformations in Crystalline Solids, Manchester, July 1968, in the press.

CONTENTS

CHAPTER 1 - INTRODUCTION

1.1 Scope of the Thesis

This thesis is an account of an experimental investigation into the behaviour of crystalline mercury under the influence of applied stress. A research programme designed to examine the mechanical properties of mercury was initiated several years ago at the University of Surrey (formerly Battersea C.A.T.) since it was thought that there existed anomalies in the reported deformation modes. Previous work has focussed attention on the identification of the operative deformation modes and has indicated that the orientation dependence of the deformation behaviour is particuarly interesting. This experimental work has been confined to two readily available temperatures, 200°K and 77°K.

The original purpose of the present investigation was to determine the temperature dependence and orientation dependence of the deformation characteristics of mercury, with the intention of elucidating the mechanisms determining the operation of slip and twinning by means of tests in tension and compression on single crystal specimens. In particular, it was felt that the possibility of an assymmetry in the slip behaviour with respect to tension and compressive tests which is now well-established in b.c.c. metals would also exist in mercury, and that further interesting information would result from the extension of the test temperature range below 77°K down to liquid helium temperatures. However, the preliminary results obtained at low temperatures proved particularly

interesting and necessitated more detailed attention. Thus two temperatures have been studied in particular, 77°K and 4.2°K.

1.2 The Crystallography of Mercury

Mercury solidifies at -39°C and the crystal structure of this normal α -phase is unique in that it is the only metal having rhombohedral symmetry to possess a single lattice structure. The α -structure has three mirror planes intersecting in a three-fold axis which contains a centre of symmetry. The structure is most convenient referred to the face-centred rhombohedral (f.c.r.) basis which is illustrated in Fig. 1.1, and throughout this thesis lattice planes and directions will correspond to this cell. It is convenient to use this cell because of its similarity to the f.c.c. cell. The axial angle of the f.c.r. cell is greater than 90° and so can be regarded as a f.c.c. cell compressed along the [111] direction, this direction being the three-fold axis of the rhombohedral lattice. The axial angle does not vary appreciably between 5°K and 77°K (Barrett 1957) and the value 98° 21.8' used by Bacon (1963) to compute lattice spacings in mercury will be assumed here. The lattice parameter does change in this temperature range and the two values used in this thesis are a = 4.5690Å at 5°K and a = 4.5785Å at 77°K (Barrett 1957).

The unique [111] direction is usually chosen for the standard stereographic projection of mercury and such a projection appears in Appendix I. A consequence of the rhombohedral symmetry is that a change in the sign of an

index does not produce a crystallographically equivalent plane or direction as for f.c.c. Thus, the (111) plane is unique being distinct from the three $\{11\bar{1}\}$ planes. Moreover directions are not in general at right angles to planes with the same indices. The three $\{1\bar{1}0\}$ mirror planes effectively divide the 111 projection into six unit triangles. All possible crystal orientations can be represented in one of these and the one used in this work is that defined by the poles 111, $2\bar{1}\bar{1}$ and $11\bar{2}$.

1.3 Slip in Crystalline Mercury

Crystallographic slip in metals normally occurs on the closest-packed planes and the predominant slip direction is the closest-packed direction. Other slip directions have been observed to operate when the resolved shear stress in the closest-packed direction is low or when high test temperatures are used. For mercury the $\{11\bar{1}\}$ planes are the closest-packed and $\langle 011 \rangle$ is the closest-packed direction, and so the expected slip mode is $\{11\bar{1}\}\ \langle 011 \rangle$.

The deformation modes of mercury were first investigated by Andrade and Hutchings (1935). Using cylindrical crystals tested in tension they reported slip on the $\{100\}$ planes in the $\langle 011 \rangle$ direction. Their crystals were not oriented and their results were deduced from measurement of angles between traces on the surfaces. However, Fisher (1943) pointed out these results could also be interpreted in terms of slip on $\{11\bar{1}\}$ and this was later confirmed by Crocker et al. (1963) using a single surface analysis (Bevis et al. 1964) on large

grain polycrystalline specimens. The results of this analysis also suggested that the predominant slip direction was not the $\langle 011 \rangle$ direction but the second closest-packed direction $\langle 1\bar{1}0 \rangle$. Further work by Rider and Heckscher (1966) on crylindrical single crystals tested in tension showed without ambiguity that the predominant slip direction was indeed $\langle 1\bar{1}0 \rangle$, the occurrence of the $\langle 011 \rangle$ direction being confined to high temperatures and only for certain orientations.

The slip traces associated with the operation of the close-packed direction was always wary in nature, as distinct from the straight slip on $\{ 11\bar{1} \} \langle 1\bar{1}0 \rangle$. Examples of straight slip and indeed of twinning in mercury, to be discussed in the next section, are given elsewhere in the thesis. However, wavy slip is not discussed in detail in this work and so it was thought to be appropriate to present a micrograph of wavy slip in this chapter. This appears as Fig. 1.2. Recently, Guyoncourt has observed non-planar slip near $\{100\}$ planes for certain restricted orientations during four-point bending tests. This was interpreted as slip on the two variants of the $\{11\bar{1}\}$ planes containing a common $\langle 011 \rangle$ shear direction, cross-slipping to form composite $\{100\}$ planes.

Thus, the predominant slip direction in mercury is $\langle 1\bar{1}0 \rangle$ and not the close-packed direction $\langle 011 \rangle$. Heckscher and Crocker (1965) have considered the dislocation geometry of the mercury structure and attempted to explain this anomalous slip result in terms of two models. The initial

attempt involved the extension of the f.c.c. tetrahedron model of Thompson (1953) by considering a distorted tetrahedron for mercury. By calculating the self-energies of the perfect dislocations for mercury using isotropic elasticity theory an explanation was sought for the predominance of the $\langle 1\bar{1}0 \rangle$ Burgers vector. This model was successful in explaining the occurrence of cross-slip for the $\{ 11\bar{1} \}\langle 011 \rangle$ mode by predicting that the dissociation of the $\frac{1}{2} \langle 1\bar{1}0 \rangle$ dislocation was more likely than for the $\frac{1}{2} \langle 011 \rangle$ type. However, the model predicted the energies of the $\frac{1}{2} \langle 1\bar{1}0 \rangle$ to be greater than the $\frac{1}{2} \langle 011 \rangle$ dislocations both before and after dissociation making the occurrence of the latter theoretically more common. This is contrary to the experimental observations.

A more satisfactory approach was based on the possible stacking faults on the $\{ 11\bar{1} \}$ mercury slip planes which in the perfect crystal have an approximate four-fold stacking sequence. Again, it was found that dissociation of the $\frac{1}{2} \langle 011 \rangle$ type leads to no reduction in energy and consequently this dislocation will remain perfect and will tend to cross-slip, producing the observed wavy traces. However, on this model the $\frac{1}{2} \langle 1\bar{1}0 \rangle$ dislocations are found to dissociate into approximately two $\frac{1}{4} \langle 1\bar{1}0 \rangle$ partials with a reduction in isotropic energy by a factor of two. Thus, the $\frac{1}{2} \langle 1\bar{1}0 \rangle$ dislocations having a lower energy than the $\frac{1}{2} \langle 011 \rangle$ will be more common and will produce the straight slip lines usually observed in mercury. The explanation of the operative slip modes in mercury in terms of the dislocation geometry thus appears satisfactory, but the significance of

the agreement is somewhat limited since the arguments assume a point lattice rather than an actual crystal structure and are based on isotropic elasticity theory. A more realistic approach has been attempted using ball models which for mercury are in the form of spheroids of axial ration 0.8 as distinct from spheres for the f.c.c. cases. Although the partial slip dislocations suggested by these models were slightly different from the ones discussed above the general conclusions concerning the predominant slip direction were the same.

An alternative treatment based on the application of anisotropic elasticity theory has been given by Tucker (1966). The elastic properties of mercury are defined by six independent constants (Gruneisen and Sckell 1934), and these have been used to calculate both the macroscopic shear moduli of the possible shear modes and the elastic energies of the various dislocations mentioned above. The shear modulus for the $\{11\bar{1}\} < 1\bar{1}0 >$ slip system is considerably lower than that for the alternative slip modes (see Table 5.10) and thus may be considered as more likely to occur. In addition, calculation of the energies of the perfect and partial dislocations based on the four-fold stacking approach as a function of orientation of the Burgers vector with respect to the dislocation line clearly shows that an edge dislocation with $\frac{1}{2} < 1\bar{1}0 >$ Burgers vector will be more favourable.

Clearly, the direct observation of dislocations in crystalline mercury would be extremely valuable in interpreting the anomalous slip results given in this section. During the course of the work described in this thesis an attempt was made to observe the dislocation structure in thin films of mercury using an X-ray topographic method. The demands of the experimental procedures necessary to achieve satisfactory results using this technique indicate that such an investigation would constitute a separate research project. Appendix III discusses some of the problems encountered and possible ways of overcoming them in order to realise meaninful results.

1.4 Deformation Twinning in Mercury

Guyoncourt and Crocker (1968) have pointed out that, in general, for metals with a single lattice structure the operative twinning plane is crystallographically equivalent to the reciprocal twinning plane and similarly for the twinning directions. In addition the associated shear strain is the smallest possible to restore the structure in the twin orientation. An examination of the operative twinning mode of mercury has shown that this metal is a notable exception to these general criteria. Several determinations of the possible twin modes for mercury have appeared (Jaswon and Dove 1956; Dove 1956, Kiho, 1954). These authors predicted the mode reported by Andrade and Hutchings (1935) but only recently has Bevis (1966) found the mode which, as will be described below, was determined unambiguously to be the operative twin mode. Table 1.1 shows all the possible modes

involving no atomic shuffles with shears less than unity. The K_1 plane of mode 1 is that reported to occur by Andrade and Hutchings. These planes could not operate as twin planes in the f.c.c. case since they would be mirror planes. The same habit plane is observed for twins in other rhombohedal metals (Hall 1954). Indeed, this mode involves the smallest shear and thus would be expected to occur. However, recent work by Crocker et al. (1966) and Guyoncourt and Crocker (1968) involving single surface and two-surface analyses has proved conclusively that the deformation twin mode is the reciprocal of mode 2 involving the irrational ' $\{ \bar{1}\bar{3}5 \}$ ' habit plane. Not only is this the only reported observation of a Type II twin in a single lattice structure, it is the only twin mode in metals involving an irrational twinning plane apart from some secondary twins in α-uranium (Cahn 1953). Further, it is surprising because it occurs in preference to two compound twin modes which involve a smaller shear. The reported twinning shear of 0.63 is exceptionally high for a metal which twins so profusely.

Two intersecting variants of the twin planes usually occur. These pairs are termed 'complementary' (Guyoncourt 1967) since they have a special crystallographic relationship which allows this morphology to be easily accommodated in the matrix. The two irrational variants concerned intersect at an acute angle, the line of intersection being very nearly a $\langle 211 \rangle$ direction. This direction is contained in a $\{ \bar{1}11 \}$ slip plane, and the two twins and the slip system $\{ \bar{1}11 \}\langle 01\bar{1} \rangle$ have approximately a common plane of shear, whose normal is

the direction $\langle 211 \rangle$. This special crystallographic relationship enables the local strains associated with the twin intersections to be almost entirely accommodated by slip. Guyoncourt (1967) also reported results of an investigation into the growth of twins and the interaction of slip and twins at 77°K by means of bend tests on square cross-section crystals.

The observation of twins in mercury on the irrational '$\{\bar{1}\bar{3}5\}$' habit plane instead of twins with a smaller shear on $\{011\}$ or its reciprocal $\{100\}$ indicates that the present theories of the crystallography of twinning are inadequate. These theories do not take into account the part played by dislocations in twin formation. By considering the irrational twin boundary as facets of two rational planes Guyoncourt and Crocker (1968) showed that this boundary may be regarded as an array of screw oriental dislocations. The Burgers vector of these dislocations is in the direction of the twin shear and so the boundary is composed of an intrinsic set of screw twinning dislocations which can cause the growth or contraction of the twin boundary. A qualitative picture of the twin composition plane has also been found using the spheroid models. The parent and twin fit together very easily at the interface suggesting that the twin boundary energy may be low, thus favouring this habit plane. The macroscopic shear moduli for the '$\{\bar{1}\bar{3}5\}$' twin mode in mercury is lower than that for the alternative twin modes and reference to Table 5.10 will show that the value is in fact less than that for $\{11\bar{1}\} \langle 1\bar{1}0 \rangle$ slip. Thus elastic accomodation of this twin by the matrix

during growth is more favourable than for the other twin modes. Further calculations of the energy density of a twin on ' $\{\bar{1}\bar{3}5\}$ ' has again shown that this twin is favoured in practice (Guyoncourt 1967).

1.5 Orientation and Temperature Dependence of Deformation Behaviour

For mercury crystals tested in tension, the predominant slip mode at the two temperatures investigated, 200°K and 77°K, has been found to be $\{11\bar{1}\} < 1\bar{1}0 >$. However for orientations in the stereographic triangle near $[110]$, where the resolved shear stress on this mode becomes low, alternative modes are observed. Thus, at 200°K these crystals exhibit wavy slip on $\{11\bar{1}\}$ planes with the close-packed $<011>$ slip direction. At 77°K, this slip mode is not operative for the same tensile tests and these crystals then deform by twinning on the ' $\{\bar{1}\bar{3}5\}$ ' planes. Slip in the $<011>$ direction on a plane near $\{100\}$ has been reported to occur at 77°K during bending tests, being observed only for orientations near $[111]$. The majority of these crystals deform by $\{11\bar{1}\}<1\bar{1}0>$ slip as for the tensile tests, but the restrictions on the occurrence of twins are more complicated.

A summary of the deformation behaviour is contained in Table 1.2. At any particular temperature, the operation of a certain deformation mode is clearly orientation dependent. Moreover, there is a marked change in deformation characteristics as the temperature is reduced from 200°K to 77°K. A similar orientation dependence does not arise for f.c.c. structures where the unit triangle occupies one twenty-

fourth of the full stereogram. For mercury, where the triangle occupies one sixth, a large range of orientations is possible and as will be shown in Chapter 3, different variants of the slip modes can occur within the one triangle, a situation not found for f.c.c. An anologous situation has, however, been found for b.c.c. metals where different slip planes are operative for different regions. (Taylor and Christian 1967, Sestak and Zarubova 1965). Observations of slip on irrational planes of maximum resolved shear stress have also been reported to occur in these metals and there is considerable disagreement about whether some of the observations are due to composite slip since all the planes lie in the $\langle 111 \rangle$ zone, the axis of which is the observed slip direction. The reported occurrence of possible composite slip at 77°K on $\{100\}$ planes in mercury and the wavy nature of the $\{11\bar{1}\}\langle 011 \rangle$ slip lines at 200°K discussed in section 1.3, raises the possibility of a similar assymmetry in the slip behaviour existing in mercury.

The results of Rider and Hecksher (1966) suggest a further investigation of the orientation dependence of the occurrence of the two slip directions as a function of temperature. Moreover, the occurrence of deformation twinning as the temperature is lowered to 77°K invites a further investigation at even lower temperatures than those previously used. No investigation of the deformation behaviour of mercury at low temperatures has been reported with the exception, perhaps, of Barrett (1957) who cold-worked a fine grain polycrystalline sample in a low-temperature X-ray diffractometer in an attempt to induce a phase transformation. The results

presented in Chapters 4, 5 and 7 of this thesis will demonstrate that the low temperature deformation behaviour of mercury is particularly interesting in that the situation is further complicated by the observation of a stress-induced phase transformation. The occurrence of this reaction in single crystals is found to be orientation dependent and demonstrates again the anomalous behaviour of crystalline mercury arising from the low symmetry structure. The observation of this phase transformation has focussed attention on the deformation characteristics of mercury at 4.2°K. Consequently the investigation of a possible assymmetry in the slip behaviour at high temperatures has not been realised. An independent research project has been initiated on this topic involving four-point bending tests and analysis of the results based on that given by Sestak and Zarubova (1965).

1.6 Low Temperature Phase Transformations

The main part of this thesis is concerned with the deformation of crystalline mercury at 4.2°K where a new stress-induced phase transformation has been reported to occur (Doidge and Eastham 1968a, Abell and Crocker 1968a, b). Reed and Breedis (1966) have suggested that the only solid state transition which can occur at low temperature is of the martensitic type. This transformation is characterised by a shape change (Bilby and Christian 1956) corresponding to a macroscopic homogeneous deformation. A feature of the reaction is a rapid growth mechanism involving the co-ordinated movement of atoms through small distances relative to their neighbours. The process does not depend on the exchange of

atoms by diffusion and is thus alternatively termed diffusionless. The rapid growth formation often manifests itself in the form of an audible click as the strain energy associated with the growth of the product within the parent matrix is released. Several reviews of martensitic transformations have been published, those relevant to this work being concerned with the crystallography of these transitions (Bilby and Christian 1956, 1961; Wayman 1964; Christian 1965a,b, 1968).

Regarding the transition in terms of a macroscopic homogeneous deformation was first found to be inadequate for transformations in iron alloys by Greninger and Troiano (1949) and led to the hypothesis that the lattice deformation is homogeneous over small regions, the deformation in different regions being combined to give the overall shape change. Bilby and Christian (1956) gave a formal definition of this type of transformation:

'A structural transformation is classed as martensitic if the atoms on a primitive lattice defined by a selected unit cell of the parent structure move to positions on a primitive lattice defined by some unit cell of the product structure, in such a way that the displacements constitute a homogeneous deformation. This deformation may be different in adjacent small regions.'

In this classification, mechanical twinning is regarded as a special type of martensitic transformation involving no change in structure.

Formulations of the general theory of the crystallography of martensitic transformations all assume that the total shape deformation is an invariant plane strain, in agreement with experimental observation. That is, there exists an interface between the parent and product structures which remains unrotated and undistorted as a result of the transformation. The lattice deformation, which allows no volume change in the transformation, is then resolved into a lattice correspondence, relating the unit cells of the two structures, and a lattice invariant shear. The combination of these two together with a rigid body rotation then defines an invariant plane strain and produces the new structure which may be internally slipped or twinned. It is generally assumed that the choice of lattice correspondence is characterised by small values of the principal strains of the associated lattice deformation. A more detailed discussion of the crystallographic theories is contained in Chapter 6, relevant to the application of the theories to this mercury transformation.

Martensitic transformation is usually achieved by rapid cooling (or heating) or by cold work. If the temperature is slowly lowered below a value T_o where the two modifications associated with the transformation are in thermo-dynamic equilibrium, a nucleation and growth process will in general determine the transition to the low-temperature phase. However, in some cases this equilibruim temperature (found by equating the Gibbs free energies of the two phases) is so low that diffusion is virtually impossible, and then a diffusionless mechanism occurs. A substantial strain energy

is required to produce the shape change associated with martensitic reactions and only when the temperature is low enough and the free energy difference favouring the low temperature phase big enough, is the driving force sufficient for the transformation to be initiated. When this driving force is not sufficient, an applied stress can supply the additional energy required to produce the low temperature phase.

The temperature at which martensitic transformation can begin spontaneously on cooling is referred to as M_s, which is considerably lower than T_o. The subsequent reversion to the high-temperature phase will not in general begin until a temperature M_r, above M_s, has been reached. In their review of low temperature phase transformations, Reed and Breedis (1966) found that prior plastic deformation above the M_s temperature can suppress or raise this temperature, while the application of hydrostatic pressure depresses the M_s temperature. As already mentioned, if the temperature is below T_o, the applied stress can induce the transformation. However, if the parent material plastically deforms, the increased defect density may inhibit the transformation, but in some cases sufficient nucleation sites for spontaneous nucleation are not present and these defects may act as such. The highest temperature at which transformation can occur during plastic deformation is called the M_d temperature, and this temperature has been associated with T_o. In general below M_s, the amount of transformation increases with strain and lowering of the temperature, but suppression of the trans-

formation may occur at very low temperatures.

It is interesting to note that a phase transformation has been found to occur in mercury at 77°K from the normal α-structure to a modification termed β-mercury (Swenson 1958) under the influence of large applied pressures. The properties of this phase have been extensively studied (Atoji et al. 1959, Schirber and Swenson 1959, 1961, 1962) and a summary of these is presented in Chapter 4, where this $\alpha - \beta$ transition is compared with the phase change found in the present study. Various workers have used electrical resistance measurements to investigate the nature and properties of martensitic transformations particularly in sodium and lithuim, copper alloys and iron-nicked systems (review, Reed and Breedis 1966). A similar method has been used here together with superconductivity measurements to demonstrate the existence of the phase change and to investigate some of the properties of the product phase. The results of these experiments are given in Chapter 4.

1.7 Conclusion

1.7.1 Notation for Deformation Modes

A convenient notation scheme for the deformation modes of mercury has been used throughout this thesis. A summary of this scheme is contained in Appendix I. Following the notation used for f.c.c. crystals, the three $\{ 11\bar{1} \}$ slip planes have been labelled A, B and C. The six variants of the irrational '$\{ \bar{1}35 \}$' twin plane can be separated into three pairs, the variants of each pair being mirror-related in a

$\{1\bar{1}0\}$ mirror-plane. Thus, the pair $(\bar{3}5\bar{1})$ and $(5\bar{3}\bar{1})$ are labelled a and a' since they have a common reciprocal twin plane which is the slip plane A. A similar relationship exists for the other pairs of twin plane variants. The corresponding shear directions are denoted by Greek letters. Thus, Θ , ϕ , ψ are the predominant $<1\bar{1}0>$ slip directions on the slip planes A, B, C, and α and α' are the twinning directions of the type $<\bar{1}21>$ on the twinning planes a and a'. A pair of twin habits such as a and a' occur as complementary modes with accommodation slip on plane A, as discussed in section 1.4. The three close-packed $<011>$ directions observed as slip directions under certain conditions at high temperatures are also indicated in this Appendix, which also includes a notation involving $\{\bar{1}13\}$ planes which will be introduced in Chapter 5. The predominant slip direction $<1\bar{1}0>$ is sometimes referred to as the long diagonal slip direction whereas the less common $<110>$ direction is termed short diagonal. This terminology was originally coined by Rider and Hecksher (1966) and is due to the fact that the $\{001\}$ faces of the f.c.r. cell have long and short diagonals parallel to $<1\bar{1}0>$ and $<011>$ respectively.

When slip occurs in a single crystal under an applied stress the operative mode is determined by the resolved shear stress on the slip plane in the slip direction. This stress is conveniently given by the geometrical Schmidt factors (Schmidt and Boas 1950) in terms of the angle χ between the direction of applied stress and the normal to the slip plane, and the angle λ between the stress direction and the slip

direction; thus

$$S = \cos\chi \cos\lambda$$

A similar relationship holds for any shear process in a single crystal defined by a plane and direction. Schmidt factors on any particular mode will then be denoted thus: S_A, S_a etc. No ambiguity arises out of this nomenclature since the $\langle 011 \rangle$ slip direction is not expected to occur at the temperatures used in this work and so a particular mode is identified by its shear plane alone.

1.7.2 Concerning this thesis

The work is reported in essentially two parts. Chapter 3 describes the experiments performed at 77°K, while the remaining chapters are concerned with results of experiments conducted below this temperature. Chapter 4 discusses the evidence of the occurrence of a new stress-induced transformation in mercury by describing results of experiments carried out at 4.2°K and comparing them with reported work on the $\alpha - \beta$ transformation in mercury. Chapter 5 is devoted to an investigation of the crystallographic features associated with the transformation and Chapter 6 includes an interpretation of the transition by the application of the current theories of martensite crystallography. Chapter 7 relates results of low-temperature X-ray diffractometer measurements aimed at determing the crystal structure of the product phase of the transformation. Where relevant, reviews of reported work have been included in the introduction to the corresponding chapter if they have not been presented in this chapter. There are three

Appendices to the thesis. The first of these shows a standard 111 projection for α -mercury and summarises the notation of the deformation modes discussed. Appendix II refers to an effect observed on the Laue back reflection X-ray plates of single crystals and Appendix III discusses the possibility of the direct observation of dislocations using the Lang topographic technique.

	K_1	K_2	η_1	η_2	g
1	$0\bar{1}1$	100	100	011	0.457
2	$\bar{1}11$	$'\bar{1}\bar{3}5'$	$'0\bar{1}1'$	$\bar{1}21$	0.633
3	100	$1\bar{1}\bar{1}$	$0\bar{1}\bar{1}$	211	0.880
4	$3\bar{1}1$	'313'	$'1\bar{1}\bar{4}'$	101	0.888
5	111	$11\bar{1}$	$\bar{1}\bar{1}2$	$\bar{1}\bar{1}2$	0.901

Table 1.1 Possible twin modes of mercury

Temperature	Predominant Mode	Secondary Mode
200°K	$\{11\bar{1}\} < 1\bar{1}0 >$ slip	$\{11\bar{1}\} < 0\bar{1}1 >$ slip
77°K	$\{11\bar{1}\} < 1\bar{1}0 >$ slip	$'\{\bar{1}\bar{3}5\}' < \bar{1}21 >$ twin $'\{100\}' < 011 >$ slip

Table 1.2 Summary of deformation modes

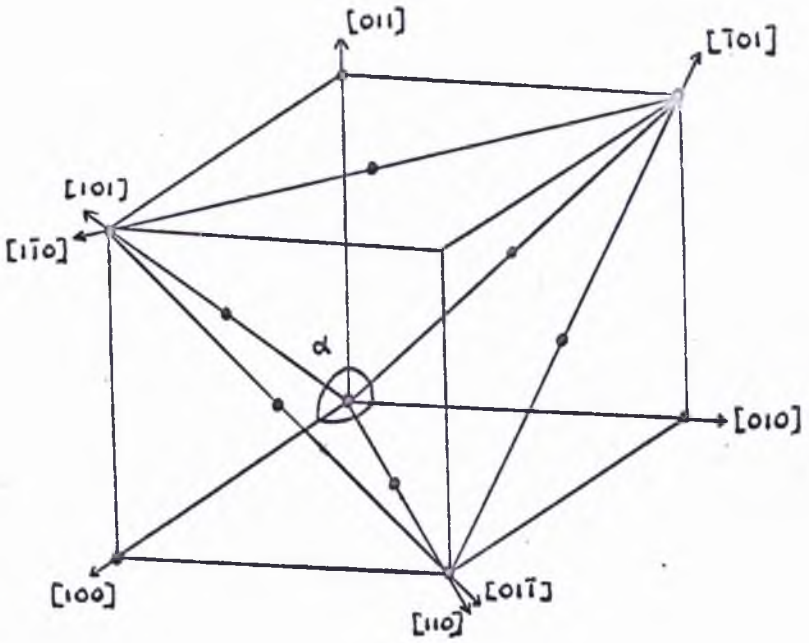

Fig. 1.1 The unit cell of α - mercury showing important directions.

Fig. 1.2 Example of wavy slip on a cylindrical crystal

CHAPTER II - GROWTH AND PREPARATION OF SINGLE CRYSTALS

2.1 Introduction

Three types of mercury crystal have been used during the programme of research in this department. Single surface analysis of traces on large grains of a flat poly-crystalline specimen enabled the determination of the slip plane (Crocker et al. 1963). 4 mm diameter cylindrical single crystals were grown for the experiments to determine the operative slip direction (Rider and Hecksher 1966). Square cross-section single crystals were used for a two-surface analysis of the twin shear elements (Crocker et al. 1966).

The work described in this thesis has entailed the use of single crystals of both circular and square cross-section. The glass moulds previously used for the growth of the cylindrical specimens were considered suitable, but a 6 mm diameter mould was chosen to exclude any possibility of twisting the specimen during the subsequent circumferential trace analysis. However, the crystals grown in 6 mm square tubes were often found to be difficult to remove, and even when this was possible surface irregularities on the glass walls left scratches along the length of the specimen. These scratches, while being useful as reference marks for goniometry provided points of stress concentration where recrystallisation frequently occurred during the subsequent anneal in the storage vessel. In, addition, using the modified Bridgman technique of Rider & Hecksher for the growth of specimens was by no means a reliable source of single crystals. Many of the crystal surfaces had characteristics resembling lineage on them, and

examination of the diffraction patterns of these crystals confirmed this in the form of splitting of the Laue spots. This not only made orienting the patterns more difficult and less accurate, but made the subsequent metallography less easy.

Thus, a need was felt for designing a new mould for the growth of the square crystals, and further, for an investigation into the factors governing the growth of good single crystals of mercury. As already indicated, the Laue back reflection technique would form an integral part of such an investigation and so a simple-to-use low temperature X-ray camera was constructed. Preliminary work on a method of growth involving cooling by means of a thermistor device has shown interesting results, particularly with reference to the detection of the growing solid-liquid interface by an ultrasonic method. However, it was felt more important to develop a method based on the existing techniques than to attempt something completely new.

Because of the observed effect of impurity content on the deformation characteristics of mercury (Greenland 1937) it was particularly important to standardize the material used. Singly distilled mercury having a total impurity content of less than three parts per million was used in all the work. The analysis was performed by Johnson and Mathey. The mercury was stored under ethyl alcohol to prevent a dust or surface film from forming.

2.2 Crystal Growth Equipment

As mentioned in the Introduction, the growth of cylindrical single crystals in the straightforward circular

cross-section tubing was considered entirely suitable for the purpose of this work. Veridia precision bore tubing of 6mm diameter was used to grow single crystals up to 6 cm in length.

A novel design was developed for the growth of square cross-section single crystals with faces particularly suitable for subsequent metallographic examination. The outer part of the mould consisted of a Veridia precision bone tube of 10 mm square cross-section shown in Fig. 2.1. Into this fit four accurately machined and polished glass slides also shown in Fig. 2.1, of such dimensions that the cross-sectional area is effectively reduced to 6 mm square. Fig. 2.2 shows the set of slides inserted in the outer tube, and a cross-section of the completed assembly appears in Fig. 2.3 showing that two of the slides are bevelled to allow smooth movement inside the tube. A specially cut rubber bung fits into the end of the mould and tends to force the slides apart thus preventing the liquid mercury escaping prior to solidification. Inserted in the centre of the bung, as is also the case for the growth of the cylindrical crystals, is a sharpened copper pin to provide a nucleation point during the subsequent growth. The special feature of this square mould becomes apparent when the crystal has been grown. The set of slides containing the single crystal are extracted as a unit from the outer glass tube, thus diminating any scratching due to the surface of the crystal sliding on the walls of the tube. The slides are then simply lifted from the crystal surfaces one by one leaving the crystal virtually undamaged.

Prior to growth of both cylindrical and square cross-section crystals the glassware was thoroughly cleaned with teepol and fuming nitric acid solutions and well rinsed with absolute ethyl alcohol. All the surfaces were covered with a layer of this alcohol before assembling the mould; this facilitates the extraction and dismantling when the crystal has grown.

2.3 Growth Rate - Crystal Perfection

2.3.1 Experimental Investigation of Growth Conditions

Crystals of various lengths between 5 and 7 mm, depending on the precise nature of the subsequent experiments to be performed, were grown using a modified Bridgman technique. Fig. 2.4 shows a demountable square mould containing mercury prior to growth suspended above a dewar containing the refrigerant. In earlier experiments (Rider and Hecksher 1966) the refrigerant used was liquid air, but it was found that the initial growth rate of the crystal was too great resulting in the frequent occurrence of 'bad' crystals. In order to reduce this failure rate in the growth of single crystals, cold absolute ethanol was used as the refrigerant at temperatures between $-60^{\circ}C$ and $-110^{\circ}C$. A copper cylinder and copper rods were placed in the dewar in an attempt to eliminate any thermal gradient in the alcohol. A temperature rise of less than $10^{\circ}C\ hr.^{-1}$ was achieved with this arrangement. The crystal growth motor, also shown in Fig. 2.4, was fitted with a gearbox so that the rate of lowering of the mould could be varied.

The growing interface was observed through an optical

microscope, the image being reflected through 90^{o} using a specially constructed sleeve, with a 45^{o} mirror, to fit over the microscope objective. The initial nucleation and growth rate are important since they control the subsequent growth. A very low temperature and fast lowering rate will cause nucleation at places other than the copper pin provided specifically for the purpose and a single crystal will not result.

A combination of temperature and lowering rate was found such that the solid-liquid interface always remained above the level of the surrounding alcohol during the growth of the crystal. Under these conditions, represented in Fig. 2.5(a), heat is drawn from the liquid phase through the interface, sites on the interface acting as nucleation points for the solidification of the super-cooled liquid. The growing crystal then takes on the atomic configuation of the interface, producing a single crystal. If the interface falls below the alcohol level, as indicated in Fig. 2.5(b), thermal paths through the walls of the mould are provided and nucleation points arise at irregularities in the glass surface. High temperatures and fast lowering rates produced this situation and resulted in lineage on the surface of the crystal which, as already mentioned, is undesirable.

The optimium experimental conditions were found to be a refrigerant temperature of $-90^{o}C$ and a lowering rate of 1 mm min^{-1}.

2.3.2 Factors Determining Growth Rate

Estimations of the dependence of the rate of growth of the interface on the temperature gradients in the two phases of low melting point elements have been reported. Goss (1953) considered the simple heat flow from the liquid plus the latent heat of solidifcation, and equated it to the heat flow in the solid. For slow growth rates and no supercooling of the liquid he gives $\frac{G_s}{R} > \frac{\rho L}{k_s}$ where G_s is the solid temperature gradient, R the growth rate, ρ the density and k_s the thermal conductivity of the solid, λ For the liquid air refrigerant, G_s can be taken as 100, which gives $R < 3$ mm min^{-1}. Now, to ensure the situation typified by Fig. 2.5(a), the lowering rate should be less than this value. Previous workers on mercury have used rates ranging from 2mm min^{-1}. (Andrade and Hutchings 1935) to 10 mm min^{-1} (Greenland 1937). Thus, one might expect that these rates resulted in the frequent occurrence of'bad' crystals. Further, as already discussed, it is felt that this temperature gradient promotes a large, undersirable, initial growth rate immediately following nucleation.

Pomeroy (1952) gives a different expression in terms of the difference between the thermal conductivities of the liquid and solid phases, thus $R < G\,(k_s - k_l)/\rho L$. For mercury, the thermal conductivity is found to increase by a factor of 3 on solidification (Gmelin 1965). Thus an estimate of $(k_s - k_l)$ can be obtained, and the corresponding value of R is approximately the same as that using the criterion of Goss. Using cold alcohol as the refrigerant at the optimium

temperature found, Gs is reduced by about a half and so then is R. Consequently, the chosen lowering rate of 1mm min^{-1} would appear suitable for this refrigerant in order that the growth situation shown in Fig. 2.5(a) exists.

2.3.3 Examination of As Grown Crystals

After extraction of the crystal from the mould, the surfaces were observed under an optical microscope. Use was made of the polarised light facility on the microscope to delineate possible grain boundaries. The square cross-section crystals were found to have smooth scratch-free surfaces and the well-defined nature of the edges of the specimens made them suitable for use as a reference direction for accurate goniometry.

Some of the cylindrical specimens had characteristic surface growth features as shown in Fig. 2.6. When observing the formation of these features, it was found that the movement of the solid-liquid interface was irregular, and periodically it apparently stops and the ridge is then formed slowly. Subsequently the interface moves on relatively quickly leaving behind the ridge on the surface. The movement continues until the next ridge is formed, again with the interface apparently stationary. It thus seems that the crystal grows more quickly in contact with the glass walls of the mould and then has to slow down while the main bulk of the specimen crystallises. However, the whole crystal was usually found to be single and was thus considered suitable for use in subsequent deformation experiments. A further indication of the perfection of the crystal was obtained by examination of the diffraction patterns

taken using the Laue back reflection technique described in the next section. Crystals showing splitting or asterism of the spots on the pattern were considered unsuitable and discarded.

The crystals were stored in specimen tubes in a large dewar containing ethanol cooled by solid carbon dioxide. The temperature was thus maintained at approximately -70°C. The crystals were usually grown in batches and were annealed under these conditions for between 1 and 4 weeks.

2.4 Orientation

The orientation of the specimen axes of the single crystals was determined by a Laue back reflection technique. A low-temperature X-ray camera was constructed for this purpose and a schematic representation is shown in Fig. 2.7. The specimen is positioned horizontally in a brass block A which is free to slide in a copper mount B so that the whole length of the specimen can be brought into the X-ray beam. The copper mount is cooled by a thick copper rod which dips into a dewar of liquid air, thus maintaining the specimen temperature at about -70°C. The specimen to film distance can be adjusted but for all the crystal orienting reported here this distance was fixed at 3 cm. Consequently, in practice only movement and adjustment of the brass cylinder is necessary prior to recording the diffraction pattern. When a groove along the length of this cylinder is aligned with the edge of the copper mount, then the correct position of the crystal face, normal to the X-ray beam, is ensured. In the case of cylindrical specimens a fiducial

mark is placed on the specimen by passing a fine wire through the collimator in the film holder.

X-rays from a 'Matchlett' sealed tube with a copper target operated at 36 KV and 15 mA were used. An exposure time of one hour gave enough Laue spots to orient the pattern and ensured that the background radiation produced shadows on the film of two pointers on the film holder. These were used as a reference direction when orienting the pattern. The diffraction patterns were oriented and the specimen axis direction identified using a table of angles computed by Bacon (1963).

Diffuse scattering rings were observed on many of the Laue photographs and these will be discussed in Appendix II.

2.5 Preparation and Mounting of Single Crystals

Two sets of chuck pieces were specially machined to take these mercury crystals and to fit into the tensile machine described in the next chapter. One set catered for the cylindrical crystals, the other for the square specimens. These chucks were also suitable for the compression tests reported in the next chapter and for the tensile jig used in the experiments at 4.2°K to be described in Chapter 4 and 5. A machined V-block, in which the chuck pieces lie allows accurate alignment of the tensile specimens.

Prior to a deformation test, a crystal was taken from the storage vessel and the excess alcohol carefully removed from the surfaces using a soft tissue. The crystal was then slowly cooled to 77°K and carefully fitted into the pre-cooled

chucks. The grub screws were tightened in turn, rotating the assembly in the V-block to keep the crystal correctly aligned. The completed assembly is shown in Fig. 2.8 with a dummy cylindrical brass specimen in position. The procedure was precisely the same for square cross-section crystals. The graduations on the chuck piece seen in this figure were used in the subsequent trace analysis to be described in Chapter 3. The completed assembly was now ready for insertion into whichever tensile jig was appropriate to the experiments to be performed. These experiments will be described in the following three chapters.

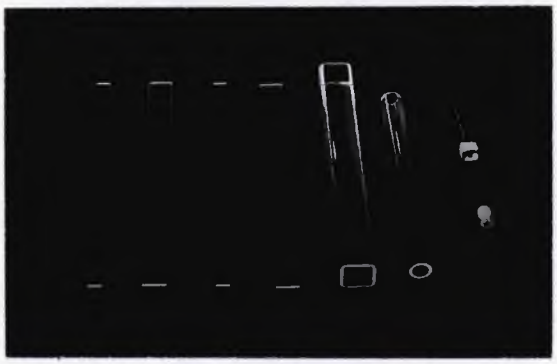

Fig. 2.1 Glass moulds used for crystal growth

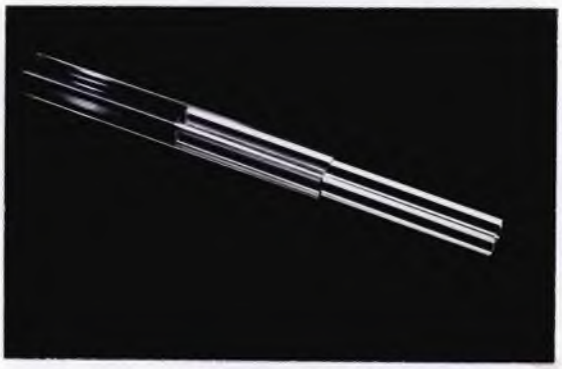

Fig. 2.2 Partially assembled square crystal mould.

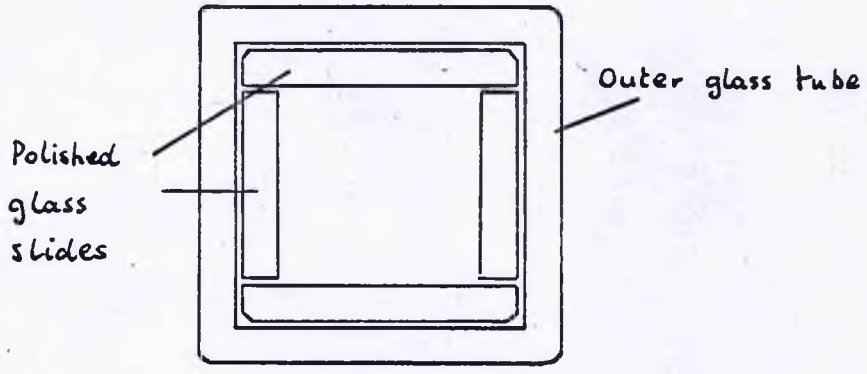

Fig. 2.3 Cross - section of square glass mould. Two of the polished slides are bevelled to permit smooth - running.

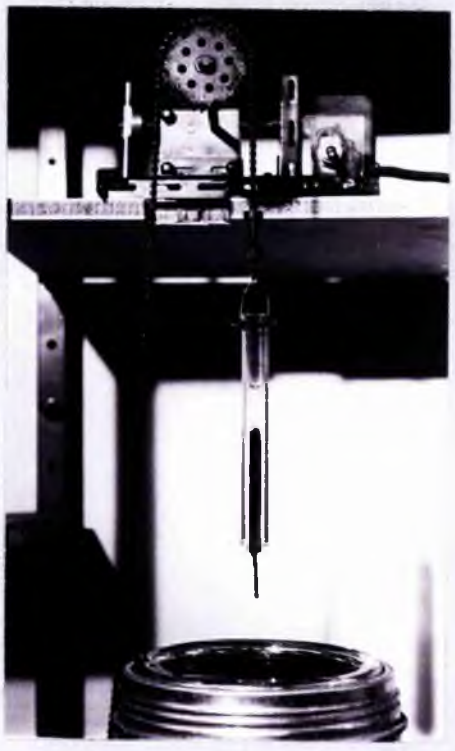

Fig. 2.4 Crystal growth equipment prior to growth of single crystal.

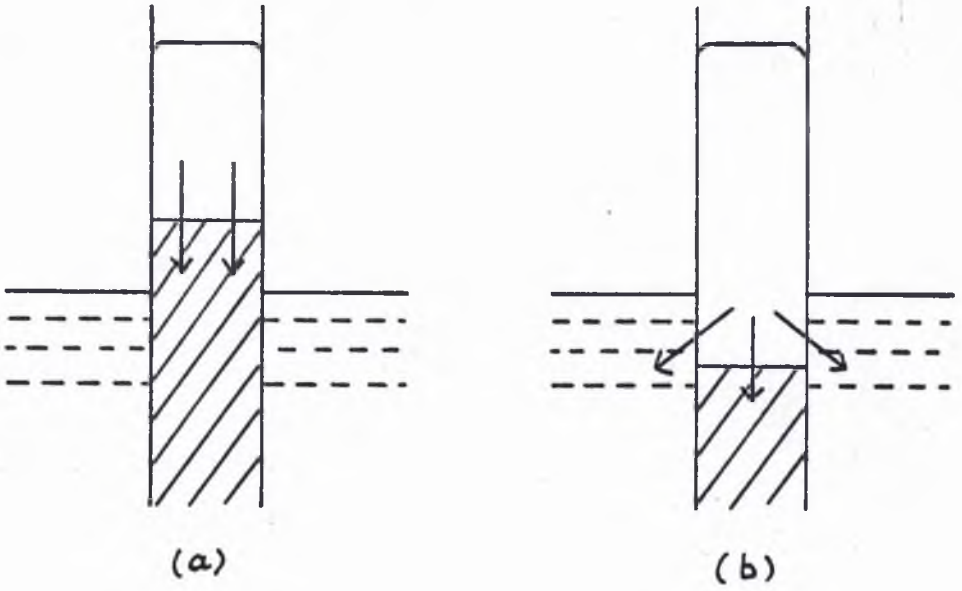

Fig. 2.5 Representation of solid - liquid interface in two growth situations.

Fig. 2.6 Growth features on a cylindrical crystal.

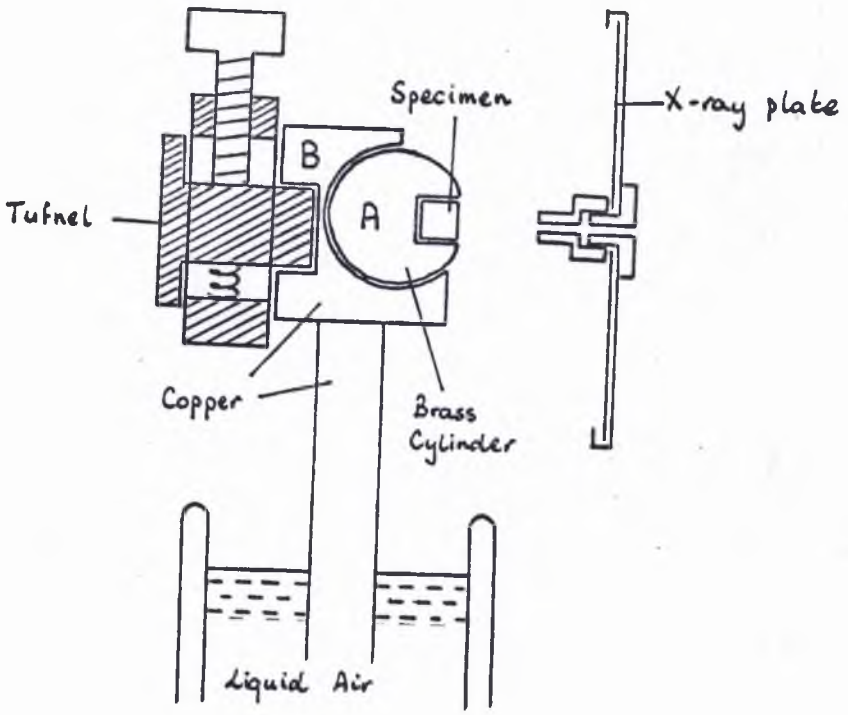

Fig. 2.7 Low - temperature X - ray camera.

Fig. 2.8 Chuck and specimen assembly.

CHAPTER III - DEFORMATION AT 77°K

3.1 Introduction

The survey of work done on mercury single crystals given in Chapter 1 has shown that further detailed investigation of the deformation characteristics of this metal at 77°K is desirable. Thus, this chapter is concerned with some results of experiments performed at this temperature. As described in Chapter 1 the large standard stereographic triangle associated with the low symmetry structure of the normal α-phase of mercury involving one sixth of the full stereogram makes the orientation dependence of the deformation behaviour particularly interesting. The results so far obtained on mercury clearly demonstrate that this is so. At 77°K the operation of a twinning mechanism for certain orientations which would have deformed by short diagonal slip at 200°K was of distinct interest. Further, as explained in Chapter 1, it was felt that the possibility of an assymetry in the slip behaviour with respect to tension and compression tests which is now well-established in h.c.c. metals (Foxall et al. 1966) would also exist in mercury.

The only published report of the measurement of stress-strain curves for single crystals of mercury is that due to Greenland (1937). In his experiments the orientations of his specimens were not uniquely determined.and indeed any approximation to these orientations was deduced assuming the operation of $\{001\}$ slip planes and $\{011\}$ twin planes following the results of Andrade and Hutchings (1935). These latter results are now known to be incorrect as described in

Chapter 1 and consequently it was considered desirable to measure again, and in more detail, the stress-strain curves of single crystals. In particular, in view of the large variety of orientations possible within the standard stereographic triangle, it was felt that the orientation dependence of the shape of such curves would be informative. Thus, testing of crystals in tension and compression has been attempted and the corresponding stress-strain curves recorded.

Of course the large standard triangle for mercury can have its disadvantages. In order to carry out a full orientation dependence, a very large number of crystals have to be grown to ensure every orientation is accounted for. As explained in Chapter 1, the exciting nature of the experiments conducted at even lower temperatures than 77°K necessitated the curtailment of the programme of work at this temperature. Thus it has not proved possible to investigate as many orientations as one would like, but even so significant results have been obtained. In the next section, theoretical considerations are used to introduce the various features resulting from the large spread of orientations possible, and the following sections deal with the experimental procedure, results and discussion of results.

3.2 Effect of Orientation on Deformation Behaviour

Rider and Hecksher (1966) have published the results of a computer plot of Schmidt factor contours for the two experimentally observed slip modes of mercury, that is $\{111\}\langle 1\bar{1}0\rangle$ and $\{11\bar{1}\}\langle 011\rangle$. These are reproduced as Figs 3.1 (a) and (b) respectively. The interesting fact to

note about these plots is that they indicate that for both types of slip the operation of more than one variant of the slip mode is possible, within the one standard stereographic triangle. This is not, of course, the case for f.c.c. metals to which the mercury structure approximates. Nor is it true for hcp metals such as zinc and cadmium. However, a similar situation has been found to exist in b.c.c. metals (Taylor and Christian 1966). Here instead of different variants of one mode being operative, a second mode occurs for various orientations, the precise position of the boundaries dividing the occurence of one mode from another being dependent on the type of test, that is, tension or compression, and the temperature (Foxall et al. 1966).

In the case of mercury, the dotted lines in Fig. 3.1 indicate the boundaries along which the resolved shear stress on two systems are equal. The particular variants having the highest value of Schmidt factor in these regions are shown using the notation for the slip modes introduced in Chapter 1. In these regions single slip on the relevant variants should theoretically occur and if one considers the lattice rotations following deformation on these systems various features become apparent. During tensile deformation the specimen axis may be regarded as rotating along a great circle towards the operative slip direction, and an indication of the relevant rotations in each case is given by the arrows in Fig. 3.1. Thus, single slip predominates until a boundary with another system is met, when double slip will theoretically begin. It now becomes clear that three types of boundary occur. Those denoted by u can be referred to as unstable in that rotations

associated with the systems either side of the boundary cause the specimen axis to rotate away from it. Thus, although double slip is theoretically possible for an orientation immediately on the boundary, this seems unlikely since a non-geometrical factor will probably cause the predominance of one system with a subsequent rotation away.

The boundaries marked s are called stable since for an orientation near these, rotation towards them will ensue and when reached the pole will theoretically remain on the boundary. Double slip will then occur with a rotation along the boundary so as to maintain the specimen axis in a plane symmetrical to the two operative slip planes. This continues until the two slip directions and the tensile axis lie in the same plane. For example, in Fig. 3.1(a) region A, when the s boundary is reached double slip will proceed with rotation to the pole $[2\bar{1}\bar{1}]$. In (b), region A, the stable point is shown as $[211]$, but in region C the position is slightly different. Double slip is possible on the stable boundary there with no rotation since the slip direction and tensile axis already lie in the same plane $(1\bar{1}0)$. It is at this sort of boundary that the phenomenon of overshoot has been observed (Tanner and Maddin 1959, Mitchell et al. 1963) in f.c.c. and b.c.c., where single slip on the initial system has continued in preference to the initiation of glide on the second (conjugate) system and the specimen axis has been found to overshoot the boundary.

The two types of boundary so far discussed are found in any crystal system and the overshoot phenomenon has been investigated in various metals particularly ones with f.c.c.

structure. The third kind of boundary does not occur in high symmetry metals and is thus not so common. We refer to it as permeable and denote it p. Here, the two rotations either side of the boundary are in approximately the same sense and so one would expect the tensile axis to pass right through it. Then, theoretically the second system would be more highly stressed, and would become more so as the rotation proceeded. Consequently, one would expect the second slip system to take over, perhaps completely, from the first, as distinct from what happens at the stable boundary where double slip is expected. One such boundary exists for each of the two slip modes in mercury as shown in Fig. 3.1. Whether the second slip system does replace the first at these boundaries or whether the overshoot phenomenon again occurs, with the secondary system taking over at higher strains, would be of particular interest.

It has already been mentioned in Chapter 1 that preliminary results at the higher temperatures on the study of assymmetry of slip in mercury have led to the initiation of a separate research project involving these temperatures. Consequently the effect of the boundaries for the $\{11\bar{1}\}\langle 011\rangle$ type slip which has only been observed at $-70^{\circ}C$ has not been investigated. Indeed the results of Rider and Hecksher indicate that this might not even be possible since the $\langle 1\bar{1}0\rangle$ direction becomes operative in the lower regions of the triangle. This is particularly disappointing since crystals with orientations in region B of Fig. 3.1(a) occur less frequently than those in region C of Fig. 3.1(b). The problem

is further complicated by the occurence of twinning in this region near $[110]$. However by raising the temperature even more, an investigation involving the permeable boundary in the latter figure might be possible.

The investigation of the overshoot at these boundaries under compressive testing is not feasible since large strains are not possible in these tests without the severe distortion inherent in the type of compression test to be envisaged. To obtain meaningful results on this aspect a compression arrangement similar to that used for testing niobium crystals (Taylor and Christian 1967) would be desirable. The experiments on compression will thus be restricted to identification of the operative deformation mechanisms together with values of associated critical resolved shear stress (henceforth abbreviated to c.r.s.s.). It is worth noting that the two boundaries within the triangle in Fig. 3.1(a) correspond to well defined zones, each being the trace of a $\{11\bar{1}\}$ type plane. This is not true, however, for Fig. 3.1(b) where the boundary is not a great circle and thus corresponds to no rational pole, but does pass through $[100]$ as shown.

Further manipulation of these two figures and their contours can be used to illustrate the results of Rider and Hecksher. If we define the ratio of the c.r.s.s. on the two modes by $\alpha = C\langle 011\rangle / C\langle 1\bar{1}0\rangle$, then for $\alpha = 1$, the c.r.s.s. on the two modes are equal, and which occurs depends on the respective values of Schmidt factor. Figs 3.1(a) and (b) then correspond to the cases of $C\langle 011\rangle = \infty$ and $C\langle 1\bar{1}0\rangle = \infty$ respectively. By varying the value of α, the experimental and

theoretical results can be correlated. Fig. 3.2 shows the result for $\alpha = 1.25$. The orientations of four crystals reported to deform on $\{11\bar{1}\}\langle 1\bar{1}0\rangle$ are superimposed on this figure. It can be seen that there is a close fit. For a lower value of α the right hand crystal would have slipped in the $\langle 011\rangle$ direction. The value of α is consistent with the range Rider and Hecksher deduced for their results. The testing of crystals at various intermediate and higher temperatures would lead to information on the temperature coefficients of the c.r.s.s. of the two modes.

Similar computation has been performed to calculate the effect of orientation on the Schmidt factor for the observed twinning mode in mercury. The result is shown in Fig. 3.3(a) and (b) where once again only the contours of the most highly stressed slip system in any particular region are shown. In this case, however, since twinning is a unidirectional process, the size of the Schmidt factor is important. In (a) the positive values are considered corresponding to the most highly stressed variant in a tension test. Similarly (b) represents the compression case. It can be seen that in a tension test one variant is expected to be predominant virtually for all orientations whereas for compression the situation is slightly more complex.

Clearly, in tension, the variant a' is highly stressed for the majority of orientations, but as previous results and those presented here have shown twinning is confined to the region near $[110]$. Here, the $\langle 1\bar{1}0\rangle$ slip Schmidt factor becomes low and it might be argued that if a critical value of the

resolved shear stress for twinning (henceforth abbreviated to r.s.s.t.) does exist, and it is much higher than that for $< 1\bar{1}0 >$ slip, only when the Schmidt factors for slip are low will the r.s.s.t. be exceeded and twinning occur. Information on the possibility of a critical value of r.s.s.t. will be reported and further discussion on a c.r.s.s. for slip especially with reference to this region.

Thus, it can be seen that there exist several interesting features to be investigated at this one temperature, particularly with reference to the orientation dependence of the occurrence of the three mechanisms observed here, slip, twinning, and kinking.

3.3. Experimental Procedure

3.3.1 Introduction

Initial experiments were performed on square cross-section crystals since as described in Chapter 2 a method had been developed to ensure surfaces which were particularly suitable for metallographic observation. As the results to be presented in section 3.4 show, the predictions postulated in section 3.2 were largely verified using these crystals. However, certain anomalies became apparent which could not be clarified using these crystals. It was thus felt advisable to use circular cross-section single crystals for the remainder of the experiments to be described. Further verification of operative slip variants, more meaningful c.r.s.s. measurements and stress strain curves were thus obtained. In addition, the elimination of stress concentrations at the crystal edges, which could result in spurious deformation, was achieved. In either case, the single crystals were grown and

prepared for testing by the methods described in Chapter 2.

3.3.2 Size of specimen

The ratio of the diameter a to the length b of a cylindrical crystal is of importance in tensile tests since the crystal should be free to deform on the system that is most highly stressed and not be influenced by the physical restraints inherent in the test. We can obtain a minimum value for this ratio by considering Fig. 3.4 which shows diagramatically the relative position of three slip planes A, B and C within a single crystal. A cylindrical crystal is being considered since this is the simplest case to treat with the dimension a being constant. Consider plane C to be gripped by the chucks of the tensile arrangement. Then the ratio a/b must be of such a value that the crystal will readily slip on plane A or B. To ensure this A or B must be more highly stressed than C. Thus a/b must be chosen such that $S_C < S_A, S_B$ where S denotes the Schmidt factor on a particular slip variant. The parameter α takes into account any assymmetry in the c.r.s.s. on the different systems. The Schmidt factors can be found in terms of a and b and by plotting a/b against α, the minimum values of the ratio are obtained corresponding to $\alpha\, S_C = S_A$ or S_B. The result of this is shown in Fig. 3.5 for $1 < \alpha < 2$, thus allowing for the c.r.s.s. on one variant to be as much as twice that on another.

In practice the crystals are grown with a/b corresponding to a value of $\alpha > 2$, i.e. $b > 3.6$ cm, since for cylindrical crystals a = 0.6 cm. This offers a wide margin of error since it is unlikely that $\alpha = 2$ for the $\{111\}\langle 1\bar{1}0\rangle$

slip mode. Thus, for tension tests the specimens were mounted with b = 4 cm in general, but for compression tests a value b = 3 cm was usually chosen since for values greater than this severe buckling became a problem.

3.3.3 Tension and Compression Tests

Both kinds of test were carried out on a Tensometer Ltd. machine using a cross-head speed of 4 mm min^{-1} except for two specimens which were tested at 16 mm min^{-1}. This machine was particularly useful in that it had a yoke attachment which facilitated the introduction of a dewar containing the refrigerant around the specimen. The refrigerant for these experiments was liquid nitrogen. A load cell was positioned in the load bearing arm its output being connected to a chart recorder having a full scale deflection of 1 mV. Thus the load was measured electrically and the associated circuitry allowed loads in ranges between 1 and 50 Kg. to be measured. This represented a considerable improvement on the previous stress measurements made on mercury crystals in this department using a mechanical method. For tension tests the specimen and chuck assembly of Fig. 2.8 is located on the yoke and load arm with dowel pins. The compression jig attachment to the testing machine was of conventional design. No sideways movement was allowed during the test this being ensured by two specially machined cylindrical pieces which locate in the ends of the chuck pieces of Fig 2.8 and in the parallel plates of the compression jig.

3.3.4 Trace Analysis

Measurement of the trace angle with respect to the

specimen axis on two adjacent faces of a square cross-section crystal is sufficient to define the plane of the trace. This can then be indexed by reference to the standard orientation stereogram. The associated macroscopic shear direction cannot be uniquely determined from these measurements without recourse to surface tilt measurement where applicable. However, as explained in section 3.2, for this temperature the operative slip variant is always identifiable from determination of the slip plane. The senses of the surface tilts associated with the twin traces were observed to check for consistency with the established twin mode, particularly because detailed examination of deformation twins in mercury have previously been restricted to compressive and bending tests. Full surface tilt measurements on twin traces were not however undertaken since the observed occurrence of only one deformation twin mode in crystalline mercury offers no ambiguity in the shear direction.

Examination of the traces on cylindrical specimens permits easy identification of the shear direction. With the specimen and chuck assembly located in a V-block the angle of a slip line or twin trace to the specimen axis was measured as a function of angular rotation about that axis. The angular rotation was measured by means of the graduations engraved on the chuck piece shown in Fig. 2.8. The shear direction was taken to be that midway between the positions at which the trace vanished.

These measurements were carried out on an optical microscope fitted with a goniometer eyepiece with the specimen positioned in a bath of liquid nitrogen and cooled ethylalcohol.

The square specimens were usually demounted from the chucks first, but in either case the specimens were suspended just above the level of the liquid refrigerant. This prevented distortion of the image of the traces and also maintained a sufficiently low temperature while keeping the surfaces free from frost. The measured angles were then plotted on an indexed stereogram and the plane and, when possible, the shear direction identified. The estimated accuracy is 2^{o} for the pole of the shear plane and 4^{o} for the shear direction.

3.4 Results

3.4.1 General Features of Deformed Crystals

The crystallographic orientations of the axes of all the specimens tested at $77^{o}K$ are shown in Fig. 3.6. The prefix S denotes a square cross-section crystal, the remainder being cylindrical specimens. The dotted boundaries shown here are those discussed in section 3.2 where predictions concerning the operative variants of the slip modes were presented. A certain amount of difficulty was encountered in the compression tests involving icing of the runners making accurate measurements impossible. Consequently, attention was focussed on the tension tests since the c.r.s.s. values were more reliable and the stress-strain curves more meaningful.

Five square and ten circular cross-section crystals were tested in tension. Of the circular crystals tested in compression two are considered here. The mechanisms by which these crystals deformed are given in Tables 3.1 and 3.2, the first of these referring to the square crystals. Three mechanisms were observed, straight slip, twinning and kinking.

The notation used in the tables is that described in Chapter 1. The majority of crystals deformed predominantly by straight slip, both in tension and compression. Deformation twinning occurred in tension on six crystals and on two of these no prior slip occurred judging from the recorded load-extension curves and the appearence of the surfaces. In these two cases twinning was observed on two variants of the twin mode while only one variant was operative in the other crystals. Between five and ten kink bands were observed on five crystals approximately evenly distributed over the gauge lengths. Crystals C5 and C7 were tested in compression and slipped on the most highly stressed variant. No twinning was observed on these specimens.

Examples of the three mechanisms, slip, twinning and kinking involved in the deformation of these crystals are shown in Figs. 3.7-11. Fig. 3.7 shows the surface of a cylindrical crystal exhibiting straight slip typical of the majority of orientations. The occurrence of slip lines is inhomogeneous and they appear to form in bands.approximately 600 μm across. The general morphology of the twinned crystals was similar to that reported by Guyoncourt and Crocker (1968), where square crystals were deformed in compression. A typical example is Fig. 3.8 where twins on two systems have formed on a circular cross-section crystal. Fig. 3.9 shows the surface of a square crystal that has twinned profusely in tension. Intersections of twins on two variants are clearly shown with the associated bands of accommodation slip. Cross-twinning, a familiar feature on mercury (Crocker et al. 1966) is also apparent on

this micrograph. Accommodation effects are necessary when one twin ends in the matrix as well as at intersections. Fig. 3.10 shows an example where an accommodation kink band has formed with fine slip within it. When only one twin variant is operative, straight slip occurs with it as shown in Fig. 3.11 where the twin has sheared the slip lines. An example of a typical kink band formation is shown in Fig. 3.12.

3.4.2 Analysis of Deformation Modes

For both tension and compression tests slip always occurred on the $\{11\bar{1}\}\langle 1\bar{1}0\rangle$ mode previously observed by Rider and Hecksher (1966) in tension tests at this temperature. The variant of the slip mode with the highest Schmidt factor, according to the scheme discussed in section 3.2, was always observed to operate. This was also true for the accommodation slip occurring at the twin intersections on the two crystals on which profuse twinning occurred, as shown in Fig. 3.9. Wavy slip, reported to occur in mercury (Guyoncourt 1967) for certain orientations during bending tests, was not observed.

Twinning occurred on the irrational $\{\bar{1}35\}$ composition plane which is now known to be the well-established deformation twin mode in mercury (Guyoncourt and Crocker 1968). The sense of the surface tilts were consistent with the $\langle\bar{1}21\rangle$ shear direction associated with this twin mode. It was seen in Section 3.2 that for the majority of orientations a' is the twin variant with the highest Schmidt factor. When twinning occurred it was always on this variant and was sometimes accompanied by twins on a. Thus when occurring in pairs the two operative variants were those possessing the unique

crystallographic relationship involving accommodation slip planes discussed in Chapter 1. Accommodation kinking sometimes occurred at these intersections as well as in situations like that of Fig. 3.10 involving one twin variant. These kinks and the ones observed on the slipped crystals always corresponded to an $\{01\bar{1}\}$ plane, the particular variant occurring being directly related to the operative slip direction. Thus for crystals in region A of the unit triangle where the slip direction is $[1\bar{1}0]$ the kinks form on $(1\bar{1}0)$.

3.4.3 Stress-Strain Curves

The load extension curves for most of these crystals were recorded. Departure for the linearity of the elastic region of these curves has been taken as the criterion for the onset of plastic flow and the corresponding load used to deduce the c.r.s.s. for each crystal shown in Tables 3.1 and 3.2. The relevant Schmidt factors for slip are included corresponding to the observed variants, these being, in each case, the ones with the highest value. For the crystals that twinned, it is the Schmidt factor of the most highly stressed variant a' that is indicated in these tables, and have been used to calculate the quoted values of the r.s.s.t.

The load-extension curves have been converted into resolved shear stress against resolved shear strain curves using equations given by Schmidt and Boas (1950). Not to consider the components of stress and strain on the operative modes would be misleading since the large lattice rotations possible and the associated changes of Schmidt factor would not be taken into account. For example the unresolved stress-

strain curves of crystals S1 and S2 showed significantly different rates of hardening which are removed when the components on the operative mode are considered. Some typical curves appear in Fig. 3.13. The two crystals which twinned profusely without prior slip are not included since the yield point coincides with a large stress-relaxation, corresponding to a burst of twin formation, at a considerably higher stress than is indicated in this figure. The stress-relaxation was accompanied by audible clicks during the test. In these cases the test was usually stopped and the surfaces examined to confirm the occurrence of twins with no appreciable rise in temperature. Upon re-testing these crystals, they were found to twin again without slipping and usually at a lower tensile stress than for the first burst. For example C10 had twin bursts at tensile stresses of 444.4 gm mm^{-2} and 343.0 gm mm^{-2}. For the crystals that slipped before twin bursts were observed, and then re-tested after observation, the load-extension curves usually showed further slip and hardening followed by further twins at higher tensile stresses.

Crystals for the majority of orientations exhibit a low work-hardening rate. The two exceptions appear to be crystals C5 and C23, where a significantly higher rate of hardening is observed. C5 was tested in compression and C23 lies just outside the region where profuse twinning is observed. C23 twinned at a higher strain than is indicated in Fig. 3.13. Reference to the distribution of orientations in Fig. 3.6 indicates that they were such that the hope of investigating overshoot at double slip boundaries could not be realised. The large strains theoretically possible on the primary glide

systems and the high deformations thus involved means that, unless a crystal has an initial orientation reasonably near a double slip boundary, the necessary metallography would be difficult.

3.5 Discussion

For the purpose of discussing the results, the unit stereographic triangle has been divided into various regions as shown in Fig. 3.14. Three of these A, B and C correspond to crystals that have slipped on the most highly stressed system according to the scheme of section 3.2. It has not proved possible to determine whether these boundaries exist in the precise form predicted. Indeed, to do so would be a difficult task because of the size of the unit triangle, and further to test the situation with respect of compression tests would entail a great amount of work. The boundary drawn within region A near [110] is the contour of $S_A = 0.15$ taken from Fig. 3.1(a). Crystals to the upper side of this contour deform by twinning alone, whereas on the other side slip is predominant with a transition region defined by C23, C13 and S5 where both can occur. This situation is in approximate agreement with the results of Guyoncourt (1967) for bending tests on mercury, except that there no twinning was observed outside the small region bounded by the contour.

In region B, the position is not quite so definite, the behaviour of crystal 11 fitting into the category of the transition region with the occurrence of both slip and twinning. The cross indicates the orientation of a crystal taken from the Rider and Hecksher (1966) paper which twinned in tension

without slipping. This helps to further define the region as shown by the dotted line. Another crystal orientation from that paper shows that the contour $S_c = 0.15$ suffices in defining the area of region C in which twinning will occur to the exclusion of slip. Within this twinning region, the present results show that two variants of the twin mode are operative, a' and a. That a' should be operative is expected since it is the most highly stressed system. Variant a occurs as well even though it is not highly stressed with respect to the direction of tensile stress. However, the local stresses in the matrix surrounding the formation of twin a' are relieved very simply by accommodation slip on system A at the intersection of twins a' and a as shown by Guyoncourt (1967).

System A will occur as the accommodation slip mode for all cases where two twin variants a' and a are operative. The operation of this mode is determined by the local stresses and the twin intersections rather than the stresses due to the applied tensile load. In the transition region this is not the case and the majority of the internal stresses are relieved by slip and only the most highly stressed twin system a' occurs A summary of the information available on the various crystals that twinned is contained in Table 3.3. It is clear that the predominance of twinning is not controlled merely by the Schmidt factor $S_{a'}$, since this increases as one goes away from [110] towards S5, whereas the occurrence of twins decreases with this trend. As already indicated in Fig. 3.14 the value of $S_{A,\ B,\ C}$ is important, and twinning only occurs when the ratio of the two exceeds 1.5. The boundary corresponding to this is indicated in Fig. 3.14. Good agreement is obtained

with experimental results for region B and part of A though not for other orientations. A more likely boundary is suggested by the remaining dotted line.

That twinning is confined to regions where slip is difficult has been observed on other materials. Bell and Cahn (1957) deliberately seeded crystals of zinc of such an orientation to prevent basal glide and found that twinning was then observed, but only after detectable pyramidal slip had occurred. This is in contrast to the present results and those of Rider and Hecksher (1966) where no slip was observed prior to twinning on some crystals. Bell and Cahn found that the r.s.s.t. was very dependent on specimen conditions and size and as such found no evidence for a critical value. Price (1960) has shown that a critical value of the r.s.s.t. does exist for dislocation free platelets of zinc, a result which is consistent with the dependence upon specimen condition.

Thompson and Millard (1952) verified the maximum shear-stress criterion for twinning in single crystals of cadmium, but later work on this material (Thompson and Hingley 1955) suggested a greater scatter of values. In these experiments crystals were chosen with small values of the angle χ between the tensile axis and the slip plane. It was found that crystals which had slipped extensively prior to twinning had a higher r.s.s.t. than crystals which had been only slightly deformed. This also seems to be the case in mercury where C23 and C13 which deformed predominantly by slip to high strains showed higher values than S5 and C11 which were hardly deformed. S3 and C10 are different in that no prior slip appeared to occur.

Taken as a whole, the r.s.s.t. values in Table 3.3 show no indication of a critcal value. However, for the two crystals S3 and C10 that twinned with no prior slip the resolved shear stresses on the twin mode are very similar. This may be evidence of the r.s.s.t. having a critical value and, if so, the ratio of that to the c.r.s.s. for slip would be in the range 2.9 to 3.4 by reference to the last column of the table. However outside this twinning region, that is for the rest of the crystals in the table, no consistency is observed. That is, when prior slip occurs the c.r.s.s. law for twinning, if it exists, is violated. For crystals S5, C11 and C13 the prior slip appears to facilitate the twinning process, whereas the opposite is true for crystal C23.

Closer examination of Tables 3.1 and 3.2 show that the c.r.s.s. for slip as calculated from the load-extension curve is not constant for all the crystals tested. The results do not indicate that one variant of the slip mode has a lower value than the others. However if the values of c.r.s.s. are plotted against the corresponding Schmidt factor the graph shown in Fig. 315 is obtained. The closed circles represent values taken from the C crystals and the closed squares from the S crystals. Although less reliable, the results from the S crystals have been included since they seem to fit into the general trend. Values for four cyrstals whose orientations were not uniquely determined but whose S values were deduced from surface traces have been included in this figure. The majority of the values are lower than the value 50 ± 17 gm mm^{-2} reported by Rider and Hecksher (1966). It is felt that the

method of testing employed by these workers involving the use of sliding grips was less reliable and accurate than the present measurements. The elastic region of the load-extension curves in the present tests were very straight and the departure from linearity well-defined. This is not always the case with the alternative method of gripping.

Ignoring for the moment crystals 5, 7 and S1, this figure clearly illustrates that the c.r.s.s. law for slip on mercury is violated at low S values. The two open points at very low S values refer to crystals S3 and C10 and represent the r.s.s. on the most highly stressed slip system at the twinning stress. Thus, they correspond to a minimum possible value of the c.r.s.s. for these specimens. Similar extrapolation of the results of the twinned crystals of Rider and Hecksher (1966) are consistent with this trend, the cross in Fig. 3.15 is an example of such an extrapolation. Crystals C5 and C7 were tested in compression and both C7 and S1 were tested at 16 mm min^{-1}. Crystals C5 and 7 could be interpreted in terms of an assymmetry in slip behaviour with respect to tension and compression tests, but to postulate this on the results of two crystals would clearly be inadvisable. The S1 result may be due to a load calibration mistake since a change of strain rate of at least an order of magnitude is usually needed to produce a detectable change in flow stress (Basinski 1960). Crystal C5 also exhibited an anomolous stress-strain curve which could again be conceivably interpreted in terms of assymmetry. However C7 also tested in compression shows an entirely different behaviour.

The majority of crystals work hardened quite slowly as might be expected during primary glide. C23 was the exception and its distinct behaviour from C13 is very marked. C13, having a slightly different orientation with lower Schmidt factor, twinned almost immediately after yield. Thus it may be that the higher work hardening rate of C23 is in some way related to the non-operation of the twinning mechanism for this crystal.

The occurrence of kink bands on crystals S4, S5, C15, 23 and 24 which are confined to one area of the unit triangle suggests that they act as a significant deformation mechanism. Kink bands usually represent a rotation of the lattice about an axis lying in the slip plane perpendicular to the slip direction. For these crystals this axis of rotation is of the $\langle 112 \rangle$ type. Roberts and Partridge (1966) have postulated that kink bands associated with twins in hcp metals are due to arrays of edge dislocations lying on adjacent planes with their extra half planes aligned thus distorting the lattice. The occurrence in mercury of accommodation kinks on $\{1\bar{1}0\}$ planes supports this interpretation this plane being perpendicular to the Burger's vector. However, a secondary slip system seems to occur within the kink band in Fig. 310. Honeycombe (1950) found a similar effect in aluminium.

The identification of kink bands on these crystals serves to explain some observations made on mercury by Greenland (1937) As mentioned in section 3.1 he based his crystal orientations on the occurrence of $\{001\}$ slip planes and $\{011\}$ twin planes. With these two modes observed by Andrade and

Hutchings (1935) he deduced that only when the heads of the twinning and glide eclipses lie on the same generator of the crystal surface, is the orientation of the crystal uniquely determined. Oddly enough, this situation is geometrically possible for these two planes and consequently his values of c.r.s.s. quoted for this particular case will be valid. However, the crystallography of the identification of the traces can now be seen to be incorrect. Slip occurs on $\{11\bar{1}\}$ planes and twins on $\{\bar{1}35\}$ and not $\{011\}$. Nor have twins been observed to occur at the temperature of Greenland's observations, between -60 and -70°C. The situation is resolved by interpreting the traces other than slip lines as kink bands. Indeed the appearance of micrographs in Greenland's paper supports this view. The relationship between the $\{11\bar{1}\}$ slip plane and the $\{1\bar{1}0\}$ kink plane is such that Greenland's deduction about the crystal orientation from this particular position of the two traces is valid.

3.6 Conclusion

The results discussed in this chapter have shown how striking is the effect of the low symmetry of the mercury structure on the deformation behaviour of single crystals. The orientation dependence of this behaviour has been investigated and three possible mechanisms are reported: slip, twinning and kink formation. Straight slip on the close packed $\{11\bar{1}\}$ planes occurs for the majority of orientations. That crystals in one standard stereographic triangle can slip on three different variants of the slip mode depending on their orientation has been confirmed. The c.r.s.s. is found

to vary by up to a factor of three with orientation, the minimum observed value being 17.5 gm mm.$^{-2}$. Twinning occurs on the irrational '{ I35 }' plane when the slip planes are lowly stressed. Two intersecting variants of this habit often occur with accommodation slip or kinks at the intersections. No conclusive evidence of a critical value of the r.s.s.t. has been found. Kink bands occur on { 1$\bar{1}$0 } planes being made up of an alignment of edge dislocations on adjacent slip planes. In general, the stress-strain curves confirm the operation of primary glide for large strains, a consequence of the large unit stereographic triangle of mercury.

Crystal	S1	S2	S3	S4	S5
Slip Variant	C	C	-	A	A
Twin Variant	-	-	a,a'	-	a'
$S_{A,B,C}$ (x 100)	45	24	09	32	26
c.r.s.s.	39.8	31.0	-	24.0	23.0
S_T (x 100)	-	-	31	-	41
r.s.s.t	-	-	200.0	-	66.0
Kink	-	-	-	$(1\bar{1}0)$	$(1\bar{1}0)$

Table 3.1 Deformation modes of square crystals.

Crystal	3	5	7	10	11	13	15	16	19	20	23	24
Slip Variant	A	A	B	-	B	A	A	A	A	B	A	A
Twin Variant	-	-	-	aa'	a'	a'	-	-	-	-	a'	-
Kink Variant	-	-	-	-	-	-	$1\bar{1}0$	-	-	-	$1\bar{1}0$	$1\bar{1}0$
$S_{A,B,C}$ (x 100)	43	40	10	12	14	17	29	44	29	14	18	35
c.r.s.s.	22.5	40.0	28.9	-	42.0	51.0	18.0	15.6	17.4	-	40.0	19.8
S_T (x 100)	-	-	-	35	20	37	-	-	-	-	35	-
r.s.s.t.	-	-	-	204.0	70.0	152.0	-	-	-	-	327.5	-

Table 3.2 Deformation modes of cylindrical crystals

Crystal	S3	C10	S5	C11	C13	C23
$S_{a'}$ (x 100)	36	35	41	20	37	35
$S_{A,B,C}$	09	12	24	14	17	18
$Sa'/S_{A,B,C}$	3.44	2.9	1.6	1.5	2.2	2.0
r.s.s.t.	200.0	203.7	66.0	66.1	152.0	327.5

Table 3.3 Summary of twinned crystals

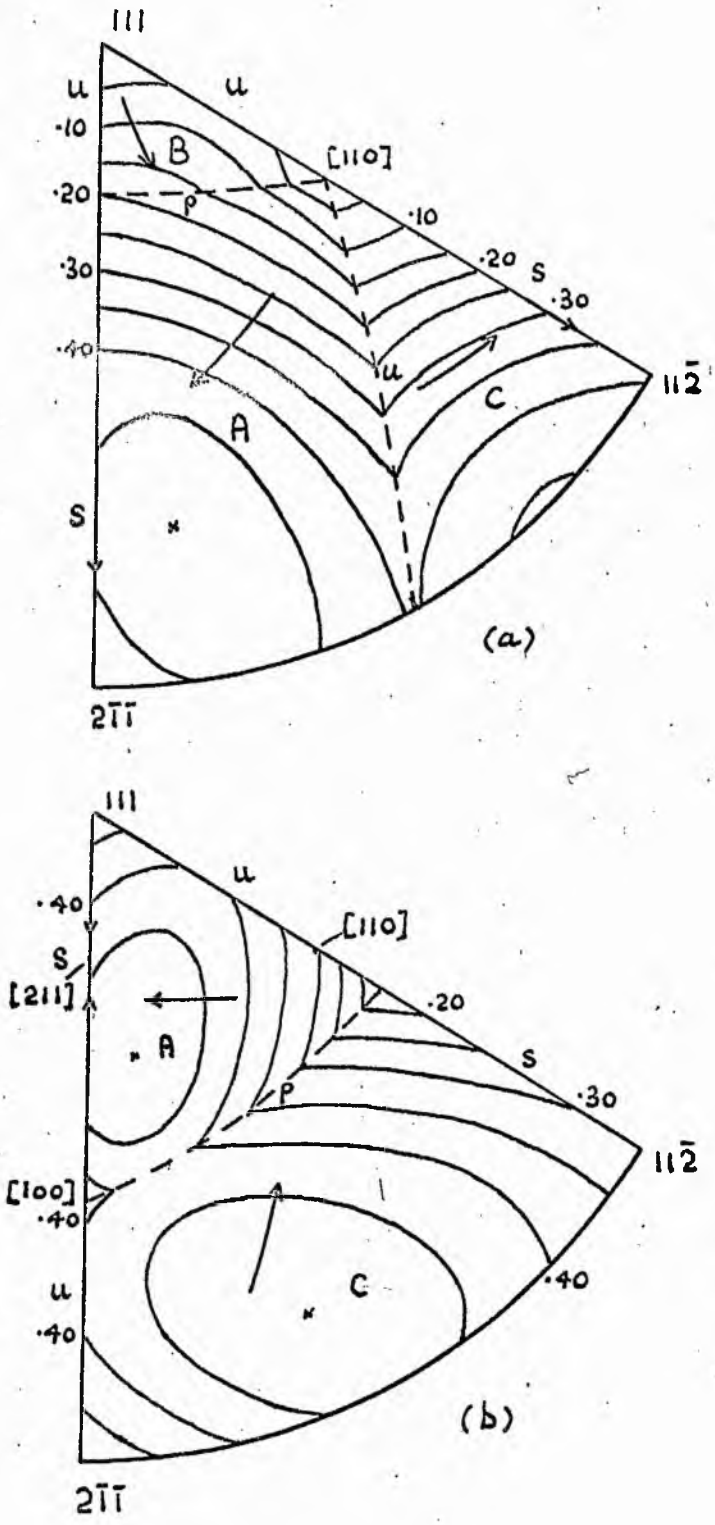

Fig. 3.1 Schmidt factor contours for slip on (a) $\{11\bar{1}\}\langle 1\bar{1}0\rangle$, and (b) $\{11\bar{1}\}\langle 011\rangle$. Lattice rotations and boundaries between different variants are indicated.

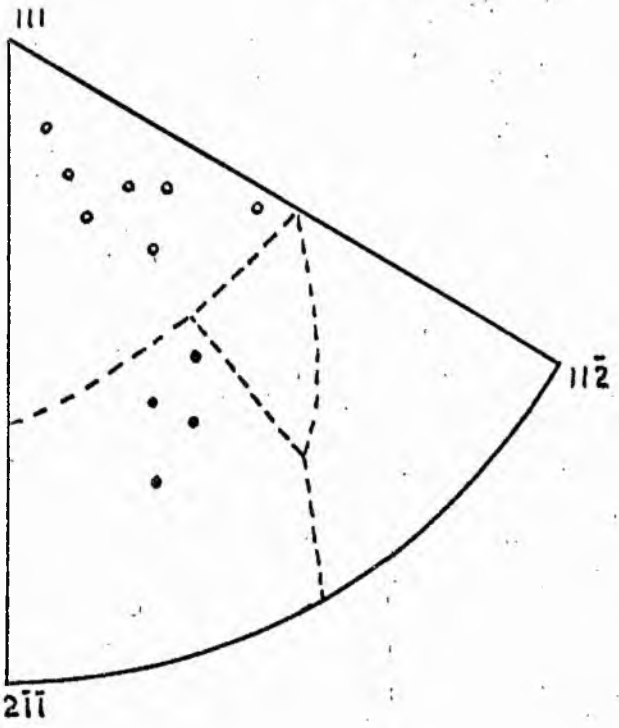

Fig. 3.2 Comparison of c.r.s.s. on the two slip modes with results of Rider and Heckscher at 200°K. Boundaries drawn assuming ratio of c.r.s.s. = 1.25. Closed circles slipped on {111}<1$\bar{1}$0>, open circles on {111}<101>.

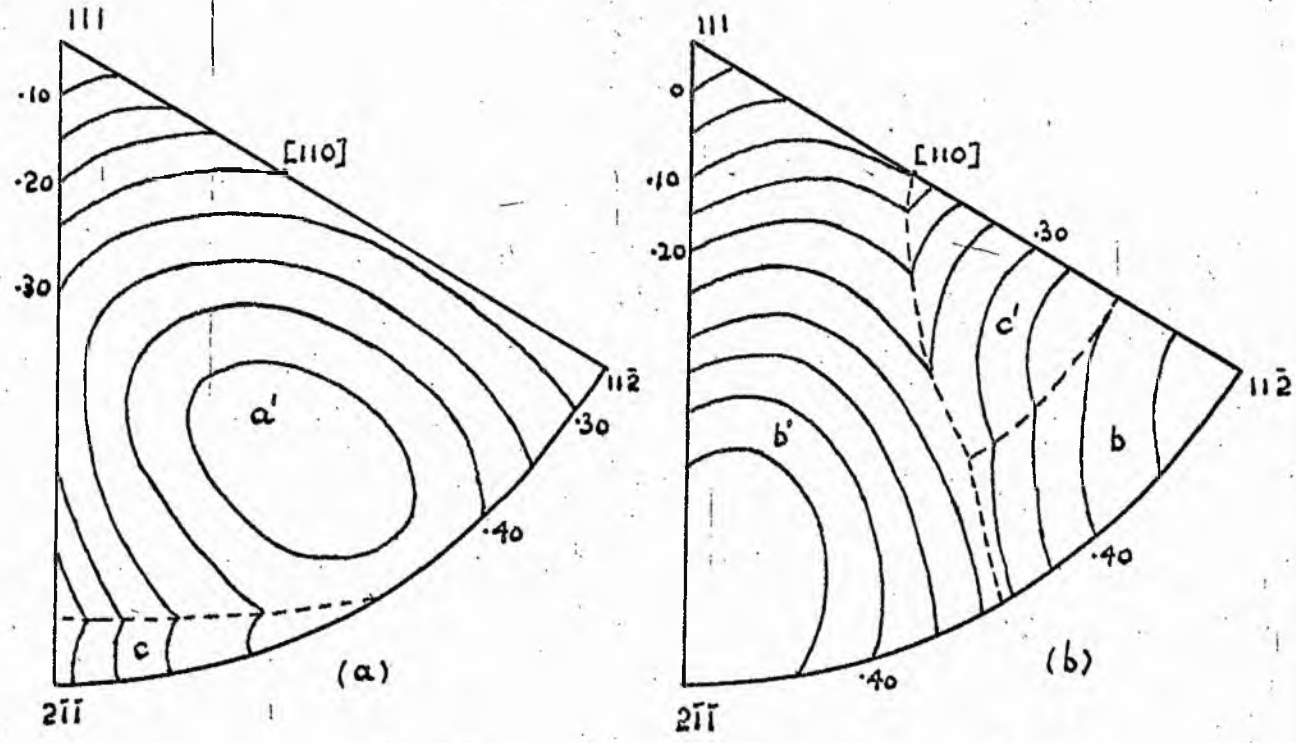

Fig. 3.3 Schmidt factor contours for twinning on '{$\bar{1}\bar{3}$5}'<$\bar{1}$21> in (a) tension, and (b) compression.

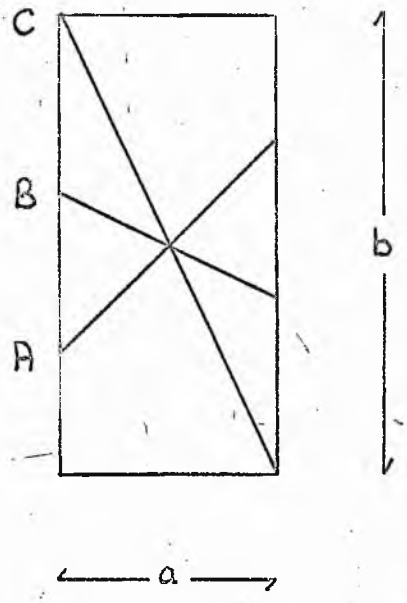

Fig. 3.4 Schematic representation of cylindrical crystal indicating three {111} slip planes.

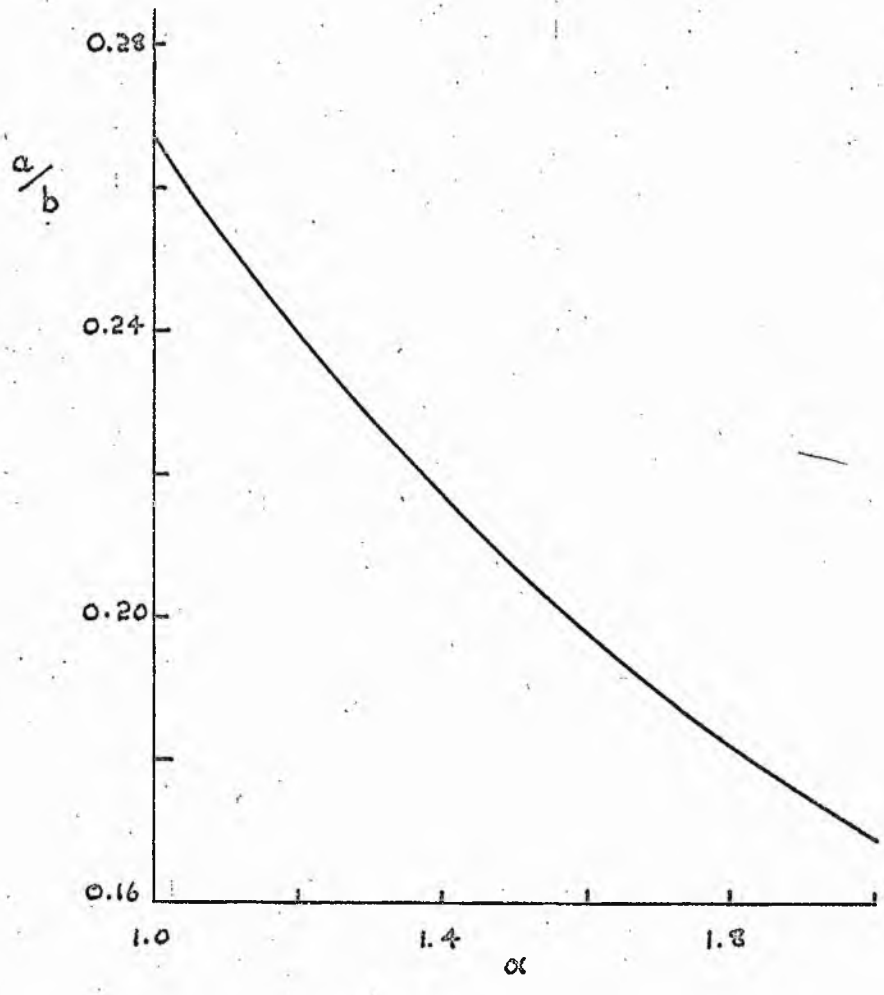

Fig. 3.5 Curve of a /b vs. α, the ratio of the c.r.s.s. on the slip planes C and A.

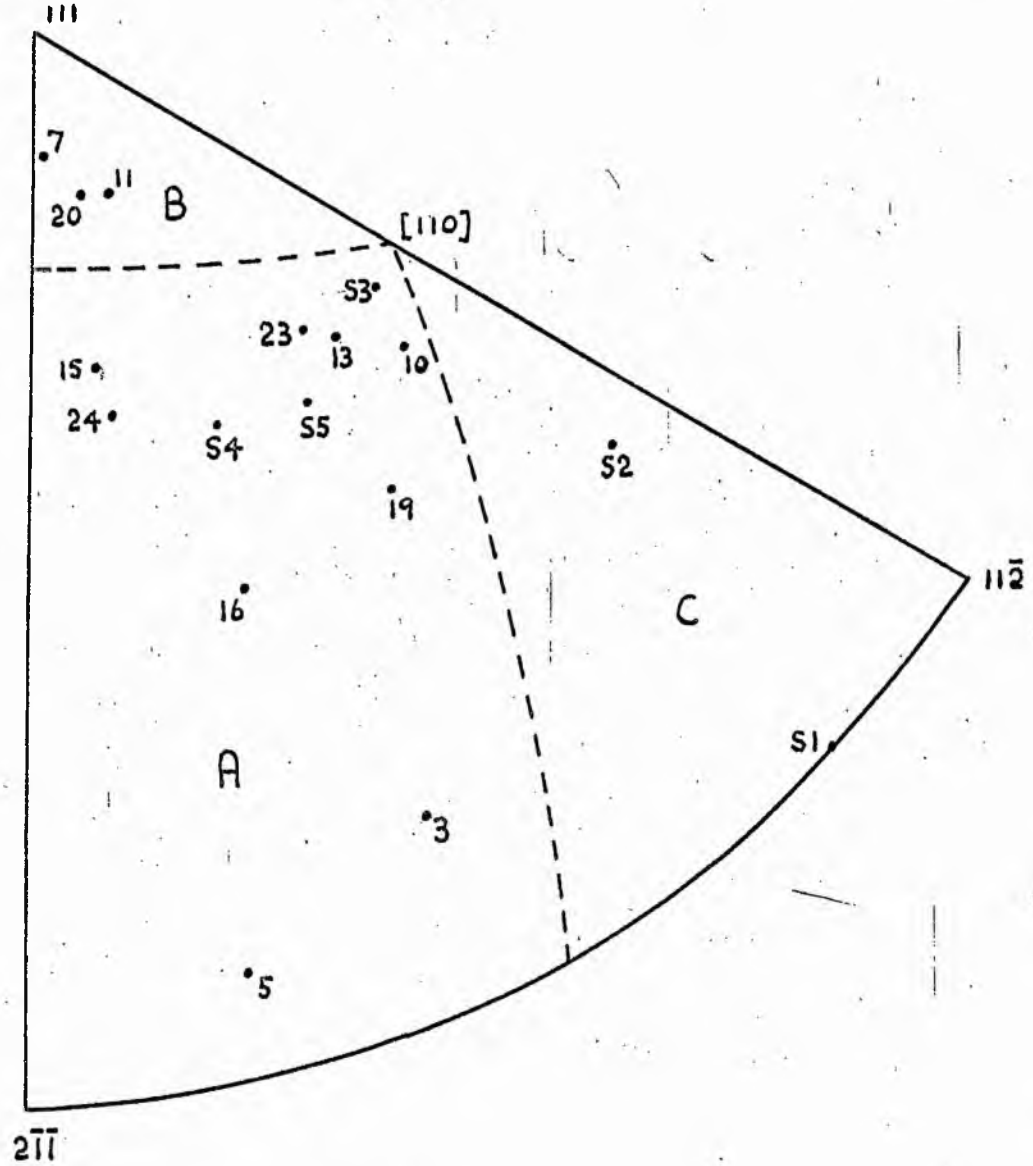

Fig 3.6 Orientations of crystals tested at 77°K.

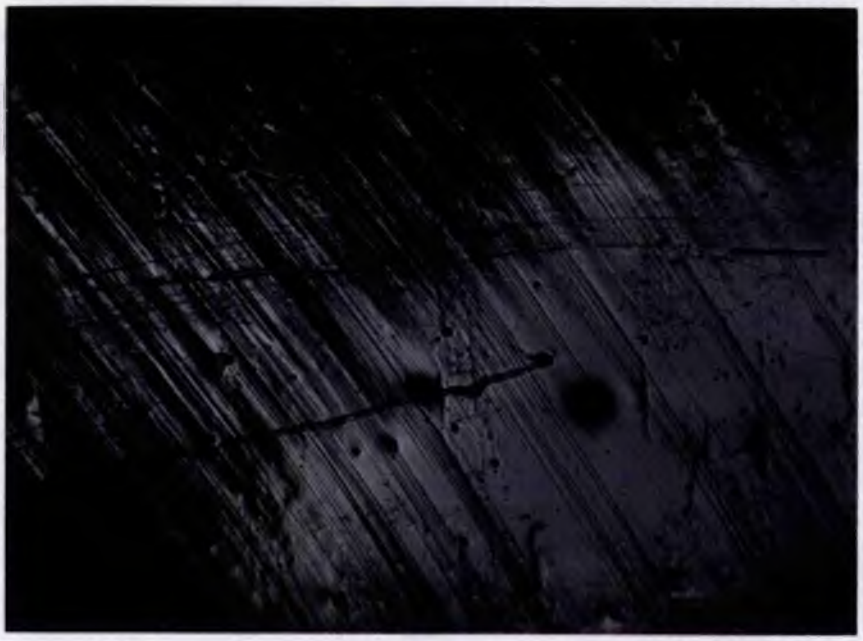

Fig. 3.7 Example of straight slip (x 80)

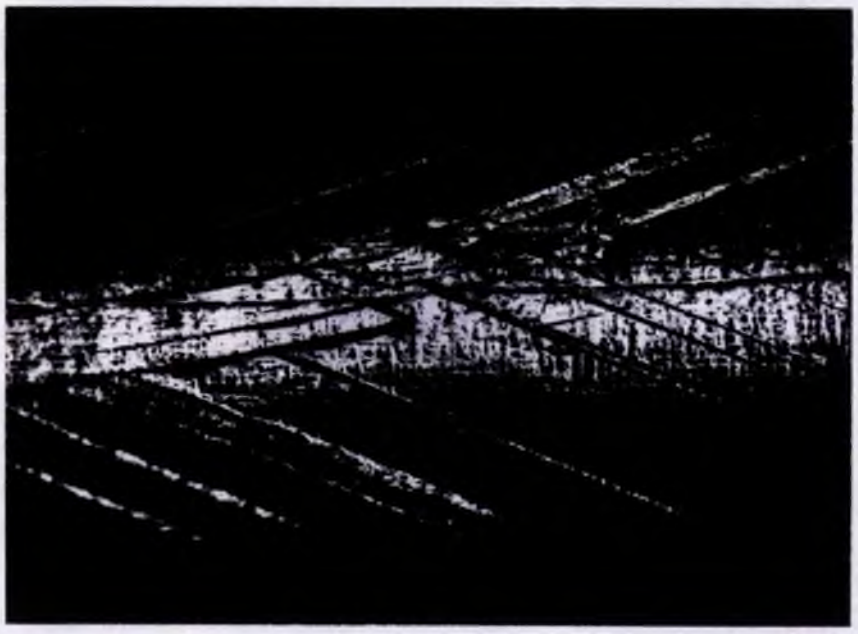

Fig. 3.8 Profuse twinning on a cylindrical crystal (x 40)

Fig. 3.9 Twin intersections and cross-twinning showing accommodation slip and kinks (x 80)

Fig. 3.10 Accommodation kinking at tip of twin (x 80)

Fig. 3.11 Slip lines sheared by a twin (x 150)

Fig. 3.12 Kink band on square crystal (x 80)

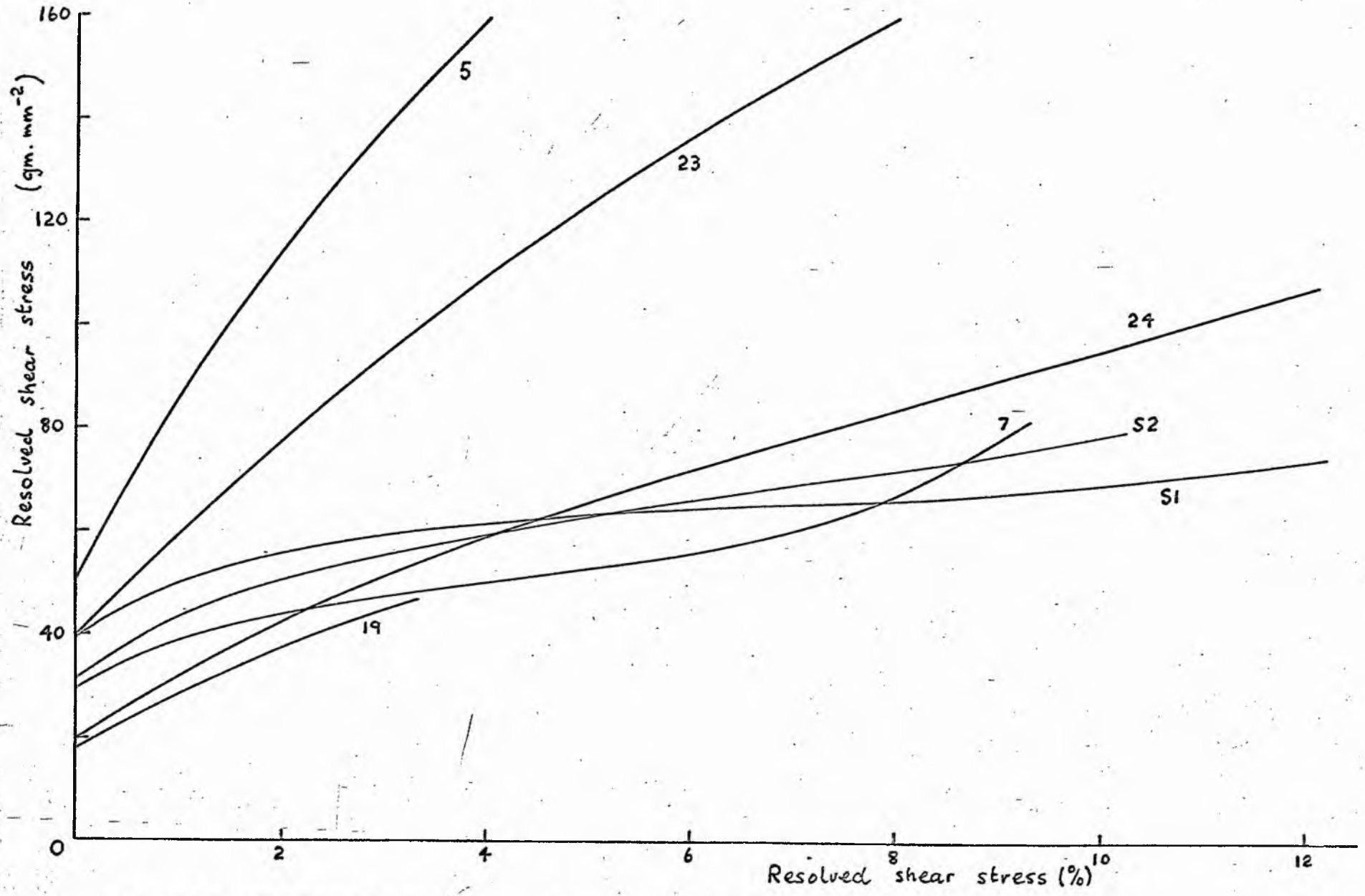

Fig. 3.13 Stress-strain curves of some crystals deformed at 77°K.

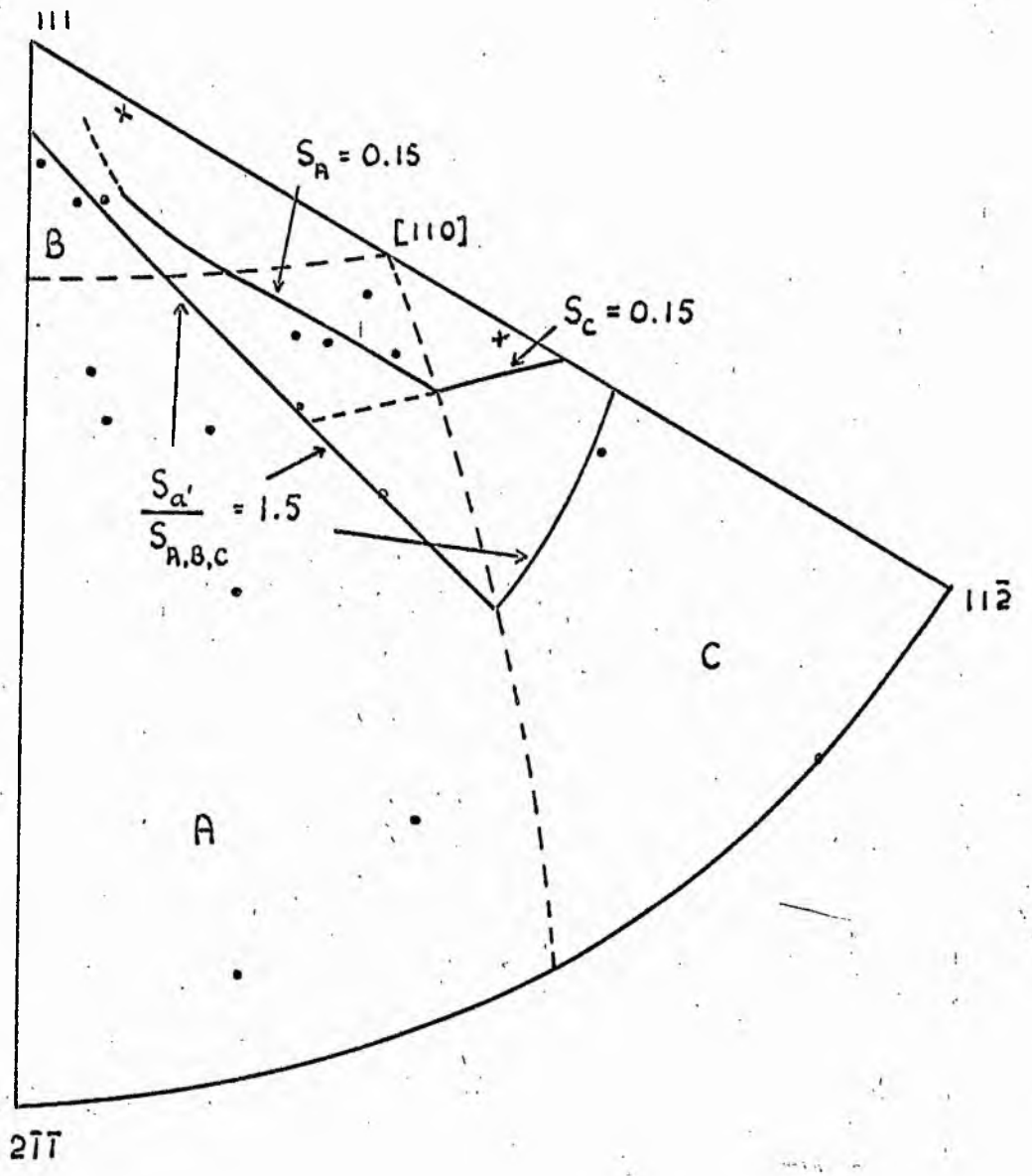

Fig. 3.14 Unit triangle subdivided according to deformation behaviour at 77°K.

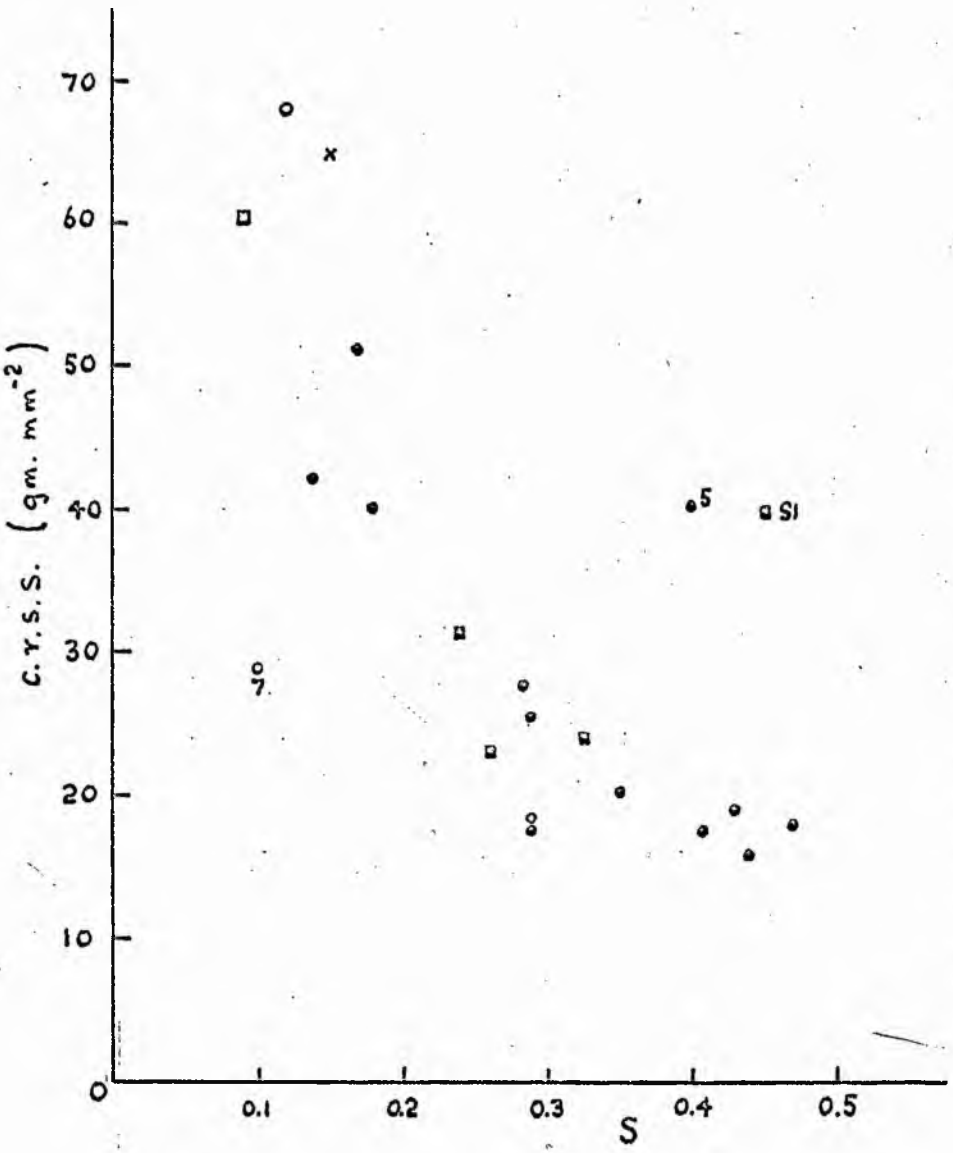

Fig. 3.15 The c.r.s.s. of crystals at 77°K plotted against the corresponding Schmidt factors.

CHAPTER IV - DEFORMATION AT 4.2°K - EVIDENCE OF THE γ-PHASE

4.1 Introduction

The remaining chapters of this thesis are concerned with the deformation behaviour of crystalline mercury at low temperatures, using liquid helium as the rerigerant. It has already been seen that lowering the temperature from 200°K to 77°K produces striking changes in the behavour of single crystals under applied stresses. It was therefore of particular interest that the operative range of temperatures should be extended to include deformation at 4.2°K.

Added impetus to this part of the work was given when some colleagues in this department reported evidence of a new phase change in mercury during the course of an investigation of the superconducting properties of various metals (Doidge and Eastham 1968a). Their results indicated a product of a different form to the second phase of mercury which had already been reported to occur under high pressure extrusion (Swenson 1958). Swenson found that, once produced, this phase was stable down to below 4.2°K. Thus, the situation with regard to the low temperature behaviour appeared rather confusing and, consequently, the experiments to be described seemed particularly relevant. It was hoped to correlate the behaviour of single crystals under applied stresses with the occurrence of a phase change and by so doing to elucidate the nature of the transformation concerned. This hope has been realised and an interpretation found in terms of the existence of a new phase of mercury. Subsequent metallographic

analysis has yielded information on the crystallography of the transformation.

Because of the reported occurrence of a β-phase of mercury, it seems appropriate to present here a summary of the relevant properties of this phase and the associated transformation, so that the results presented in this chapter can be discussed with reference to this product. This will be presented in the next section and the following sections illustrate two different techniques by means of which the existence of the third phase, γ, of mercury has been established. Preliminary metallographic observations on the transformation appear in section 4.5.

4.2 The β-Phase of Mercury

A solid state transition was first observed in mercury by Bridgman (1935). The production and properties of the second phase have been extensively studied and reported in a number of papers. The normal rhombohedral α-phase of mercury is stable to absolute zero under atmospheric pressures, but a transition to a product phase labelled β occurs at high pressures (Swenson 1958). In particular, a hydrostatic pressure of 5000 atmos. is required to initiate the transition at 4.2°K, and 10,000 atmos. for the transition to go to completion. It is found that 4000 atmos. is needed at 78°K for a complete transition even though the phase diagram indicates that at this temperature the β-phase should form spontaneously at zero pressure. Once formed, the β-phase is more stable than α-Hg below 79°K, is metastable between 79 and 90°K and

anneals rapidly and irreversibly to the α-phase above 90°K. The electrical resistance of α-Hg has been found to be approximately twice that of the β-phase (Schirber and Swenson 1959).

Both the α - and β - phases are superconductors and the critical fields of the two phases as functions of temperature and pressure have been measured (Schirber and Swenson 1961). The temperature dependence of the critical field is presented in Fig. 4.2 where curves from the α - and β - phases are indicated. Schirber and Swenson (1961) give the superconducting transition temperatures of the two phases as $T_{c\,\beta}$ = 3.949°K and $T_{c\,\alpha}$ = 4.153°K. β-Hg has been found to crystallise on a body-centred tetragonal lattice whose parameters measured at 77°K are a = 3.995 Å and c = 2.825 Å (Atoji et al. 1959). In a discussion of the nature of the α - β transition, Schirber and Swenson (1962) suggest that it has characteristics which can be explained qualitatively in terms of a martensitic behaviour. However, the application of a modified form of the Wechsler, Liebermann and Read (1953) theory of martensite crystallography was reported to be unsuccessful.

4.3 Superconducting Properties of Mercury Under Applied Stress

The possibility of the existence of a third phase of crystalline mercury has been suggested by the work of Doidge and Eastham (1968a). This section represents a summary of their results obtained on single and polycrystalline samples. During the course of an investigation of the effect of strain on the superconducting properties of various metals and alloys,

they found that their results on mercury could be interpreted in terms the occurrence of a new phase. These results are represented in Figs. 4.1 and 4.2. Fig. 4.1 shows a typical set of magnetisation curves in increasing field applied longitudinally to a mercury crystal held in the superconducting state at 2.1°K. The as-grown α-phase specimen shows the usual sharp transition for a Type I superconductor from the superconducting to the normal state at a critical field denoted $H_{c\alpha}$. After an increment of strain in tension in the cryostat, curve 2 is obtained showing that the magnetisation finally drops to zero at the same critical field $H_{c\alpha}$, but first deviates from the perfect diamagnetic associated with the superconducting state at a lower field. Upon progressively increasing the strain (curves 3 and 4) the transition at the lower field becomes more and more marked and always occurs at the same field. This lower field is denoted $H_{c\gamma}$ as it is believed that this transition corresponds to the new phase, γ, ceasing to be superconducting at a lower field than the original α-phase. The partial transformation to the γ-phase must have been induced by the applied tensile stress. After obtaining curve 4, where nearly all the transition appears to take place at $H_{c\gamma}$, the crystal was allowed to warm up to 77°K for 12 hours and then recooled to 2.1°K with no further deformation. The simple α-phase magnetisation curve 5 was again obtained.

Fig. 4.2 shows the critical field curve for the present transformation product plotted together with those for α - and β-Hg after Schirber and Swenson (1961) discussed in section 4.2. The different behaviour with temperature of this product

again demonstrates the distinct nature of the new phase. It should be noted that the α-phase critical field curve of Doidge and Eastham (1968b) agreed exactly with the one indicated in this diagram. Three distinct values for the zero field critical temperature derive from this data given by $T_{c\alpha} = 4.153^{\circ}K$, $T_{c\beta} = 3.949^{\circ}K$ and $T_{c\gamma} = 3.74 = 0.05^{\circ}K$. As the critical temperature of this product is less than that of either the α- or β-phases it may be concluded that it does not correspond to a mixed state of these two phases, since, if this were the case, $T_{c\gamma}$ would lie intermediate between these two values.

It thus appears that a stress-induced transformation occurs in Hg at $4.2^{\circ}K$ to a product structure exhibiting different properties to the low-temperature modification already reported. Independent confirmation of this transformation was sought by means of electrical resistance measurements on specimens strained at $4.2^{\circ}K$, the results of which are described in the following section.

4.4 Electrical Resistance Measurements

4.4.1 Introduction

As described in Chapter 1, the courses of diffusionless or martensitic phase changes can be readily followed by electrical resistance measurements as a function of temperature. A change in the scattering power of the electrons will in general result from a change in the lattice structure associated with the phase transformation. Previous workers who have measured the electrical resistance of both single

and polycrystalline samples of α-mercury have found continuous temperature dependence curves in the range $1^{o}K$ to $228^{o}K$ (Sckell 1930, Andrew 1949, Aleksandrov et al. 1967). Thus if an applied stress at $4.2^{o}K$ produces a phase transformation, a significant change in resistivity should be produced in addition to that due to the increase in dislocation density and that due to the change in size factor. More particularly, on subsequent warming, a discontinuity would be expected in an otherwise smooth resitance versus temperature curve corresponding to the temperature, M_r, of reversion from the new phase to the normal α-phase.

Further, if the phase transformation exists and is diffusionless or martensitic in character, a well-defined shape change on an otherwise flat surface of the specimen is always observed to occur. In some cases this surface tilt remains even when M_r has been exceeded, and even if this is not the case some surface marking is usually found to remain. Consequently, single crystal specimens of square cross-section were used in these experiments to enable naked eye observation of the surfaces while still at $4.2^{o}K$, and subsequent metallographic examination at higher temperatures to reveal the more detailed nature of the surface traces. The method of measuring the resistance as a function of rise in temperature was chosen to detect the transformation instead of measuring the resistance change with strain at $4.2^{o}K$. This obviated the necessity to correct for the change in size factor inherent in the second technique.

4.4.2 Experimental Procedure

Square cross-section single crystals approximately 8 cm. long were grown and oriented by the methods described in Chapter 2. After preparation in the manner also described in that chapter, current and potential leads of 18 S.W.G. enamelled copper wire were attached at either end of one face of the crystal leaving approximately 5 mm. at each end to be secured in the chucks. This ensured a specimen gauge length having an appreciable electrical resistance at 4.2°K of the order of 5×10^{-6} ohms. To ensure good electrical contact all that was required was to form a butt joint by allowing solder to run down the leads onto the cooled specimen. No prior tinning of the specimen was necessary and so virtually no damage was caused. Care was taken to minimise frosting of the surface as this did affect the efficiency of the bond. A copper-constantan thermocouple was attached in a similar manner to an adjacent face at one end to leave as much of the gauge length as possible free for the subsequent two surface analysis. In some cases a second thermocouple was affixed at the other end to enable any temperature gradients in the specimen to be recorded. The specimen was then mounted in the chucks as described in Chapter 2. This assembly was inserted vertically in a tensile jig, shown in Fig. 4.3, designed to fit into the inner dewar of a usual double concentric dewar system used in liquid helium temperature work. Since in these experiments the primary interest was in trying to relate the surface traces with the production of the new phase, measurement of stress using the tensile machine and load cell described in

Chapter 3 was considered unnecessary.

The jig was placed in a precooled double dewar system and liquid helium transferred until the whole specimen was immersed, the specimen being located at the bottom of the inner dewar. A constant current of about 1 amp was supplied by a stable d.c. current supply available in this department (Foxon and Selway 1966). The potential drop down the specimen and across a standard resistor were both measured on a Tinsley Diesselhorst potentiometer capable of measuring to better than 0.1 μV. A thermoelectric free reversing switch was included in the circuit, direct and reverse current readings being taken to eliminate thermal emfs. This measuring apparatus is fully described by Foxon (1965). To facilitate taking the temperature at the same time as the current and potential readings, the thermocouple emf was displayed on a chart recorder with an event marker. The full-scale deflection of the recorder was 1 mV and with the hot junction at 77^{o}K the maximum measured emf was 0.775 mV corresponding to 4.2^{o}K. To measure temperatures higher than 77^{o}K, the leads are of different polarity and only need switching over.

The experimental procedure adopted was to extend the specimen at 4.2^{o}K, estimating the strain from the pitch of the thread. Observation of the specimen surface was possible through the unsilvered strip in the double dewar system. The stress was relaxed and a set of readings recorded as the temperature rose. This rise was achieved by initially boiling off the helium until none was in contact with the jig, and then allowing thermal radiation produce a much slower rise in

temperature. On completion of the resistance measurements at approximately 100°K, the leads were removed and metallographic observations carried out at 77°K or between 150 and 200°K with the surfaces covered by ethyl alcohol to prevent frosting.

4.4.3 Results

Five square cross-section single crystals were successfully tested by the procedure described in section 4.4.2. The testing of these crystals was always accompanied by audible clicks or 'crying' similar to the behaviour usually associated with diffusionless processes such as phase transformations and mechanical twinning. Various macroscopic strains up to 15% were employed, anything higher being found unsuitable since the severe surface distortion made subsequent optical examination difficult. Fig. 4.4 shows a curve of resistance as a function of thermocouple emf in the range 4.2 to 100°K. All the curves have one feature in common - a discontinuity where the specimen resistance increases sharply over a comparatively small emf range, this range being the same for all specimens. Even though the calibration curve for the thermocouple is not linear in the range 4.2 to 100°K, it is a smooth continuous curve and so, when plotted against the corresponding temperature, any discontinuities in the resistance curves will be due to specimen behaviour.

The observed emf intervals have been converted to the corresponding temperatures, M_r, and are given in Table 4.1 together with the proportional reistance changes and the macroscopic strains. The discontinuity in all cases lies in the temperature range 49 - 56°K, and reference to the curves shows

that no further steps were observed up to 100°K. The size of the resistance step varies from specimen to specimen being a function of the amount of transformation achieved by the applied stress at 4.2°K.

4.4.4 Discussion

The sharp increase in resistance at a reproducible temperature described in section 4.4.3 can only be interpreted as corresponding to a transition from one crystal structure to another with an associated change in the periodicity of the lattice and hence its scattering power. We thus conclude that the normal α-phase of mercury is wholly or partially transformed to the new phase under the influence of the applied stress at 4.2°K and, once formed, this phase remains stable up to 49°K; it rapidly reverts directly back to the α-phase above 56°K with a corresponding increase in electrical resistance, and is regarded as being metastable between these temperatures. The justification of referring to the transformation product as a new γ-phase of mercury is thus further emphasized by this behaviour, since it contrasts directly with a similar property of the β-phase where the metastable region lies between 79 and 90°K.

These results are in agreement with the preliminary resistance measurements of Doidge and Eastham (1968a) where strains at 4.2°K of up to 30% were used. We can thus say that in the range of strains used up to 30%, the reversion temperature of the transformation appears to be independent of the applied strain at 4.2°K. The reproducibility of this discontinuity at the temperatures mentioned explains why curve 5

of Fig. 4.1 was obtained. The anneal at approximately 77°K exceeded the reversion temperature of the transformation and thus on subsequent cooling only the superconducting magnetisation curve for the α-phase was obtained.

In both the superconductivity and resistivity experiments the specimens have been subjected to very similar treatments prior to recording the various measurements which indicate the existence of the transformation; that is, they have been inserted in a jig at 77°K and cooled to 4.2°K and subsequently strained by varying amounts. Barrett (1957) has reported that the mere cooling of α-Hg down to 4.2°K produces no transformation detectable by X-ray diffraction and the present results certainly confirm this. Consequently the applied tensile stress is the controlling factor in initiating this transformation. Swenson (1958) reports that, once produced, the stable form for crystalline mercury below 79°K is the β-phase having a b.c.t. structure (Atoji et al. 1959). However, they found that to initiate the transformation at 4.2°K a pressure of at least 5000 atmos. was required and approximately 10,000 atmos. for it to go to completion. By comparison the experiments reported here show that a simple tensile stress is sufficient to initiate a transformation. The implied pressures of the present tests and those of the extrusion experiments to produce β-Hg are hardly comparable. This ease of production together with the other observed properties associated with this transition clearly indicate that it is not the previously observed $\alpha - \beta$ transition.

4.5 Preliminary Metallography

The occurrence of a phase transformation is invariably accompanied by the appearance of some kind of surface feature on the specimen. One of the particular characteristics of a diffusionless transformation is that it results in a well-defined surface shape change in such a way that a previously flat surface is tilted in the region of the transformation product, these regions usually occurring in the form of plates which can extend through the whole of the specimen. An examination of these restivity specimens of mercury was thus performed in an attempt to identify any striking surface features. As described in section 4.4.2 this examination was carried out between 150 and 200°K in cooled ethyl alcohol and it is worth noting that, to the naked eye at least, the morphology of the surfaces do not change at all during the rise in temperature from that of the test of 4.2°K to approximately 100°K. where the last resistance measurement is recorded, and subsequently to the observation temperature.

The surfaces of all five specimens were observed and on all of them the predominant markings were unlike any features seen on mercury crystals deformed at higher temperatures. These traces were similar to those seen on the superconductivity specimens; however, they could not be easily related to the appearance of those resistivity specimens of Doidge and Eastham which were examined, as much higher strains were employed in their experiments, the resultant distortion of the surface making an optical examination very difficult. The traces were straight and corresponded to regions where the surface

had been tilted, the sense of the tilt being discernible but not as easily as in the case of deformation twins in mercury. It was found that these traces usually extended through the whole of the cross-section of the specimen. Three of the crystals were chosen for a preliminary two-surface analysis because of the suitability of the surfaces and their features. This analysis, according to the procedure set out in sections 3.3.4, revealed characteristic slip lines on the close-packed $\{11\bar{1}\}$ planes on most of the specimens. The predominant unfamiliar traces were so analysed and tested for consistency with the already known deformation modes of α-Hg, that is slip, as described above, and twinning on the well-established irrational $\{\bar{1}35\}$ composition plane, both these modes being found at higher temperatures (See Chapter 3).

The new traces could not be interpreted in terms of either of these modes, but the poles of the traces did show a consistency among themselves. Ten sets of these traces on the three crystals were identified and they all appeared to lie near crystallographic planes of the type $\{\bar{1}13\}$ of the f.c.r. cell. Although only three crystals were examined in this way, these new surface traces were observed on all the resistivity specimens tested. The orientations of these crystal axes were fairly diverse but because of the size of the α-Hg unit triangle, all possible orientations could not be used in these experiments. However, what we can say is that all these crystals of various orientations tested in this way show the discontinuity in the resistance against temperature curves which is associated with the transformation, and exhibit identical

surface markings. In addition these features are similar to those observed by the author on the specimens used in the superconductivity experiments, a different technique which also demonstrates the existence of the transformation. Although these traces could be interpreted in terms of a completely new operative twinning mode, and this suggestion is discussed in more detail in the next chapter, it does seem more .. logical to associate them with the transformation and to suggest that they correspond to regions of the γ-phase in the α-phase matrix.

4.6 Conclusions

By reporting the results of experiments involving two independent techniques it has been demonstrated in this chapter that the normal α-phase of crystalline mercury undergoes a stress-induced transformation at 4.2°K to a product phase which appears to exhibit different properties to those of the previously reported modification of mercury labelled β. This new product is therefore called the γ-phase. Three points may be made to emphasize the distinction between the β- and γ-phases.

(a) at 4.2°K very high pressures are necessary to initiate the transformation from α- to β-Hg; γ-Hg is produced by a simple tensile stress.

(b) The zero-field critical temperatures for the two phases are significantly different being given by $T_{c\beta} = 3.949^{\circ}K$ and $T_{c\gamma} = 3.74 \pm 0.05^{\circ}K$ compared with the α-phase $T_{c\alpha} = 4.153^{\circ}K$.

(c) The β-Hg anneals back to the α-phase between 79 and 90°K; the reversion temperature for the α - γ transformation lies between 49 and 56°K.

The occurrence of a well-defined surface shape change on specimens undergoing the transformation suggests that the reaction is diffusionless or martensitic in nature. This view is supported by the audible clicks associated with the testing of crystals and the well-defined discontinuity in the resistance-temperature curves.

Detailed metallographic observations on the γ-phase of mercury are presented in the next chapter involving the determination of the shear elements associated with the transformation, and in Chapter 6 the application of the current theories of martensite crystallography to this transition will be considered.

Crystal	M_r °K	$(R_\alpha/R_\gamma)_{M_r}$	Strain %
3	55	1.20	7.5
4	50 - 54	1.25	12.0
5	50 - 56	1.33	15.0
6	49 - 55	1.26	14.0
7	49 - 54	1.26	13.5

Table 4.1 Resistivity Specimens tested in tension at 4.2°K

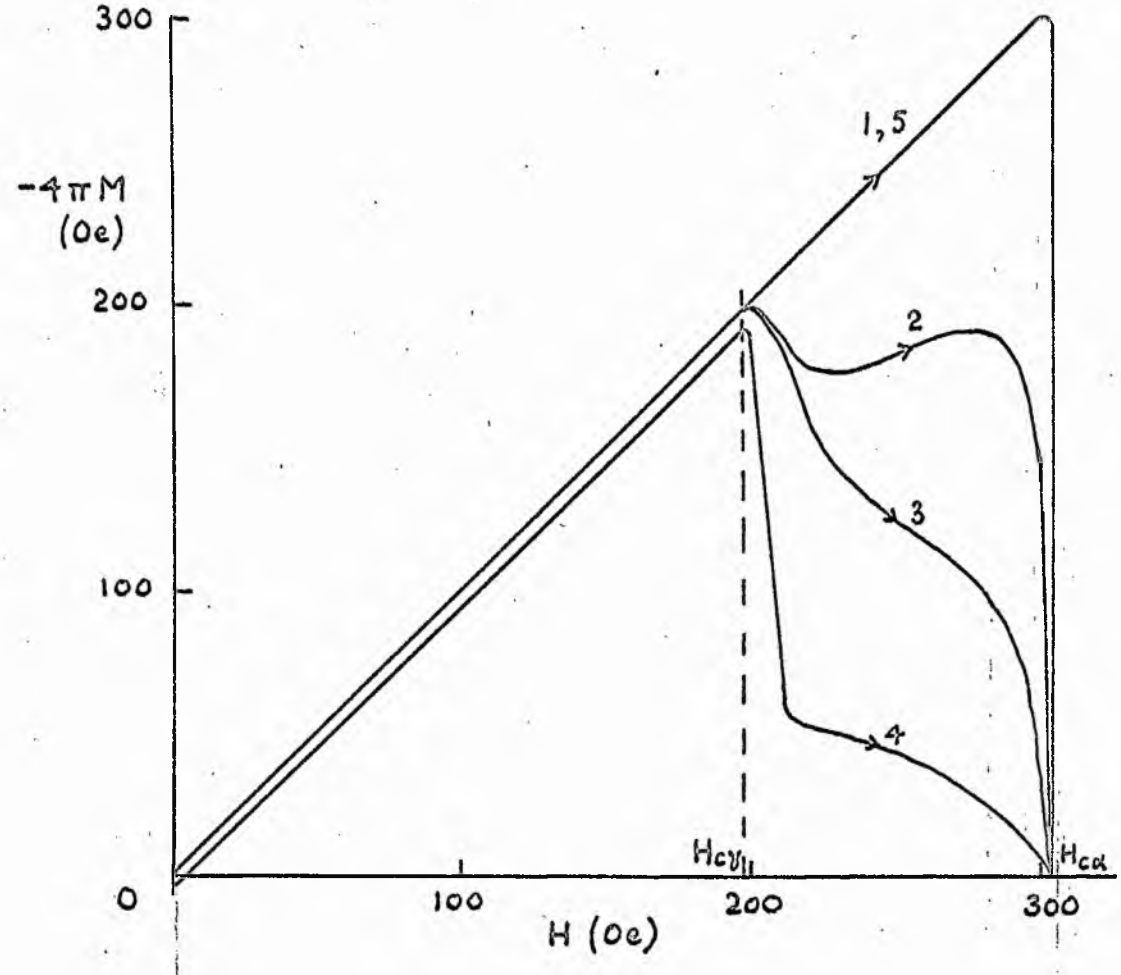

Fig. 4.1 Superconducting magnetisation curves of a mercury crystal after increments of strain taken at 2.1°K.

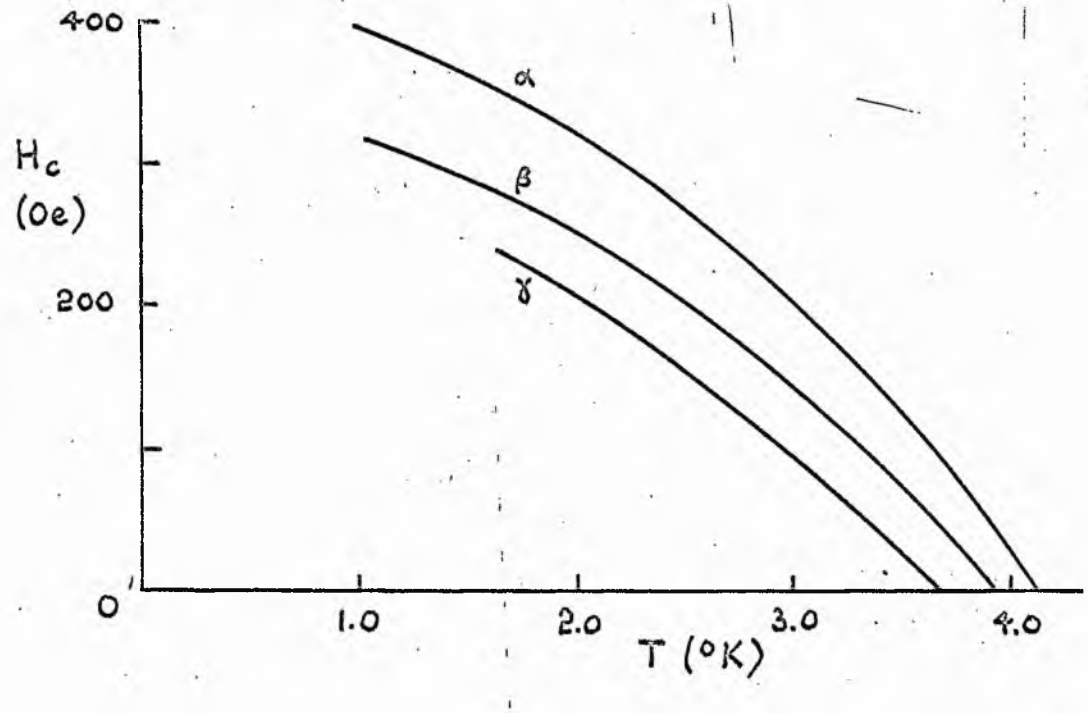

Fig 4.2 Variation of critical field with temperature for the three phases of mercury.

Fig. 4.3 Tensile jig used in experiments at 4.2°K.

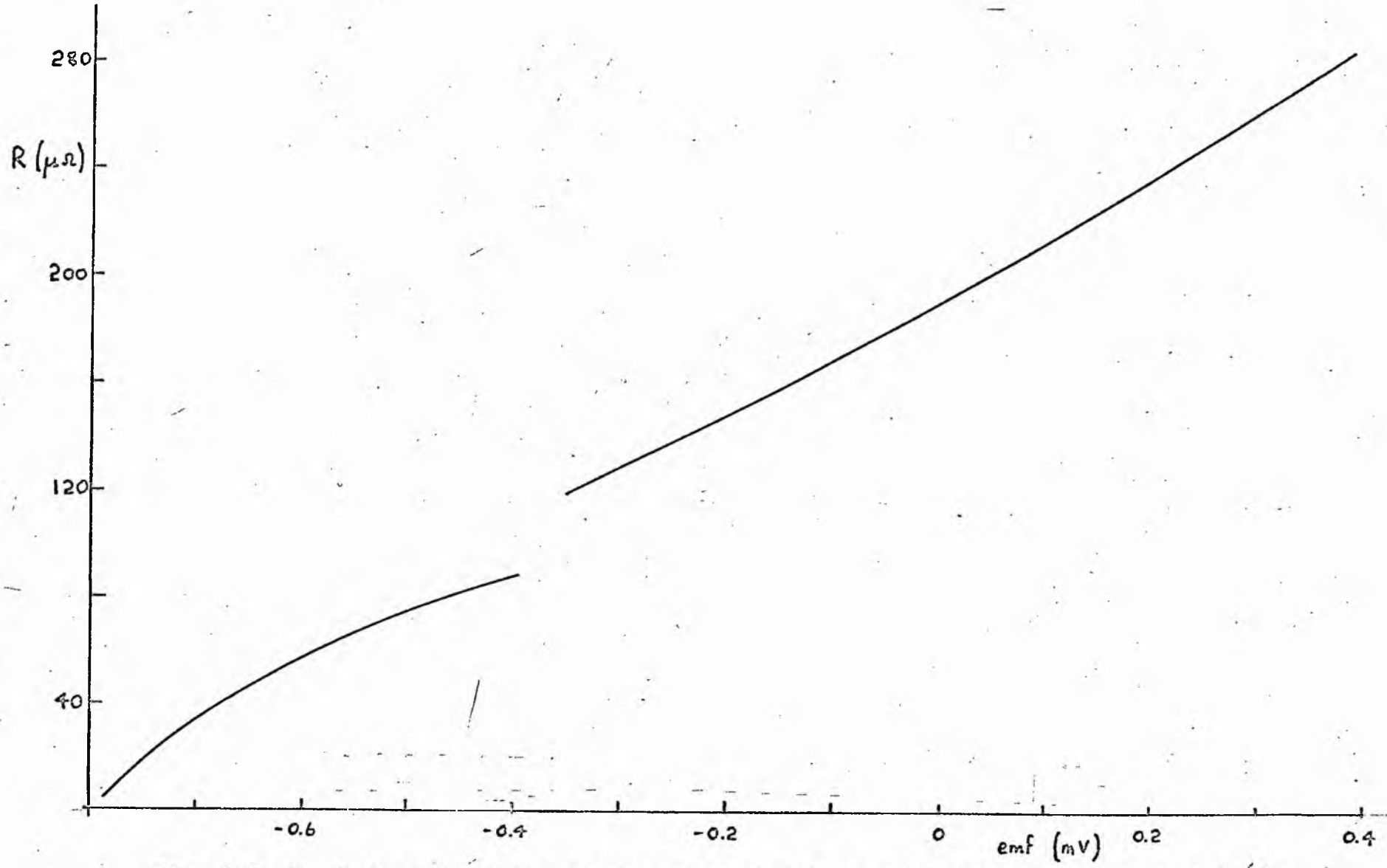

Fig. 4.4 Typical resistance - thermocouple emf curve of a crystal deformed at 4.2°K.

CHAPTER 5 - METALLOGRAPHY OF THE γ -PHASE

5.1 Introduction

The results presented in the last chapter clearly indicate that the normal α-phase of mercury undergoes a stress induced transformation at 4.2°K. It has further been suggested that the nature of the transformation and the properties of the product show that this observed transition is distinct from the previously reported α - β transformation. It is thus assumed for convenience in this chapter that the product is a different low-temperature modification and will be referred to as the γ -phase. In fact, the validity of this assumption does not affect the results to be described in this chapter. Irrespective of the nature of the product, the occurrence of this transformation in single crystal specimens offers a unique opportunity of investigating the crystallographic features associated with the transformation. This is in contrast to the reported work concerning the β -phase where no such observations were possible. Consequently, the metallographic results presented here refer to the stress-induced phase transition occurring in the α-phase of mercury at 4.2°K, the product of which is believed to be a distinct third phase of crystalline mercury.

The observation of a well-defined surface shape change, as described in section 4.5, demonstrates the existence of a macroscopic shear process associated with the transformation. The occurrence of such a shear process demands the determination

of the associated shear elements, that is the habit plane, shear direction and shear strain magnitude. The results of section 4.5 showed that, in general, the transformed regions extended through the whole of a specimen. This simplified to some extent the identification of the shear elements, but it was also noted in that section that the surface tilts would be rather more difficult to measure than, for instance, those for twins in mercury.

Square and circular cross-section single crystals grown and prepared by the methods of Chapter 2, were used in this part of the work. The tensile jig of Fig. 4.3 was again employed to induce the transformation at 4.2°K, and the trace analysis performed as described in section 3.3.4. The additional experimental technique used in this work was a method of measuring the surface tilts of the transformed regions. The technique employed has been described by Guyoncourt and Crocker (1968) and involves the use of an optical goniometer whose plane of rotation is mounted vertically. The angle between strong parent and product reflections then gives the surface tilt associated with the transformed region.

The results of the determination of the shear elements are presented in the next section with a discussion of the morphology of the occurrence of the γ -phase. Other aspects of these metallographic observations are described in the remainder of this chapter. Section 5.3 is concerned with the orientation dependence of the occurrence of the transformation in single crystals and an interpretation is found by regarding the shear process associated with the transformation as a

conventional deformation mode. A discussion of the results appears in section 5.4,

5.2 Results - Crystallography

5.2.1 General Features

Twenty three single crystals were tested by the procedures mentioned in section 5.1. Five of these were cylindrical specimens, the remainder having square cross-section The orientations of the axes are shown in the unit stereographic triangle of mercury in Fig. 5.1 where it can be seen that most of the triangle has been investigated. The prefices S and C in the figure refer to square and circular crystals respectively. The test temperature for all these crystals was 4.2°K and the mode of testing tension. Apart from six square crystals, the specimens were found to be soft on testing.

The rise in temperature necessary for the subsequent metallographic observation of the surfaces again appeared to have no effect on the morphology of the features. On fourteen crystals, the predominant surface markings were those which, as discussed in Chapter 4, have been associated with regions of the γ-phase. On many of these, straight slip lines were also observed. All these specimens had been observed to 'cry' or click on straining at 4.2°K. Three other specimens which exhibited audible clicks did not have any such traces, but in these cases profuse twinning, having similar morphology to twins found at 77°K, had occurred. Slip lines characteristic of specimens deformed at 77°K were observed on the remaining crystals, together with, in some cases, kink bands. No trans-

formation traces were seen on these crystals.

Thus the three main types of different surface morphology enable the specimens to be grouped according to their behaviour By correlating the orientation of the crystals with this behaviour, an orientation dependence for the occurrence of these different surface features becomes apparent and the unit stereographic triangle may then be subdivided according to this dependence. The result of this is shown in Fig. 5.1 where the broken lines indicate empirical boundaries between regions of differing behaviour. Thus, crystals with axes in the central regions of this triangle exhibited slip and twin traces typical of crystals tested at 77°K. In the figure these regions are labelled S and T respectively. In the remainder of the triangle, labelled M_1 and M_2, the traces corresponding to the transformation were predominant although some slip lines were also observed. Of the six specimens found to be hard on testing, three had orientations in region M_2 of the triangle, while the other three defined region T of this triangle.

Examples of slip and twinning in the crystals are shown in Figs. 5.2 and 5.3. It can be seen that the general appearance of these features is similar to that observed at 77°K and discussed in Chapter 3. The slip lines are straight and evenly spaced indicating a more homogeneous deformation than occurs at 77°K where bands of slip lines were more common. Twins on two variants occurred on all the crystals that twinned and the usual intersections with accommodation slip are clearly seen in Fig. 5.3

The general appearance of a transformed crystal is shown in Fig. 5.4 where it is clear that regions of γ-Hg form on two habit planes. The preliminary results of section 4.5 indicated that these were two variants of one crystallographic plane. This deduction was found to be valid as will be described in the next section. A higher magnification micrograph of the same crystal is shown as Fig. 5.5 where intersections between transformed region are clear. Shearing of the slip lines by the γ -Hg regions is also seen, demonstrating the existence of the shear process associated with the transformation. The regions of product structure of a transformation are often referred to as plates. In this case, the plates of γ -Hg usually occur in pairs, these pairs always intersecting at an obtuse angle as typified by Fig. 5.6 of a circular cross-section crystal. Acute-angled intersections have never been observed, and indeed appear to be actually avoided as shown in Fig. 5.7. Fig. 5.8 shows a series of intersections between two plates which appear to successively reduce the thickness of the large plate in a well-defined manner. The occurrence of the γ -Hg on two habits often gives the surface an appearance similar to that observed when cross-slip occurs in other metals. There is evidence of this in the micrographs 5.5 - 5.8. The plates of γ -Hg usually occur in bands and are often inhomogeneously distributed within these bands as in Fig. 5.6.

The result of a two-surface analysis of the slip lines both of specimens in regions S and T of Fig. 5.1 and on those exhibiting the γ -Hg plates as predominant markings, showed that slip had occurred on the close-packed $\{111\}$ planes.

This was confirmed by the circumferential analysis of the cylindrical crystals which, further, fixed the operative shear direction as the second closest-packed direction $\langle 1\bar{1}0 \rangle$. This is the predominant slip mode found at 77°K and described in Chapter 3. Similar analysis of the twin traces showed that the composition plane of the twinning process was identical to that occurring at the higher temperature, namely the irrational '$\{\bar{1}35\}$' type plane. The sense of the surface tilts of these twins was consistent with the previously observed shear direction $\langle \bar{1}21 \rangle$.

The transformation traces were subsequently analysed but in rather more detail to obtain the full shear elements associated with the transformation. Perhaps the easiest feature to determine in association with these traces is the habit plane of the shear process giving rise to them. The result of this determination is given in the next section and the following sections describe the identification of the remaining elements of the transformation shear process.

5.2.2 Habit Plane

Ten square and four circular crystals which exhibited transformation traces as predominant markings were analysed. On most of these more than one set of such traces were observed, pairs of intersecting traces, as described in section 5.2.1, being the most frequent morphology. Consequently the poles of sixteen traces were identified, and after compensating for the rotation of the traces due to the applied strain (Cullity 1956), the poles were plotted such that they could be

illustrated in one unit stereographic triangle. A part of this triangle appears in Fig. 5.9. It is clear that the experimentally observed poles are clustered near the $(31\bar{1})$ pole and in no case are the traces more than 5^{o} from this crystallographic plane. It is worth reporting at this stage that when the particular variants of this habit plane that operate in pairs are noted, a system becomes apparent. Thus, three distinct pairs of variants arise: $(\bar{1}13)$ and $(1\bar{1}3)$ occur together as a pair, as do the other variants obtained by rotating these indices orderly.

5.2.3 Shear Direction

A more detailed circumferential analysis of the traces on the four circular crystals was performed to identify the macroscopic shear direction associated with the transformation process by the method described in section 3.3.4. Seven such identifications were made and are again represented stereographically in Fig. 5.9. Although the nature of these measurements does not allow as great an accuracy in this determination as in that of the habit plane, the poles of the shear directions correspond very closely to the close-packed direction $[110]$ of the α-structure. The traces on crystal C1 did not permit a full circumferential analysis so the shear direction could not be determined unequivocally but the measurements were consistent with the results presented in this figure. However, determination of the sense of the operative shear direction from the sense of the surface tilts of these traces does indicate that it is such that the habit plane denoted $(\bar{1}13)$ is sheared in the $[\bar{1}\bar{1}0]$ direction.

5.2.4 Shear Strain Magnitude

Three square cross-section crystals, having in all six sets of transformation traces were chosen as suitable for surface tilt measurements. The orientations of these crystals lay in the region M_1 of the stereographic triangle. The metallographic measurements were then processed by two methods. (Guyoncourt and Crocker 1968), one stereographic, the other algebraic to determine the magnitude of the shear strain associated with the transformation. The results obtained are shown in Table 5.1. In general there is close agreement between the values obtained by the two methods, the average value for the stereographic method being 0.49 and that for the algebraic method 0.47. The algebraic value will be the more accurate since the only error arises from the experimental measurements, whereas the stereographic method can involve procedural inaccuracies.

These measurements also enabled the operative shear direction to be checked during the course of the stereographic determination of the shear strain. The results are shown in Table 5.1 where deviations from $\langle \bar{1}\bar{1}0 \rangle$ of the experimentally observed shear directions associated with these traces are given. The negative sense and the nearness to $\langle \bar{1}\bar{1}0 \rangle$ of the operative shear direction are again demonstrated. Although only three square crystals were examined in this way to yield the operative shear direction, it may be added that on the remaining square crystals, the sense of the surface tilts on all but three crystals were consistent with the operative shear direction being in a negative sense. The three exceptions had

orientations lying in region M_2 of the unit triangle. They will be discussed in more detail in section 5.3.

5.2.5 Crystallography of the Transformation Shear Mode

There are six variants of the crystallographic plane $\{\bar{1}13\}$, one of which lies in each of the six unit triangles of the $[111]$ projection of Appendix I. However, there are only three variants of the close-packed direction $\langle\bar{1}\bar{1}0\rangle$ as can be seen in this projection. Thus, each close-packed direction lies in two variants of this plane. If the habit plane of the transformation is assumed to be exactly this crystallographic plane, then the occurrence of plates of γ-Hg in pairs is readily explained. The two operative variants of the $\{\bar{1}13\}$ habit plane are those containing a common $\langle\bar{1}\bar{1}0\rangle$ shear direction. This is in agreement with the observation of section 5.2.2 on the habit plane of the transformation, where the specific variants occurring as a pair were noted as being of the type $(\bar{1}13)$ and $(1\bar{1}3)$ and are those containing a common $\langle\bar{1}\bar{1}0\rangle$ direction.

The lack of any accommodation affects at the intersection in the surface is further indication of the ease of self-accommodation of this pair of traces. Thus, if the habit plane is the crystallographic $\{\bar{1}13\}$ plane, then the most likely interpretation is that the associated shear direction is the close-packed direction $\langle\bar{1}\bar{1}0\rangle$. It was also noted in section 5.2.1., that the two habit plane variants were never observed to meet at acute angles; indeed it appeared that such intersections were actually avoided, as is clear in Fig. 5.7.

The reason for this now becomes apparent. Reference to Fig. 5.10 shows that such an intersection involving the accommodation of opposite shears would be extremely difficult without the occurrence of the usual accommodation effects, such as are observed at complementary twin intersections in mercury. Diagram (a) shows an obtuse intersection of two plates and a section through AB shows the surface appearence. The two plates are readily accommodated. (b) shows a hypothetical acute intersection where kinking of the surface is necessary to accommodate the two plates.

The occurrence of the habits in pairs provides a convenient notation scheme for the crystallographic variants. Thus, the habit planes $(3\bar{1}1)$ and $(31\bar{1})$ are denoted as L and L' respectively and their common shear direction $[0\bar{1}\bar{1}]$ is labelled 1. Similarly the pair of planes $(\bar{1}13)$ and $(1\bar{1}3)$, and the pair $(13\bar{1})$ and $(\bar{1}31)$ with corresponding shear directions $[\bar{1}\bar{1}0]$ and $[\bar{1}0\bar{1}]$ are represented by the letters M, M', N, N' and m, n. Modes such as L1 and L'1 which occur as a pair, we term complementary modes. The positions of these planes and directions in the standard $[111]$ projection together with a summary of the notation is to be found in Appendix I.

5.2.6 Summary

In section 5.2 it has been established experimentally that the habit plane of the transformation shear process lies within 5° of the crystallographic plane $\{\bar{1}13\}$ of the f.c.r. unit cell of α-mercury. Almost invariably the operative macroscopic shear direction in this plane is $\langle\bar{1}\bar{1}0\rangle$, the

closest-packed direction of this cell. The occurrence of the plates of γ-Hg on two intersecting variants of the habit plane has been explained in terms of the crystallography of this direction. The associated shear strain magnitude has been measured as 0.47 $\pm$ 10%. The occurrence of the transformation in single crystals appears to be orientation dependent; crystals not exhibiting the transformation deform by the modes previously observed at 77°K.

5.3 Results - Orientation Dependence

5.3.1 Introduction

The orientations of the axes of all the crystals tested in association with the $\alpha - \gamma$ transformation have been collected together in Fig. 5.11. In this figure the prefix p refers to these specimens discussed in Chapter 4, whose resistance was measured as a function of temperature, and C and S to the circular and square specimens respectively. A correlation between orientation of specimens and the crystallography of the transformation yields a systematic orientation dependence confirming that of section 5.2.1 inferred from the surface morphology of several specimens.

Crystals with axes in regions S and T of Fig. 5.1 of the triangle deformed by $\{111\}$ slip and '$\{\bar{1}35\}$' twinning processes typical of crystals tested at 77°K and yielded no indication that the transformation had occurred. In region M_1 the transformation appeared to occur easily. The existence of the product phase for specimens in this region was demonstrated by either one or both of the two observed features:

a discontinuity in the resistance-temperature curve, or the appearence of the surface traces corresponding to the well-defined shape deformation having the $\{\bar{1}13\}$ habit plane. Three of the crystals found to be hard on testing in section 5.2.1 help to define the second region M_2, in which the transformation appeared to occur, apparently less easily than in region M_1. No resistivity specimens had orientations in this region, and so this deduction is made from the morphology of the traces and the occurrence of the $\{\bar{1}13\}$ habit. Thus the orientation dependence serves to explain why all the resistivity specimens did in fact show the discontinuity in the resistance-temperature curves and the associated audible clicks; their orientation was such that the transformation could easily occur. In this respect it is perhaps unfortunate that a crystal of the 'wrong' orientation was not tested in this series of experiments to demonstrate that the discontinuity would not always occur. The single crystals grown for the superconductivity experiments were not oriented before testing and thus cannot be related to this scheme.

A quantitative appraisal of the differing behaviour of the single crystals tested can be found by regarding the transformation shear process as a conventional deformation mode for mercury at these low temperatures. The behaviour can then be analysed in terms of the relative Schmidt factors of the various possible modes for any particular crystal orientation. In the next three sections the regions in the unit stereographic triangle will be considered separately and the results interpreted in this way.

5.3.2 Region M_1

For the purpose of this discussion it is assumed that the habit plane and shear direction of the transformation are the crystallographic $\{\bar{1}13\}$ plane and $\langle\bar{1}\bar{1}0\rangle$ direction. If this mode is correct and we consider it as a conventional deformation mode, the variant which occurs in practice should have a relatively high resolved shear stress. This is conveniently indicated by means of the Schmidt Factor S_M. For the six crystallographically equivalent variants of the $\{\bar{1}13\}$ $\langle\bar{1}\bar{1}0\rangle$ shear system for each of the fourteen crystals examined in this region, the values of S_M are given in Table 5.2. Since the observations in this region indicate that the process is uni-directional, the sign of these Schmidt factors is significant and for the present tension tests, only variants with positive values should occur. Examination of Table 5.2 now indicates that for each crystal, four or five, and in some cases six transformation habits have favourable Schmidt factors and in each case, one of these, indicated in the [illegible] row, is in fact the predominant operative mode. Indeed, for all the crystals, the predominant mode is the one with the largest positive factor. This result provides striking additional verification of the $\{\bar{1}13\}\langle\bar{1}\bar{1}0\rangle$ shear process.

As has been discussed in section 5.2, the transformation habits frequently occur in pairs, thus facilitating the accommodation of the regions of γ-mercury in the α-phase matrix. The second of the habits operative in this way is determined by the shear direction common to both habits and so the transformation shear process tends to occur on pairs of

habits even where the resolved shear stress on the second system is unfavourable. For example, in crystal S5 of Table 5.2 the second system L occurs in preference to M which has a higher Schmidt factor because L', having the highest factor, is operative and L and L' possess a common shear direction as discussed in section 5.2.5.

Closer examination of the Schmidt factors for crystal S8 proves particularly interesting in connection with the consequences of this special crystallographic relationship of two paired variants. Modes L and L' occur as might be expected. However, the pair of habits M and M' are also operative even though another mode N' is over five times more highly stressed than M'. A possible reason for this can be found by noting that the Schmidt factor for mode N, the complementary mode to N', is in fact negative and thus cannot be operative in tension. This fact, therefore, appears to prohibit not only the operation of mode N but also of the complementary mode N' although this is favourably stressed. This implies that the pair morphology facilitates the accommodation of the plates of γ-Hg more readily than the occurrence of a single variant, and consequently if a pair is prevented from forming as in this case, another pair may be operative even though one of the pair is relatively lowly stressed.

It is clear from the results in Table 5.2 that the assumption that the transformation composition plane and associated macroscopic shear direction can be regarded as a conventional deformation mode for mercury at this low temperature is justified. On this basis the Schmidt factors of this shear

process have been compared with those of other possible modes for these crystals. In particular slip has been considered since on some crystals this has been observed to occur as a secondary mode, and especially with reference to crystal C1 where slip was in fact predominant. Table 5.3 shows the result of this comparison. The values S_s are the Schmidt factors of the most highly stressed slip mode and S_M those of the most highly stressed $\{\bar{1}13\}\langle\bar{1}\bar{1}0\rangle$ mode, only those which could be operative in tension being considered. The ratio of these values together with the observed modes make up the rest of the table, the predominant mode being underlined.

The ratio R of the factors for the slip and transformation processes indicate that the predominant mode is that which is most highly stressed. Moreover, the results lead to the suggestion that the c.r.s.s. for the $\{\bar{1}13\}\langle\bar{1}\bar{1}0\rangle$ mode is lower than that for slip. Two crystals, p2 and p6, whose orientations have been shown in Fig. 5.11, were not included in Table 5.2 since a full metallographic observation was not performed on them. They have been included in this table to test their consistence with the general results found for the other crystals examined in full. Both these crystals demonstrated the existence of the transformation in the resistance measurements. Crystal p2 appears to be identical to p4 in orientation and behaviour and is thus considered to be consistent. The ratio of Schmidt factors for crystal p6 is large indicating that slip was likely to be predominant. However, in both this crystal and also in crystal C1, the transformation has been found to occur. Both these crystals

have orientations very near the boundary, shown in Fig. 5.1, constructed to demarcate crystals on which transformation traces were observed from those on which they were not. On crystal S6, discussed more fully in the next section, whose orientation lay just on the other side of this boundary, only slip was observed. Anticipating slightly the results of that section we may quote the value of R for S6 as 2.37. Thus a slip mode has to be approximately twice as highly stressed as the $\{\bar{1}13\}\langle\bar{1}\bar{1}0\rangle$ mode for slip to occur to the exclusion of the transformation shear process. Thus an intermediate region appears to exist in the unit triangle between regions S and M_1 where the transformation occurs but not as the predominant feature of the deformation.

The two crystals in this region which are shown at the bottom of Table 5.3 are anomolous in that the conditions of testing were varied from those of the majority of the crystals in this chapter. Thus, in the light of the results presented here, crystals S15 and C6 were favourably oriented for the occurrence of the transformation, but in these cases the test temperature was either 55°K or above and the $\{\bar{1}13\}\langle\bar{1}\bar{1}0\rangle$ shear process was not observed.

5.3.3 Regions S and T

As described in section 5.3.1 crystals with orientations in these two regions deform on the well-established modes observed at higher temperatures. Because of their similarity to the behaviour at 77°K, these regions have been grouped together. Table 5.4 gives the Schmidt factors of the three possible slip variants for each crystal in these regions. The

operative modes are also shown, being underlined when occurring as the predominant feature. It is clear that when $\{11\bar{1}\}$ slip occurs as a deformation mode, the most highly stressed system is always operative, in accordance with the scheme discussed in Chapter 3. However, when observed as an accommodation mode with twinning, this criterion does not always apply, the operative variant here depending on which twin mode occurs. Thus, on crystal S13, twin variants b and b' occur with accommodation slip on mode B, although mode A is just as highly stressed.

The maximum values of the Schmidt factors, S_s, corresponding to these operative modes havebeen used in compiling Table 5.5 where they are compared with the Schmidt factor, S_M, of the transformation shear mode, as was done for crystals in region M, in the previous section. Except for two crystals the ratio R of these Schmidt factors are all greater than 2 which confirms the suggestion made in the previous section that if $R > 2$ the transformation will not occur. Crystals S12 and S13 are anomolous in this respect, but in these cases the twinning mechanism is predominant as is the case for these orientations at 77°K. The values of S_s are low for both these crystals and S_M is also low for S12. But for crystal S13, the $\{\bar{1}13\}\langle\bar{1}\bar{1}0\rangle$ mode is six times more highly stressed than the slip mode. But in both these crystals the twin mode is more highly stressed than either of the other modes, and is operative. Slip then occurs as an accommodation effect at intersections of pairs of twins as discussed in Chapter 3. Closer inspection of the Schmidt factors, S_T, for

the twinning mode for all the crystals in this group indicates that this mode is often very highly stressed. However only when the ratio of this factor to that for the slip mode exceeds the value 1.5, does twinning actually occur. This is in agreement with the discussion of this point in Chapter 3.

Crystal C5 is included at the end of Table 5.5 although it does not conform directly to this shceme since the mode of testing used in this case was compression at 4.2°K. The pre dominant feature was $\{11\bar{1}\}$ slip with some twins on the '$\{\bar{1}\bar{3}5\}$' mode, these probably occurring because of the high strain rate inherent in the shock loading method. The value of S_M quoted here is in fact a negative one, since the direction of stress is reversed, giving a value of R = 1.3. Thus, by analogy with the scheme developed here, the transformation could occur, but the indication is that it does not readily do so in a compression test.

In this region, then, the values of S_M decrease more rapidly than S_s as one approaches $[111]$, the limiting case being exemplified by crystal S_2 where all the values of S_M become negative implying non-operation in a tension test. For orientations near $[110]$ both S_S and S_M become very small and crystals deform by the twinning process also observed at 77°K.

5.3.4 Region M_2

The boundary of this region is less well defined than the others as only a few crystals with these orientations have been tested. Crystals with orientations near $[111]$ are very

rare and when they do occur, their deformation characteristics are particularly unusual. For example, the observation of wavy slip on one such specimen during a bend test by Guyoncourt (1967). However in the present tests, when slip occurs, it does so on the most highly stressed $\{11\bar{1}\}\langle\bar{1}10\rangle$ mode in accordance with the scheme of Fig. 3.1(a).

The inference from crystal S2 of the previous section 5.3.2, which had all negative factors for the $\{\bar{1}13\}\langle\bar{1}\bar{1}0\rangle$ mode, is that the three crystals in this region, being nearer $[111]$, will also have negative values. An examination of these values shows that this is so. The macroscopic shear direction for these crystals was not determined. The surface morphology and distribution of traces was not considered to be as suitable as the other crystals examined in this way. However the habit plane was identified and the results were included in section 5.2.2 where the habit plane was determined to be $\{\bar{1}13\}$. The present Schmidt factor considerations for these crystals implies that some other mechanism involving the $\{\bar{1}13\}$ habit plane is operative for orientations near $[111]$ and as such the traces are not associated with the occurrence of the $\alpha-\gamma$ transformation. However, as shown in a micrograph of these traces, reproduced as Fig. 5.12, the morphology of the traces, involving interesections of pairs of them at obtuse angles, is similar to that of crystals in region M_1. The cross-slip type formation between two sets of planes is again seen, as Fig. 5.13 demonstrates. Thus, it is extremely tempting to suggest that the operative macroscopic shear direction in this case is just the opposite sense of the

operative shear direction for crystals in region M_1, that is $\langle 110 \rangle$.

With this in mind, the Schmidt factors were calculated for each of the six crystallographically equivalent variants of the $\{\bar{1}13\}\langle 110 \rangle$ mode for these three crystals and are given in Table 5.6. Again, the sign of the factors are significant, and it is seen that not only are they all positive, implying possible operation in tension, but they all have extremely high values, thus supporting the suggestion that $\langle 110 \rangle$ is the operative shear direction. Assuming this is so, the maximum values of the Schmidt factors, $S_{\langle 110 \rangle}$, corresponding to the operative habit plane, have been used in a comparison with the slip factors in Table 5.7. It is clear that the $\{\bar{1}13\}\langle 110 \rangle$ mode is much more favourably stressed than the slip mode. The occurrence of the $\{\bar{1}13\}$ habit plane as a predominant deformation feature on these crystals is thus readily explained if the $\langle 110 \rangle$ shear direction is assumed to be operative.

If this result is correct, then it appears that the shear process associated with the transformation is non-unidirectional in nature. This is an extremely surprising and unexpected result. In diffusionless processes associated with transformations and twinning in this and other materials, a particular sense of the macroscopic shear direction is consistently operative. However it must be remembered that the occurrence of the transformation on specimens in this region was inferred from the determination of the habit plane of the traces and from their morphology. No confirmatory evidence in the form of resistivity measurements was possible for these

specimens. Thus the possibility of a completely different mechanism, for example deformation twinning or a second martensitic transformation, involving the same habit plane as the established transformation, cannot be ruled out. With only speculative evidence for the operative shear direction in these cases, this possibility seems even more likely although the observed pair morphology would then appear confusing.

As reported in section 5.2.4 a preliminary examination on the surface tilts on these crystals showed that they were not consistent with the operation of the $\{\bar{1}13\}\langle\bar{1}\bar{1}0\rangle$ mode of region M_1. At that stage, a full determination of the shear elements, by surface tilt measurements, was not performed mainly because the surface morphology of these specimens was not particularly conducive to this type of observation. However, in the light of the present analysis the implications of which are very striking, it was decided to attempt such observations on one of these specimens, namely S19, so as to elucidate the operative mechanism for these crystals. Two sets of traces on this crystal were examined. The stereographic analysis confirmed that the associated shear direction was $\langle 110\rangle$ to within 2° and 5° as shown in Table 5.8. The corresponding values of the shear strain magnitude were checked using the algebraic method and good agreement was again found as can be seen in the table. The average values for the two methods were 0.25 and 0.235. These values serve to distinguish this mechanism from that observed for region M_1, even though the other shear elements are surprisingly similar.

A few twins were observed on all these specimens again on the most highly stressed mode as indicated in Table 5.7. The ratio of the Schmidt factors for twinning and slip exceeded the value 1.5 for these three crystals, in agreement with those crystals in region T.

5.3.5 Discussion

In section 5.3 the orientation dependence of the crystallography of the deformation characteristics of single crystals of mercury has been investigated. Slip and twinning occur on the most highly stressed modes as was found at 77°K. Twinning is confined in general to the region near $[110]$ except for crystal C5 which was tested in compression at a far greater strain rate than the remainder of the specimens. Provided the ratio R of the Schmidt factors for $\{11\bar{1}\}$ slip and the transformation shear mode $\{\bar{1}13\}\langle\bar{1}\bar{1}0\rangle$ is greater than 2, slip will occur to the exclusion of the transformation mode.

The results obtained on the three crystals with orientations near $[111]$ imply that the opposite sense of shear on $\{\bar{1}13\}$ is possible when the resolved shear stress on other modes is very low. The magnitude of the macroscopic shear direction associated with the traces on these crystals does suggest, however, that a different mechanism is in fact operative in these cases, and the traces do not necessarily correspond to a transformation process and almost certainly not to the $\alpha - \gamma$ transformation occurring in region M_1. That these three crystals were found to be hard on testing suggests that although this mode is highly stressed, the shear

process does not occur nearly as readily as when the more usual sense of the shear direction is operative, as in region M_1. This observation is consistent with the operation of a different mechanism.

If $\{\bar{1}13\}\langle 110\rangle$ is a possible shear mode, then for consistency the Schmidt factors for this mode should be calculated for crystals in regions M_1, S and T. This has been done, and for M_1 the values are all low or negligible, the value S_M for the usual shear mode implying that it is at least twice as favourable. The one exception is crystal C1, but here slip is over twice as favourable and occurs. In region S and T the Schmidt factor values for $\{\bar{1}13\}\langle 110\rangle$ are higher but in most cases slip is still more favourable. However, two crystals S2 and S16 are interesting in this respect. For S2 the Schmidt factors for $\{\bar{1}13\}\langle 110\rangle$ are all positive, the highest value being 0.43, and for S16 five are positive the largest being 0.41. Thus, if mode $\{\bar{1}13\}\langle 110\rangle$ can operate it would be more favourable than slip for these crystals. However, no indication of the operation of this mode was found on these two crystals, confirming that if it does occur it does so only with difficulty and only when the S_s values become very small, as is the case near $[111]$. This is again consistent with the operation of a different mechanism involving similar shear elements, and this problem will be taken up again in section 5.4.

In an attempt to define the boundaries between these regions on a more quantitative basis, the procedure employed in Chapter 3 was used to compute curves of constant Schmidt

factor for orientations within the unit triangle. The result is shown in Fig. 5.11. The contours for the mode $\{\bar{1}13\}\langle\bar{1}\bar{1}0\rangle$ have been plotted using values of the particular variant having the largest positive Schmidt factor. For the majority of orientations mode M is most highly stressed, with mode L' predominant in the left lower corner. The dotted line through $[110]$ shows where the factors reduce to zero and beyond this line they become negative. By comparing the contours with those for slip given in Fig. 3.1(a), we can determine quantitatively the boundary separating the occurrence of these modes. If we consider that the resolved shear stress on $\{\bar{1}13\}\langle\bar{1}\bar{1}0\rangle$ has only to be half that on $\{11\bar{1}\}\langle1\bar{1}0\rangle$ for the former to operate, then by comparing corresponding Schmidt factors in the same ratio we obtain Fig. 5.14. The boundary between modes A and M corresponds almost exactly to that found by experiment.

If we now consider the possibility of $\{\bar{1}13\}\langle110\rangle$ being an operative shear mode and compare it to the slip mode in a similar manner, we have to assume that the c.r.s.s. on $\{\bar{1}13\}\langle110\rangle$ is four times that on the slip mode for a reasonable approximation to the experimental boundary to be achieved. The result is shown in Fig. 5.14. In the region near $[110]$ these boundaries become meaningless since, as we have seen, in this region the twinning mechanism becomes predominant.

5.4. Discussion of the Metallographic Observations

This chapter has been primarily concerned with the crystallography of the α-γ transformation based on metallo-

graphic observations performed on single crystals of various orientations. The results show that the habit plane of the plates of γ -Hg, in all cases, lies very close to the crystallographic plane $\{\bar{1}13\}$, and the macroscopic shear direction near $\langle\bar{1}\bar{1}0\rangle$. The possible theoretical composition planes of such a transformation cannot at present be reported and compared with this result, and consequently this remains essentially an experimental result. Thus it may be that the actual habit plane is irrational although the pair morphology involving a common shear direction and no accommodation effects at the interesection suggests a crystallographic process. The well-defined plane of intersection of the type $\{1\bar{1}0\}$ as shown in Fig. 5.15 supports this view.

The intersection shown in Fig. 5.8 illustrates a reduction in martensite boundary energy due to formation of the complementary plates of γ -Hg. A similar phenomenon is found for complementary twins in mercury (Guyoncourt 1967). There is evidence in this micrograph, and in Figs. 5.6 and 5.7, that growth of the plates is controlled by a dislocation mechanism. Growth of the product on one plane appears to initiate production on adjacent planes and the regions of the γ -phase extend outwards rather like Lüders band formation of slip lines. Indeed, the fact that the transformation is stress-induced is a clear indication that a dislocation mechanism controls the process. The cross-slip type formation of the complementary habits is probably due to obstacles in the matrix which the dislocations in the interface readily avoid by crossing to a complementary habit plane.

During the course of these observations, information has been obtained which indicates that the transformation is diffusionless or martensitic in nature. The audible clicks accompanying the testing of crystals at 4.2°K are typical of this kind of transformation (Machlin and Cohen 1951) or of mechanical twinning, and not of a nucleation and growth mechanism. However, on all the crystals in region M_1 no deformation twins on the well-established '{I35}' composition plane were observed. The well-defined shape deformation is again characteristic of a diffusionless process (Bilby and Christian 1956) and since the conventional twinning mode can be discounted this is best interpreted in terms of a martensitic transition. Certainly the observed characteristics are consistent with the criteria given by Bowles and Mackenzie (1954) for the occurrence of a lattice invariant plane, a predominant feature of the theories of martensite crystallography. Of course this type of plane occurs in a twinning mechanism, and so the possibility of interpreting this shear process as deformation twinning on a previously unobserved and unpredicted mode arises. However, as discussed in Chapter 4, the more logical deduction is that the traces are associated with the $\alpha - \gamma$ transformation. The reproducibility of the shear elements in region M_1 is again indicative of a martensitic nature.

It is interesting to note that the surface relief effects, due to the production of the γ -phase, still remain at the observation temperature even though the reversion temperature of 50°K has been exceeded. A similar behaviour is observed for deformation twins in mercury, after the

analogous process of recrystallisation, and in transformations in other materials (Barrett 1955-56). However in many cases, the surface tilts due to a transformation disappear on passing through the reversion temperature and in other cases, such as beta-brass (Reynolds and Bever 1952) and In - Tl (Burkart and Read 1953), stress-induced plates disappear with the removal of the stress.

The possible interpretation of the observed effects in terms of a deformation twin mode ought now to be given some more thought. A theoretical study of the crystallography of possible twinning modes in the mercury structure carried out by Bevis (1966) gave rise to five modes involving no atomic shuffles with shears less than unity, together with the corresponding five reciprocal modes. These modes were discussed in Chapter 1 and are listed in order of increasing shear magnitude in Table 1.1. It will be seen that the reciprocal of mode two is the observed mode at 77°K and in the present study has also been found to occur at 4.2°K. At both these temperatures under tensile test conditions, the occurrence of this twinning mode has been limited to orientations where the Schmidt factors for slip have been very small, namely near $[110]$ and $[111]$. Thus, for twinning to occur, even though it may be on a new mode, over most regions of the triangle where these slip Schmidt factors are their highest, seems highly unlikely. It is interesting to note that mode 4 of Table 1.1 involves a $\{\bar{1}13\}$ composition plane identical to that observed for the transformation traces. However, the corresponding irrational shear direction '$\langle 14\bar{1}\rangle$'

and the associated shear strain magnitude of 0.888 do not agree with the observed shear elements. In addition it seems unlikely that a crystal which can deform by slip and twinning on the established modes would also choose to twin on a mode involving a considerably higher shear strain.

Thus the possibility of the shear process occurring in region M_1 of the standard triangle being twinning can be discounted. In region M_2 where the slip Schmidt factors do become low as do those for the ' $\{\bar{1}\bar{3}5\}$ ' twinning mode it would seem more likely that this mode 4 could operate, even though the shear strain magnitude is high. However, the observations on crystal S19 are not consistent with this possibility. Thus an interpretation of the occurrence of these traces having a $(\bar{1}13)$ habit plane in terms of a deformation twinning process must be ruled out.

A possible explanation of the occurrence of the $\{\bar{1}13\}\langle\bar{1}\bar{1}0\rangle$ shear mode as a deformation mode of crystalline mercury at low temperatures has been found in section 5.3 by considering the relative Schmidt factors of possible modes. An alternative approach has been given by Tucker (1966) by the application of anisotropic elasticity theory to aspects of plastic deformation. The results of this theory are only strictly applicable to small strains, but have been used to tentatively explain the anomalous slip and twinning results for mercury crystals tested at higher temperatures. Based on this analysis the anistropic shear moduli for various modes have been calculated and the results are presented in Table 5.9.

The values of G_1 and G_2 are derived from the reciprocal of the compliances and stiffnesses respectively. The values indicate the ease with which the crystal may be sheared elastically on a certain mode. A direct comparison of values of the two processes on $\{\bar{1}13\}$ gives no indication of why the $\langle\bar{1}\bar{1}0\rangle$ shear direction is preferred. The values of mode 3 suggest that the usual twin mode would be the most favourable. The justification of applying this theory here lies not only in its previous success in helping to explain the slip behaviour, but also in the fact that for the present case the product phase must be accommodated elastically by the matrix during growth.

These values of shear moduli can be further used in conjunction with a criterion suggested by Hall (1954) for determining which twin mode is likely to operate in a metal. He expresses the energy density of a twin by $E = \frac{1}{2}g^2G$. By analogy we may calculate the energy density of a martensite plate and compare it with similar values for possible twin modes in mercury. It is likely that the operative mode will have the least value of E. The results of this comparison are shown in Table 5.9, with two values of E corresponding to the two values of G. The observed mode has considerably smaller values for E than the twin mode with the same habit, and smaller than those for the '$\{\bar{1}\bar{3}5\}$' mode. This may serve as a partial explanation of why, of the two processes on the $\{\bar{1}13\}$ plane, the observed mode occurs preferentially.

Although a full realisation of why a particular habit plane and macroscopic shear direction occur in connection with a

martensitic transformation cannot be found without considering the nature of the product crystal structure and the crystallographic relationship it has with the parent, it has proved extremely valuable in this case to regard these shear elements as a conventional deformation mode and to compare it with other possible modes. This is particularly valid in this case, of course, since the transformation is stress-induced and the geometry of the crystallographic planes with respect to the applied stress is a controlling factor in the production of γ-phase.

The remaining point of discussion lies in the possibility of different mechanisms being operative in the two regions, M_1 and M_2, of the unit stereographic triangle. The wealth of experimental evidence in region M_1 indicates that the macroscopic shear direction is the $\langle \bar{1}\bar{1}0 \rangle$ direction, and such a process is invariably found to be unidirectional. Thus the observation in region M_2 of a positive $\langle 110 \rangle$ shear direction on the same composition plane is rather confusing. To demonstrate that these two directions are not crystallographically equivalent, the lattice geometry of the $\{\bar{1}13\}$ planes has been considered. Fig. 5.16(a) shows two $\{\bar{1}13\}$ planes possessing a common $\langle \bar{1}\bar{1}0 \rangle$ direction in the f.c.r. unit cell, and in (b) is a representation of part of one such plane. The interesection of this $(\bar{1}13)$ plane and the (010) plane defines the direction $[301]$. There is a lattice site at $\frac{1}{2}[110]$ and one at each of the other corners of the parallelogram.

The projected position of atoms in the neighbouring $(\bar{1}13)$ planes may be obtained by considering atoms lying along the close-packed direction $[101]$. The projected sites will lie on the direction $[13, \bar{2}, 5]$ indicated in (b). The closest $(\bar{1}13)$ plane is the one containing an atom at $\frac{1}{2}[101]$ which projects on to OABC to the point D, where $OD = (9 + 7c)(198 + 58c)^{-\frac{1}{2}}$. The neighbouring plane then occupies the dotted position relative to OABC. It is clear from the relative atomic positions that the two senses of the $[110]$ direction are not equivalent. It should be added that such a simple representation is in no way indicative of which sense should be operative during the transformation, since to regard the production of the new phase as being achieved merely by a simple shear process and not by any growth process perpendicular to the habit plane would be misleading. Thus the mechanism involved in region M_2 with shear elements $\{\bar{1}13\}\langle 110\rangle$, $g = 0.24$ remains unexplained.

The most striking result associated with this transformation and reported in this chapter is the observed value of the shear strain magnitude. The mean experimental value of 0.47 is remarkably large compared with those for other martensitic transformations (Bilby and Christian 1955). Thus, in order that the mercury transformation be energetically favourable, the atomic mechanism involved is likely to be particularly simple. The fact that the transformation is stress-induced suggests that it might be instructive to compare it with deformation twinning of α-mercury for which the shear strain of 0.63 is also large. No atomic shuffling

following the twinning shear is necessary and the same seems likely to apply to this transformation. The shear strain magnitude is an indication of strains involved in the transformation and consequently will depend on the nature of the lattice deformation implied by the lattice correspondence relating the parent and product structures. This aspect of the $\alpha - \gamma$ transformation in mercury will be discussed in the next chapter.

Crystal	Shear Strain		Shear Direction Deviation from $\langle \bar{1}\bar{1}0 \rangle$
	Stereographic	Algebraic	
S9	0.46	0.46	$2\frac{1}{2}^{o}$
	0.54	0.56	3^{o}
S10	0.46	0.51	2^{o}
	0.50	0.42	2^{o}
	0.48	0.42	4^{o}
S18	0.50	0.46	4^{o}

Table 5.1 Measurements of shear direction and shear strain for the transformation

Crystal Variant	S1	S4	S5	S8	S9	S10	S18	p4	p5	p7	C1	C2	C3	C4
M	$\bar{1}$8	11	27	32	00	06	16	09	00	24	22	40	01	30
M'	$\bar{0}$4	24	15	03	$\bar{0}$8	$\bar{1}$5	23	42	00	46	17	46	05	49
N	00	45	02	$\bar{0}$5	26	11	37	39	06	35	08	19	38	39
N'	00	23	$\bar{1}$1	17	42	42	03	27	15	15	24	05	42	15
L	32	$\bar{0}$8	20	47	15	31	$\bar{2}$0	$\bar{1}$1	43	02	$\bar{0}$6	01	12	$\bar{0}$2
L'	16	01	44	39	06	20	05	08	33	$\bar{0}$1	31	09	03	04

Table 5.2 Schmidt factors (x 100) for the six variants of $\{\bar{1}13\}\ \langle\ \bar{1}\bar{1}0\ \rangle$ for crystals in region M_1.
Operative modes are underlined. Negative indices are indicated by a line over the number.

	S1	S4	S5	S8	S9	S10	S18	p2	p4	p5	p6	p7	C1	C2	C3	C4	S15	C6
S_S	20	32	37	48	29	44	43	46	46	30	47	40	47	34	30	43	40	35
S_M	32	45	44	47	42	42	37	42	42	43	26	46	31	46	42	49	48	47
R	.62	.71	.84	1.0	.69	1.0	1.2	1.1	1.1	.70	1.8	.87	1.5	.74	.71	.88	.83	.75
Op. Mo.	$\underline{S_M}$	$\underline{S_M}$	$\underline{S_M}$	$\underline{S_M}$	$\underline{S_M}$	$\underline{S_M}$ S_S	$\underline{S_M}$ S_S	-	$\underline{S_M}$ S_S	$\underline{S_M}$	-	$\underline{S_M}$	$\underline{S_M}$ S_S	$\underline{S_M}$	$\underline{S_M}$	$\underline{S_M}$	S_S	S_S

Table 5.3 Comparison of Schmidt factors (x 100) for slip and transformation mode for region M_1.

Crystal Variant	S2	S3	S6	S11	S12	S13	S16	S17	
A	14	<u>40</u>	<u>44</u>	04	05	04	17	29	02
B	03	01	05	<u>40</u>	03	04	06	11	34
C	17	40	42	35	02	01	<u>24</u>	<u>40</u>	<u>36</u>
Twin	cc'				aa'	bb'			

Table 5.4 Schmidt factors (x 100) for the three slip variants for regions S and T. Operative modes are underlined.

Crystal	S2	S3	S6	S11	S12	S13	S16	S17	C7	C5
S_s	18	40	45	39	05	02	24	40	36	42
S_M	0	08	19	09	05	24	03	19	05	18
$R=\frac{S_s}{S_M}$	-	5.0	2.4	4.6	1.0	>10	8.0	2.1	>10	1.3
Operative Mode	S_s,S	S_s	S_s	S_s	S_T	S_T	S_s	S_s	S_s	S_s,S_T
S_T	32	33	34	37	30	28	36	43	34	-
S_T/S_s	1.8	0.8	0.8	0.9	6.2	7.0	1.5	1.1	0.9	-

Table 5.5 Comparison of Schmidt factors (x 100) for slip, twins, and transformation in regions S and T.

Crystal	S7	S14	S19
M	45	49	44
M'	46	41	40
N	41	42	34
N'	45	48	50
L	49	41	45
L'	40	43	33

Table 5.6 Schmidt factors (x 100) for possible mode $\bar{1}13$ 110 for crystals in region M_2.

	S_s	S_M	$S_{\langle 110\rangle}$	$\frac{S_s}{S_M}$	$\frac{S_s}{S_{\langle 110\rangle}}$	S_T	$\frac{S_T}{S_s}$	Op. Mode
S7	05	0	46	-	0.1	11	2.2	$S_{\langle 110\rangle}, S_s, S_T$
S14	05	0	49	-	0.1	11	2.2	$S_{\langle 110\rangle}, S_s, S_T$
S19	11	0	50	-	0.2	17	1.6	$S_{\langle 110\rangle}, S_s, S_T$

Table 5.7 Comparison of Schmidt factors (x 100) for slip, twins, and $\{\bar{1}13\}\langle 110\rangle$ in region M_2.

Crystal	Shear Strain		Shear Direction
	Stereographic	Algebraic	Deviation from $\langle 110\rangle$
S19	0.24	0.23	2°
	0.26	0.24	5°

Table 5.8 Shear direction and shear strain for a crystal in region M_2.

Mode	G_1	G_2	g	E_1	E_2
$\{11\bar{1}\}\langle 011\rangle$	9.83	5.09	-	-	-
$\{11\bar{1}\}\langle 1\bar{1}0\rangle$	4.94	3.49	-	-	-
$\{\bar{1}\bar{3}5\}'\langle\bar{1}21\rangle$	4.72	3.24	0.63	0.95	0.65
$\{\bar{1}13\}\langle\bar{1}\bar{1}0\rangle$	7.81	3.41	0.47	0.86	0.38
$\{\bar{1}13\}'\langle 14\bar{1}\rangle'$	6.32	3.85	0.89	2.49	1.52
$'\{3\bar{1}\bar{3}\}'\langle 101\rangle$	13.05	6.41	0.89	5.15	2.53

Table 5.9 Shear moduli and energy densities

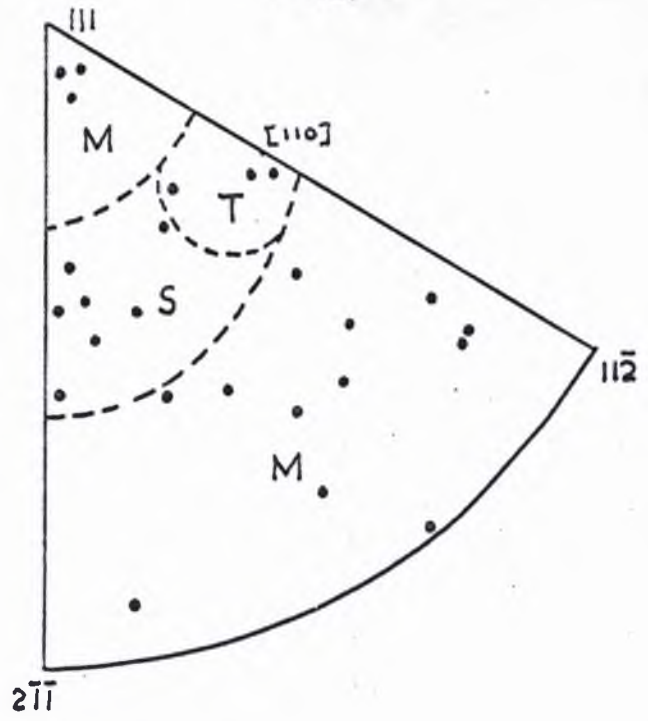

Fig. 5.1 Orientations of crystals used for metallographic analysis. Boundaries drawn according to the predominant features on the crystals.

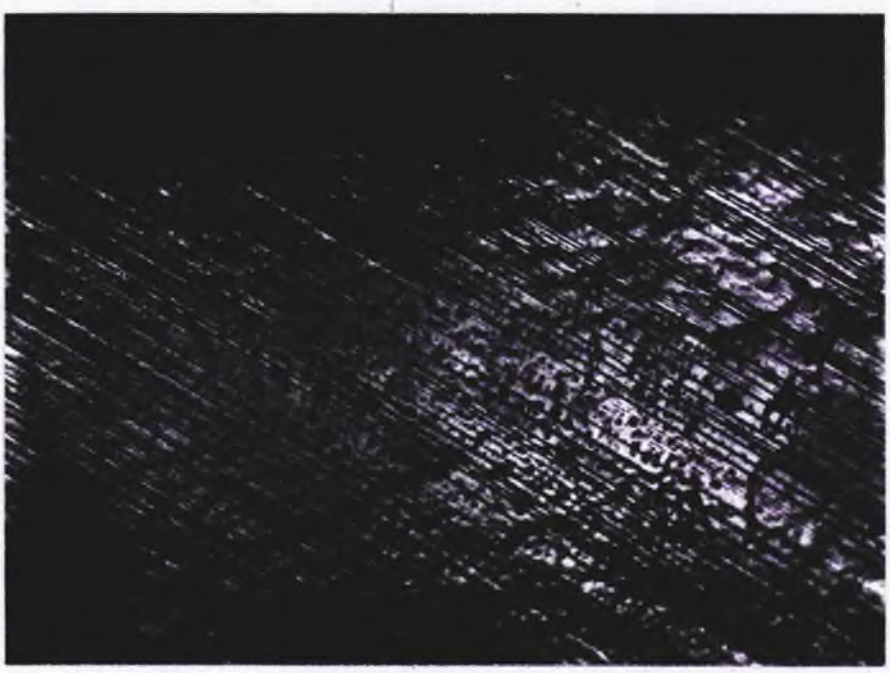

Fig. 5.2 Straight slip lines on crystal C6 (100x).

Fig. 5.3 Twin intersection showing accommodation slip (x 100)

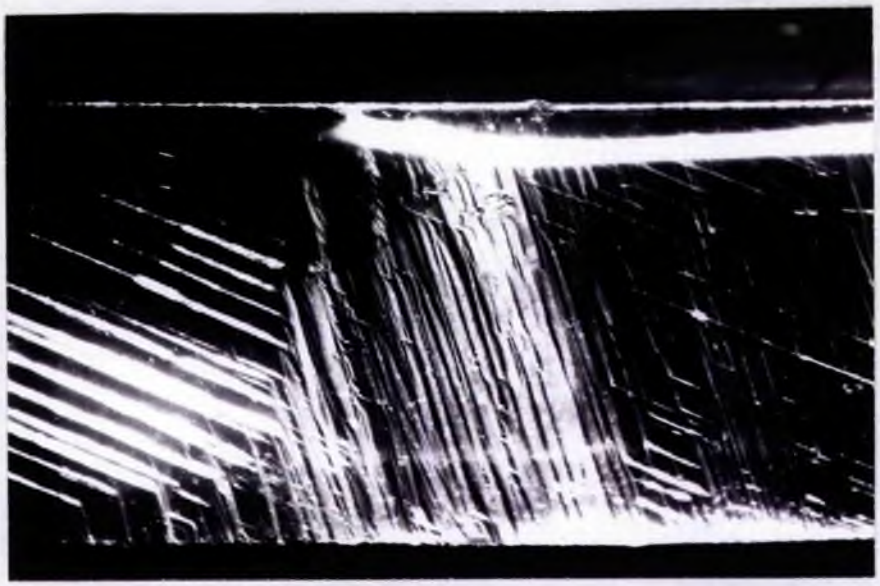

Fig. 5.4 General appearance of transformed crystal (x 10)

Fig. 5.5 Close-up of crystal in Fig. 5.4 showing obtuse intersections between plates of γ-mercury (x 80)

Fig. 5.6 Complementary plates sharing common macroscopic shear direction (x 80)

Fig. 5.7 Plates of γ-mercury on cylindrical crystal indicating that acute-angled intersections are avoided (x 80)

Fig. 5.8 Reduction of interface energy by occurrence of complementary modes (x 100)

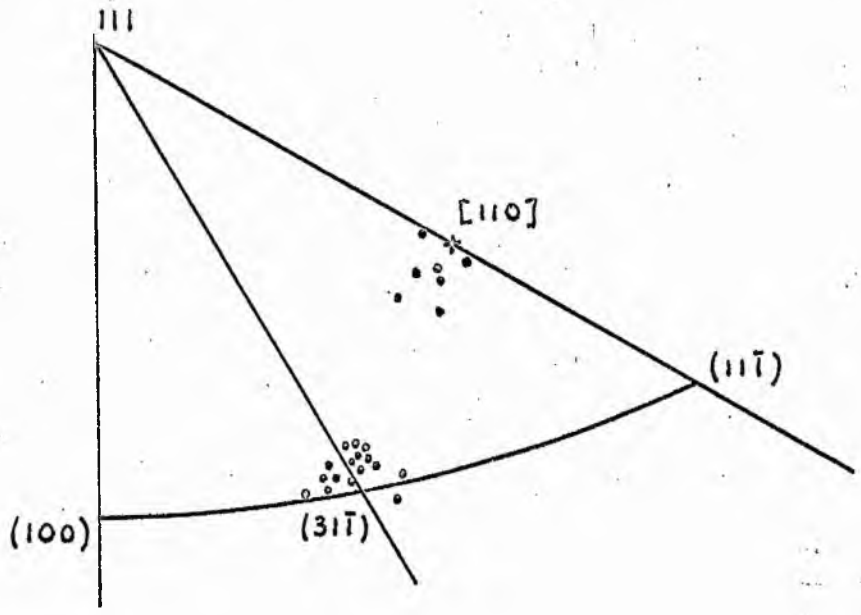

Fig. 5.9 Part of the unit triangle showing the experimentally observed poles of the habit plane and shear direction associated with the transformation.

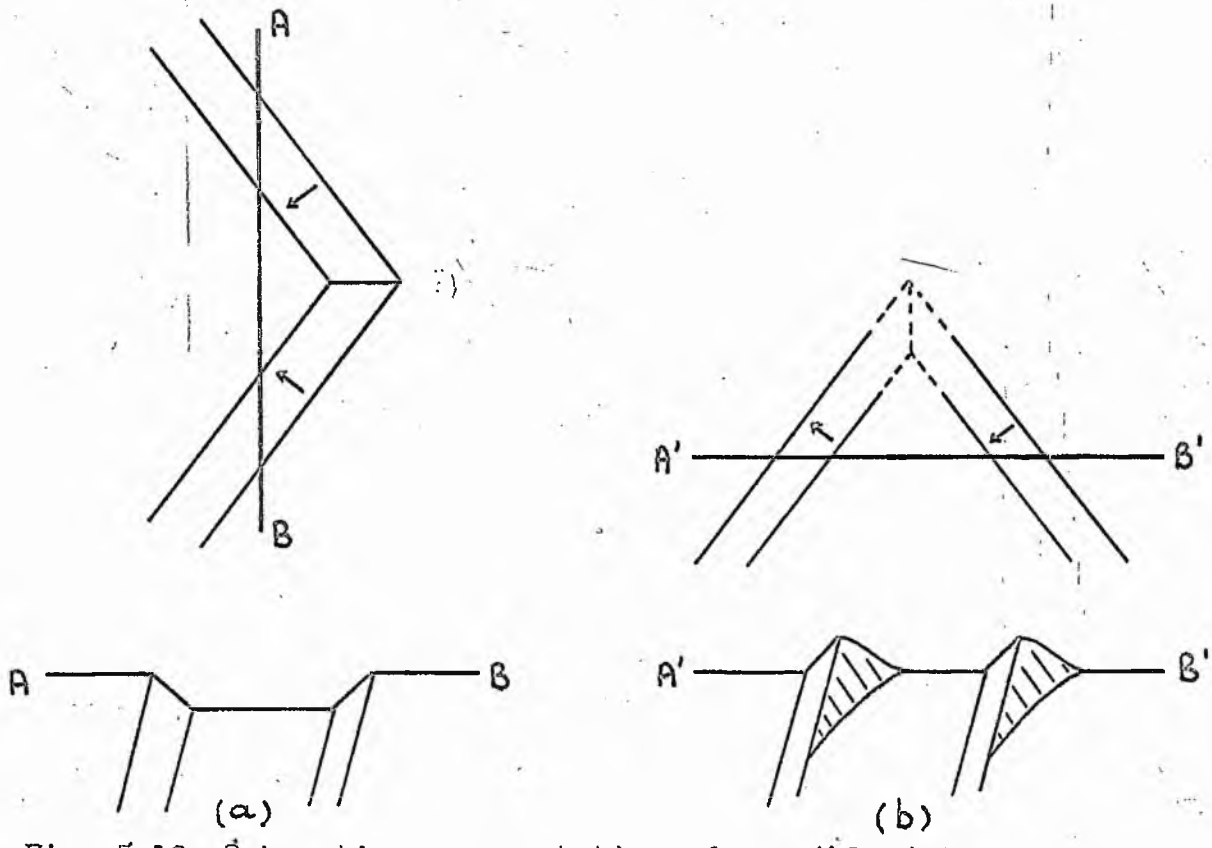

Fig. 5.10 Schematic representation of possible intersections between 'complementary' plates of γ-Hg showing (a) ease of accommodation at obtuse intersection and (b) kinking necessary at acute intersection.

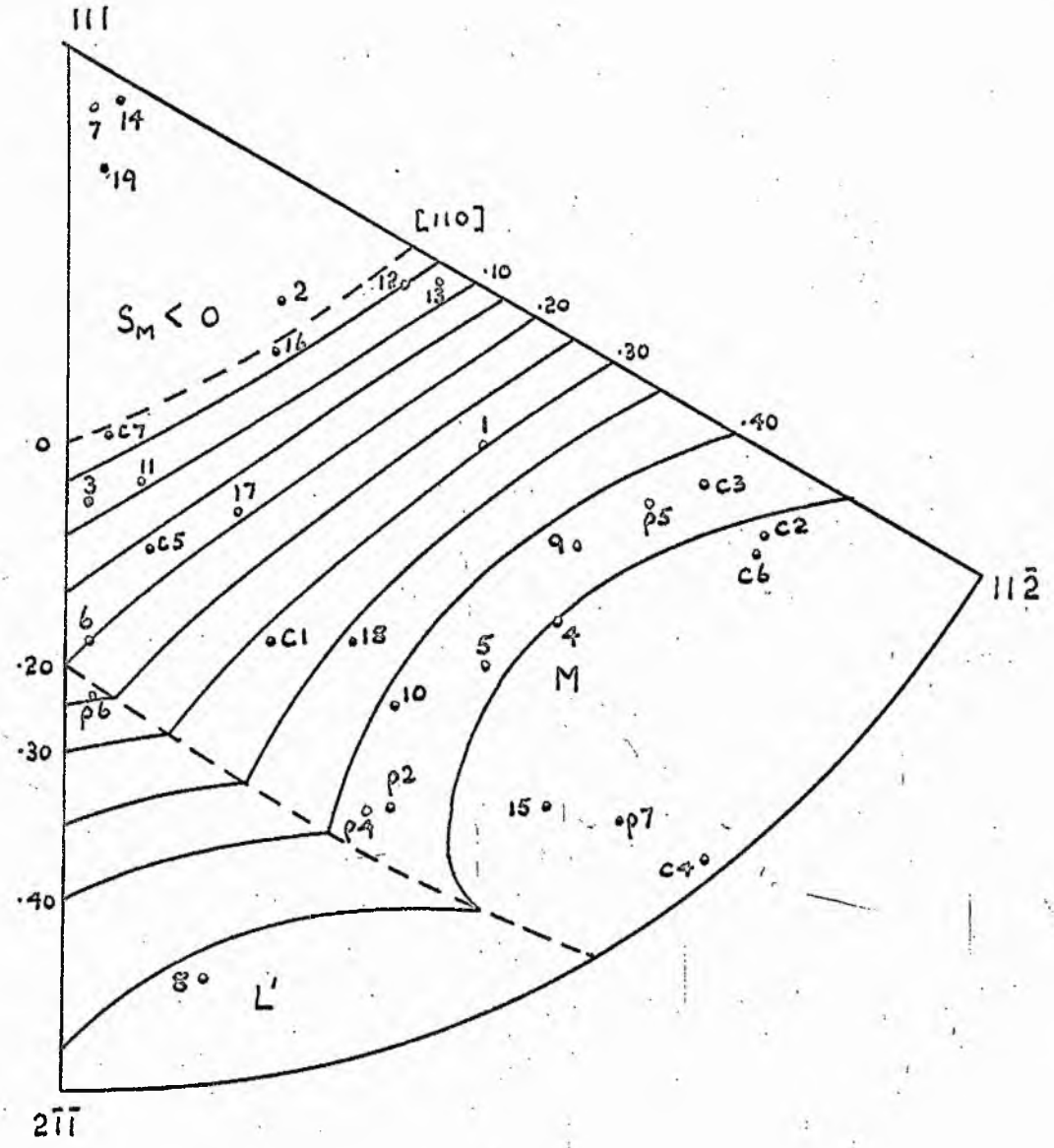

Fig. 5.11 Orientations of all crystals deformed at 4.2°K. Contours of maximum Schmidt factor on $\{\bar{1}13\}\langle\bar{1}\bar{1}0\rangle$ are drawn.

Fig. 5.12 Surface features on crystal S19 in region M_2 indicating intersections at obtuse angles (x 50)

Fig. 5.13 Features on S19 showing apparent 'cross-slip' type formation (x 50)

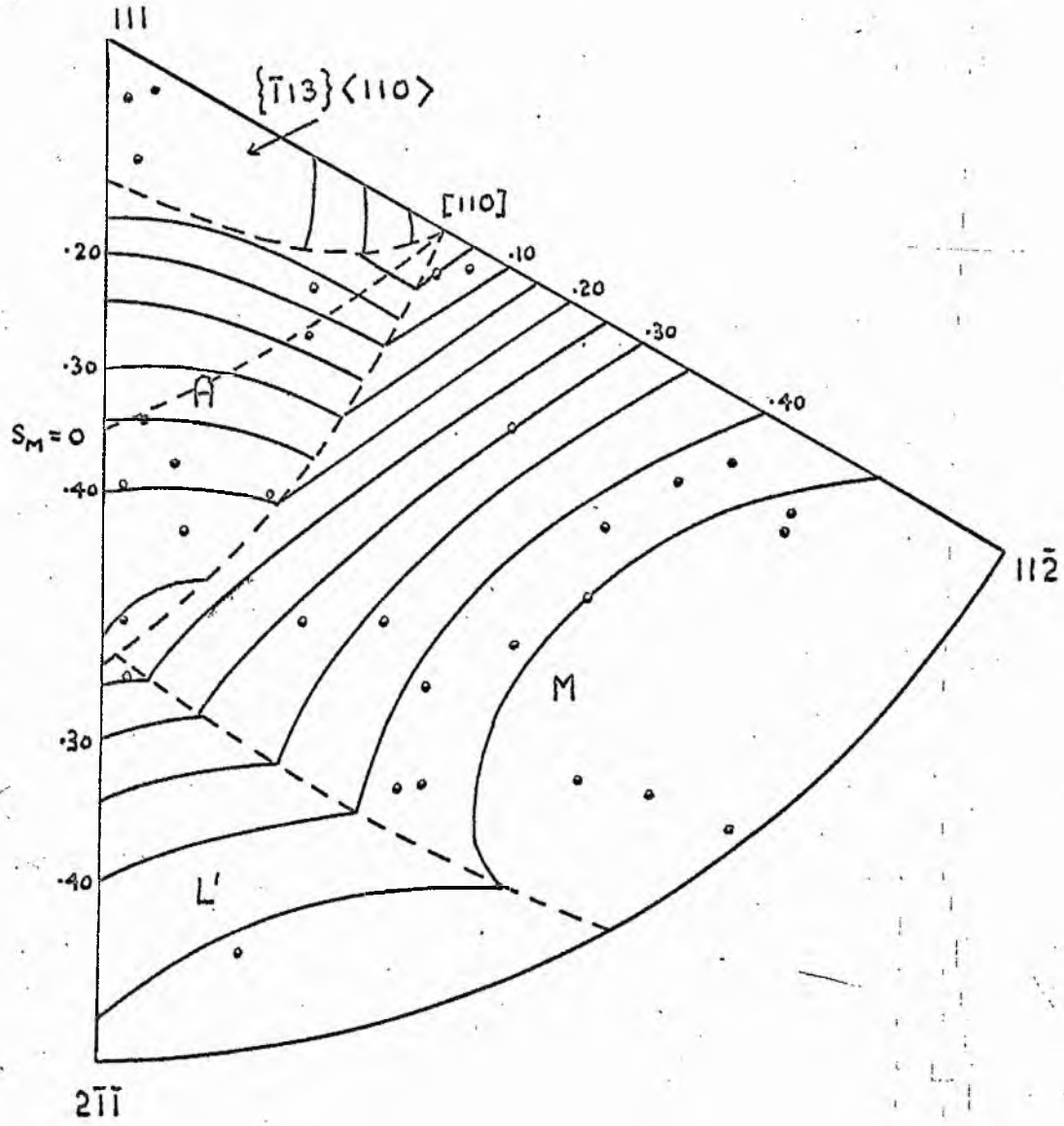

Fig. 5.14 Comparison of c.r.s.s. on deformation modes at 4.2°K assuming $C\{\bar{1}13\}\langle\bar{1}\bar{1}0\rangle = \frac{1}{2}C\{11\bar{1}\}\langle1\bar{1}0\rangle$, and $C\{\bar{1}13\}\langle110\rangle = 4C\{11\bar{1}\}\langle1\bar{1}0\rangle$.

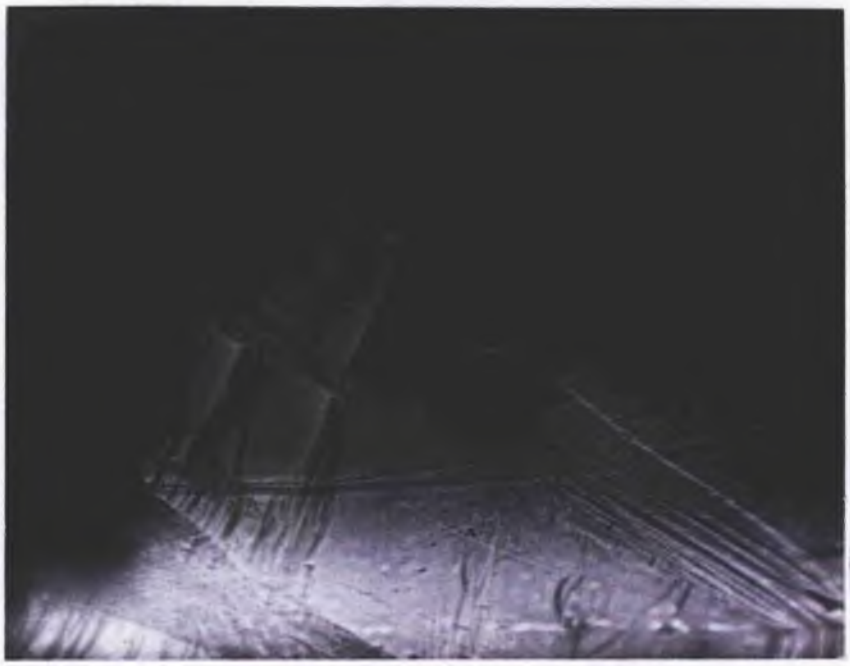

Fig. 5.15 Intersection of 'complementary' plates of γ - Hg. Plane of intersection is a $\{1\bar{1}0\}_\alpha$ mirror plane of the parent structure.

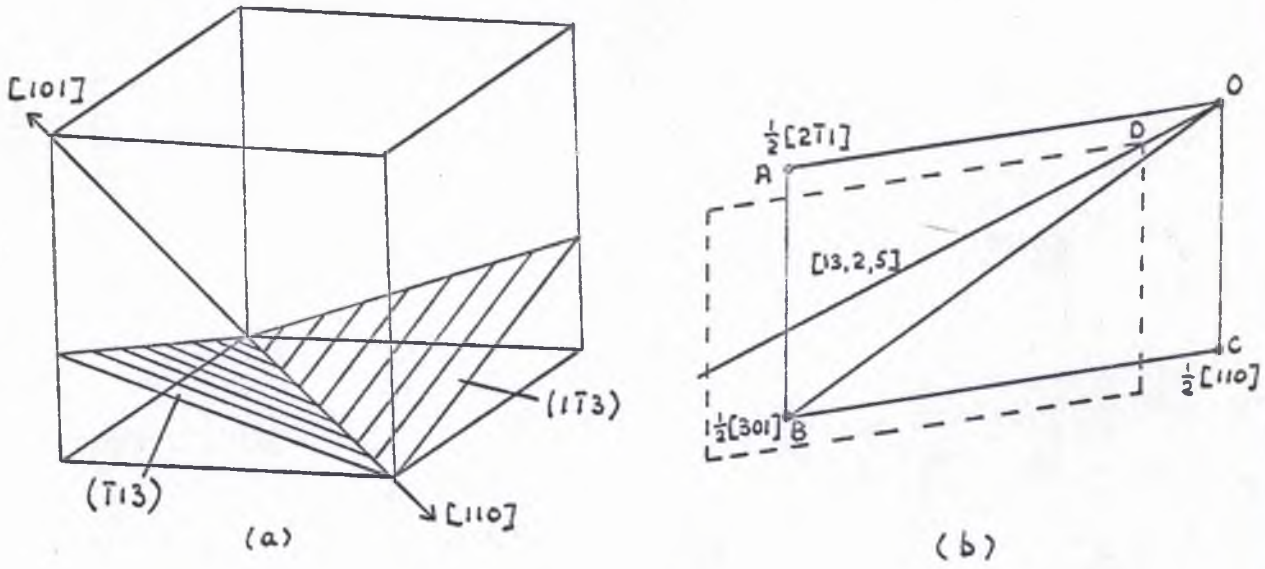

Fig. 5.16 (a) α-Hg unit cell showing two $\{\bar{1}13\}$ plane, (b) the $(\bar{1}13)$ plane with its nearest neighbour shown dotted.

CHAPTER VI - CRYSTALLOGRAPHY OF THE α - γ TRANSFORMATION

6.1 Introduction

In Chapters 4 and 5, the occurrence of a stress-induced transformation in mercury at 4.2°K has been established and the shear elements associated with this transformation have been experimentally determined as $\{\bar{1}13\}\langle\bar{1}\bar{1}0\rangle$, $g \simeq 0.47$ The transformation has been deduced to be martensitic in character and has been shown to exhibit different properties from the second phase β - mercury, and is called the γ -phase. In this chapter an attempt is made to elucidate the mechanisms concerned in the α to γ transformation by way of the application of the current theories of martensite crystallography. This is obviously of importance since the results so far obtained are essentially experimental in nature and has yet have no validification in any theory involving the mercury parent structure, nor indeed of the product. A successful application should account for all the observed features and may in particular shed light on the anomalously high shear strain associated with this transformation.

A review of the essential features of the theories is first presented followed by the introduction of a possible structure for the new γ -phase based on the pseudopotential theory of metals. The remaining sections are concerned with the application of the theories to this transformation. Two versions of the theories have been used: the stereographic analysis of the Wechsler-Liebermann-Read theory developed by Liebermann (1958), and the surface dislocation theory due

to Bullough and Bilby (1956).

6.2 Theories of Martensite Crystallography

Reviews of the current theories of the crystallography of martensitic transformation have been published (Bilby and Christian 1955, 1961, Christian 1968) and it is thus considered unnecessary here to present a detailed literature survey. The aim of this section is merely to point out the essential features of the various theories, the assumptions made, and the information necessary for a possible application to a particular transformation. Any such theory must readily account for all the experimental observations. The most obvious geometrical chacteristic of a martensitic transformation is the shape deformation in the form of a surface tilt on a previously flat surface. Examination of the surface relief effects indicates that straight lines are transformed into straight lines and planes into planes, with a definite orientation relationship between the two phases. Further experimental evidence suggests (Bowles and Mackenzie 1954) that the interface between the two phases is usually an invariant plane, that is a plane left undistorted and unrotated by the transformation. That the total shape deformation is an invariant plane strain is essentially a common feature of all the formulations of the theory. For any crystallographic theory to be successful it must predict this habit plane, the shape deformation and the orientation relationship.

Four main versions of the general theory have appeared. Two of these, due to Bowles and Mackenzie (1954) and Wechsler,

Liebermann and Read (1953), henceforth referred to as BM and WLR respectively, are essentially equivalent analyses enabling the prediction of the above features using only the lattice parameters and crystal structures of the parent and product phases. The Bullough and Bilby (1956) theory focuses attention on the nature of the interface and regards the transformation as being achieved by a glissile surface dislocation moving in the interface. In this analysis and in the WLR theory there is no shape deformation of the interface but the BM theory does allow a uniform dilation of this interface, giving the theory greater flexibility. The BM theory restricts the simple shear components to those corresponding to twinning in the product and then chooses the dilation to give the best agreement between observed and predicted habit planes. Provision for varying the shear components is inherent in the Bullough and Bilby version with no shape deformation of the interface. The same is true of the fourth version of the theories due to Bilby and Frank (1960) who devised an analysis where prismatic structural units of the two phases match up at the interface.

Because of its inherently simpler nature it was decided to use the theory which is fundamentally common to both the WLR and BM theories, for the initial application of the crystallographic theories to this martensitic transformation in mercury. At the same time it was felt that from an illustrative point of view, the stereographic analysis based on these theories (Mackenzie and Bowles 1954, Bowles and Mackenzie 1954b, Liebermann 1958) should be used for this initial treatment, since this approach would be consistent

with much of the other work presented in this thesis. A full numerical treatment based on the matrix algebra formulation of Bullough and Bilby was subsequently performed. Inherent in the theories are two assumptions; one of a lattice correspondence relating the structures of the parent and product phases, the other of a lattice invariant shear. These, used in conjunction with a rigid body rotation to retain the habit plane unrotated, then define the shape deformation in the form of an invariant plane strain.

The application of the theory thus depends upon a knowledge of the parent and product crystal structures. The parent α -structure of mercury is of course well-established but a full experimental determination of the structure of γ -Hg has not yet proved possible. A possible structure has, however, been predicted for this new phase (Weaire 1968b) based on the pseudopotential theory of metals. This will be introduced in the next section followed by a discussion of the lattice correspondences and invariant shears which will be assumed for the subsequent application of the crystallographic theory.

6.3 Crystal Structure of the γ -Phase

6.3.1 Introduction

The publication of evidence of the α - γ transformation (Doidge and Eastham 1968) in mercury and the subsequent investigation of the nature of the transformation and the properties of the martensite phase, has prompted Weaire (1968b) to report a possible product crystal structure, which he had predicted using the pseudopotential theory of metals. This

theory had in fact been used previously to predict successfully (Weaire 1968a) the structures of both α -mercury and the alternative low-temperature modification, β -mercury. This success, and the present absence of an experimental determination of the structure, has encouraged us to adopt this predicted γ -phase structure in the present analysis. A brief summary of the essential features of this theory will be given followed by the results obtained on considering the α -, β - and γ -structures.

6.3.2 Pseudopotential theory of Metals

The development of this approach to the variations of structure in simple metals was due to Cohen (1962) and Harrison (1963, 1966) and carried on by Heine and Weaire (1966) The theory begins by expressing the structure-dependent part of the total energy of a metal as a sum of two terms, by $U = U_E + U_{BS}$. The first, U_E, arises from the electrostatic interaction of the ions and is referred to as the Ewald term; the second, U_{BS}, is the interaction of the electrons with the ions and with each other and is called the band structure term. It is this term which is treated by the pseudopotential method.

It has been observed (Animalu and Heine 1965) that the pseudopotentials of most elements are very much alike, characterised by a value q_o at which the potential has its first zero. A consequence of a structural weight term in U_{BS}, dependent on a set of reciprocal lattice vectors g, is that if such a set has magnitude $g \approx q_o$ it will contribute very little to the binding energy. Thus, in the choice of a

structure, say between f.c.c. and h.c.p., the effect of q_o is to favour a structure having a distribution of structural weight which avoids q_o. However, if a structure has a set of reciprocal lattice vectors such that $g = q_o$ a lowering in the total energy can be achieved by a distortion of the lattice which splits this set into two or more. Thus, it is seen that this U_{BS} term favours a low symmetry structure, whereas the converse is true for the Ewald term which is found to increase upon distortion from a high symmetry structure such as f.c.c. The actual structure is then determined by the balance of these two tendencies.

6.3.3 Structures of α - and β -Mercury

Application of the pseudopotential method to the structure of mercury has been considered by Heine and Weaire (1966) who regarded the α- and β-structures as distortions of the face centred cubic structure leading to a significant lowering of the band structure energy as discussed in the preceeding section. In particular the α-structure was attributed to instability of the f.c.c. structure with respect to rhombohedral distortion, such a distortion splitting the (111) set of reciprocal lattice vectors and decreasing the energy. For the β-structure they suggested that the f.c.c. structure should be metastable with respect to tetragonal distortion. Calculations of the variation of energy of the f.c.c. structure with respect to such distortions confirmed this explanation (Weaire 1968a) but agreement with the observed amount of distortion was not obtained, there being in both cases too great an instability.

Such quantitative agreement is determined by the balance of the two terms in the total energy expression. The electrostatic self-energy of the ions, the Ewald energy, favours stability while the electronic interaction, the band structure energy, favours instability. By a reduction of 40% in this latter term, good quantitative agreement was achieved (Weaire 1968b). The curves obtained are reproduced as Figs. 6.1 (a) and (b) and both curves have minima at values of the distortion of correct sign and magnitude corresponding to the observed structures. The parameter, δ, used for the distortion is the linear compression along the axis of distortion relative to f.c.c.

6.3.4 Structure of γ -mercury

The pseudopotential approach successfully accounts for the observed structures of α - and β -mercury, and further considerations qualitatively explained the low melting point of this metal (Weaire 1968a). Now observations of Fig. 6.1(b) clearly suggests a possible structure for the new γ -phase reported in this thesis. This is the structure produced from f.c.c. by the opposite rhombohedral distortion to that of α-Hg, giving an axial angle of the face-centred cell of approximately 82°. If the cell has an axial angle which is the exact supplement of the α -structure axial angle of 98° 22', then this structure becomes particularly convenient since, being a product structure of a transformation, it will have the same volume as the parent cell, which, in this case, means that the lengths of the edges of the two cells are identical.

Another possibility discussed by Weaire (1968b) is the hexagonal close-packed structure. He points out that this would have a c/a ratio very different from the ideal 1.63 value, since a mercury structure having this ideal axial ratio would show instability to distortion similar to that discussed here for f.c.c. Similar calculations showed that hexagonal mercury would have a c/a ratio of about 2.0. Based on this approach, the possibility of any other structure was considered unlikely (Weaire 1968b).

On deciding which of the two predicted structures should be considered for the subsequent crystallographic analysis, more confidence was felt in the validity of the rhombohedral version as reference to Fig. 6(b) will indicate, since the magnitude of the instability for this case is approximately the same as for the observed α-structure. In the absence of direct experimental information on the product structure, the opportunity presented by the prediction of a possible structure on the basis of such a well-deformed minimum in the energy curve could not be overlooked. Weaire has recently (1968c) supported this choice as being the more suitable of the two. Consequently the new γ-phase of mercury was considered, for the purpose of the application of the theories of martensite crystallography, to have a face-centred rhombohedral structure with unit cell dimensions equal to that of the α-structure and axial angle approximately 82°. As both structures are referred to the rhombohedral basis, the indices of planes and directions will be the same and suffices α and γ will be used to differentiate.

It is of interest to note at this stage that this product γ -structure means that the (111) plane still remains unique as in the α -structure, but in this case it becomes the closest packed plane and is thus likely to be an operative slip plane, as distinct from the $\{11\bar{1}\}_\alpha$ planes being operative in the α -structure. In addition, the closest packed direction in this plane is of the $\langle 01\bar{1}\rangle_\gamma$ type, which was the second closest packed in the α -structure; while the second closest packed direction in the γ -cell is the $\langle 011\rangle_\gamma$ type which, however, does not lie in the closest packed $(111)_\gamma$ plane. Consequently if the closest packed plane is the operative slip plane in this γ -structure, there will be three possible variants of the $\langle 01\bar{1}\rangle_\gamma$ slip direction in this plane. But there will be no ambiguity as to the crystallographic nature of this slip direction as existed for the α -structure where in certain cases both the $\langle 011\rangle_\alpha$ and $\langle 01\bar{1}\rangle_\alpha$ could occur. Indeed, by analogy, the ambiguity in this case could be in the operative slip plane as there is only one close packed $(111)_\gamma$ plane compared with three variants of the $\{11\bar{1}\}_\alpha$ close packed slip plane.

6.4 Lattice Correspondences

The lattice correspondence defines the relationship between corresponding planes and directions in the two phases. The choice of correspondence is in reality a matter of informed guesswork and it is probably that a criterion of minimum strain energy at least partially dictates which correspondence is in general applicable. Having adopted this predicted structure for γ -mercury, two particularly simple distinct

correspondences relating the parent and product unit cells, both of which are face-centred rhombohedral, are immediately apparent. These relationships are illustrated schematically in Fig. 6.2. In the first of these illustrated by diagrams (a), (b) and (c) the product unit cell is obtained from the parent by means of an extension along the $[111]_\alpha$ direction and a uniform contraction in the $(111)_\alpha$ plane to give no volume change. The associated correspondence formed the basis of the preliminary analysis of the crystallography of the transformation (Abell and Crocker 1968a), since the simple nature of this correspondence greatly facilitates the stereographic analaysis used in this initial treatment. These results will be described in detail in section 6.6.

The second relationship may be described by a similar extension in the $[111]_\alpha$ direction, but only until a face centred cubic structure is obtained, followed by a further extension in one of the three directions derived from $\langle 11\bar{1} \rangle_\alpha$ This sequence is illustrated by Fig. 6.2 (a), (b), and (d). For the case of a product face-centred rhombohedral angle which is exactly the supplement of the parent angle the correspondence implied by this second mechanism may be shown to be equivalent to that associated with a simple shear on a parent $\{100\}_\alpha$ plane. This is demonstrated by Fig. 6.3. An additional strain is necessary if, as is likely, this exact angular relationship does not hold. Thus the lattice correspondences specify which vectors of the parent transform into given vectors of the product. The implied lattice deformation is then characterised by the pure strain

associated with the correspondence. This pure strain leaves certain vectors unchanged in direction but not necessarily in magnitude, and the principal distortions η_i, and hence the principal strains (η_i -1) along these principal directions may be readily obtained by the proceedure described by Crocker and Ross (1968).

A simple illustration of the effect of the lattice deformation is to be found by considering the first correspondence described for the mercury transformation, involving the extension along $[111]_\alpha$ and uniform contraction in the $(111)_\alpha$ plane. Here the three principal directions are $[111]_\alpha$, and two directions chosen in the $(111)_\alpha$ plane namely, $[1\bar{1}0]_\alpha$ and $[11\bar{2}]_\alpha$. The transformation strain is then represented diagrammatically in Fig. 6.4 by considering a sphere as the initial lattice and an ellipsoid of revolution as the final lattice. Vectors OA and OB are unchanged in length due to the deformation, but are merely rotated. The associated cones are termed the initial and final cones of unextended lines. The principapal distortions then define the equation of the ellipsoid thus

$$\frac{x_1^2}{\eta_1^2} + \frac{x_2^2}{\eta_2^2} + \frac{x_3^2}{\eta_3^2} = 1$$ where x_i are the principal directions. For the present mercury case, the uniform contraction in the (111) plane implies $\eta_2 = \eta_3$ and the final lattice is represented by a spheroid. The situation is not so clear for the second correspondence as the principal directions involved are not such low-indexed crystallographic directions.

The principal strains associated with these two correspondences are smaller than those for all alternatives if atomic shuffles are not allowed, as appears likely in view of the large macroscopic shear strain, as discussed in Chapter 5. They have been determined using the proceedure described by Crocker and Ross (1968) and for a product rhombohedral angle of 82^{o}, found to be (0.34, -0.14, -0.14) and (0.16, -0.14, -0.00) respectively. Thus if the choice of correspondence is governed by a criterion of minimum strain, the second relationship is clearly to be preferred. However, for completeness both in fact were used in the subsequent analysis, the first in the stereographic analysis as previously mentioned, and both in the application of the algebraic version of the theories due to Bullough and Bilby (1956). It is interesting to note that the principal strains quoted above are in general large which suggests that the associated macroscopic shear strain might also be large. A large macroscopic shear strain is of course one of the main experimentally observed features of this transformation, as shown in Chapter 5.

A typical lattice correspondence does not in general satisfy the condition that the habit plane be undistorted, as suggested by experiment. Bilby and Christian (1955) formulated this in general terms by stating that if an undistorted plane is to result from a homogeneous distortion, one of the principal distortions must be greater than unity, one must be less than unity, and the third one must be unity. This is clearly not true for the correspondences considered here. Consequently, the next stage in the application of the

theories is to postulate a lattice invariant shear to accompany the pure strain already discussed, to ensure that the lattice deformation satisfies this condition.

6.5 Lattice Invariant Shears

A graphical analysis of shear (Schmidt and Boas 1950) is shown schematically in Fig. 6.5 where a unit sphere is sheared on an equatorial plane K_1 in direction d. This shear plane remains undistorted after shear. The plane K_2 represents the initial position of a plane K_2' which is also undistorted as a result of the shear, their relative positions being dependent on the amount of shear involved, given by $\tan \alpha = |g|/2$. Thus, some vectors remain unchanged in length as a result of simple shear. The same result was obtained in the preceeding section by considering the lattice deformation and cones of unextended lines. The object, then, of the crystallographic theories is to find vectors which are increased in length due to the lattice deformation and are correspondingly decreased in length due to the simple shear on a given system. These vectors are then invariant in length due to these two deformations and define planes which in theory could be operative habit planes, since they remain undistorted as a result of both operations. Reference to Figs. 6.4 and 6.5 shows that these operations rotate planes and vectors relative to their original positions, and the same will be true of these habit planes. Thus the mathematical formulation of the theory must include a rigid body rotation designed to rotate the undistorted plane to its original position, then the habit plane will be undistorted and unrotated as is observed experimentally.

The lattice invariant shear usually occurs in the product phase of martensitic transformations but, when using the theories, it is convenient to formally refer the shear plane and direction to the parent structure using the correspondence. The situation is somewaht simplified in the present case as the parent and product have the same symmetry. Indeed, for the first correspondence this change of basis is trivial because due to its simple nature, associated rational planes and directions in the two structures do in fact have the same indices. For an internally twinned martensite plate it has been assumed that the two twin-related regions in the plate derive from the parent by means of crystallographically equivalent correspondences (Christian 1965). This implies that for Type I twins, the rational habit plane arises from a mirror plane in the parent (Mackenzie and Bowles 1954), and for Type II twins, the rational shear direction from a two-fold axis in the parent (Ross and Crocker 1969). The observed deformation twin mode in mercury is of Type II, and it is possible that the f.c.r. structure assumed here for γ-Hg will exhibit similar Type II twins. However, no direct experimental information is available on the operative shear modes and so several possibilities were considered.

Some of these possible shear modes are given in Table 6-1. It is seen that mode 1 is the predominant observed slip system of α-Hg and mode 2 is the most likely slip system of γ-Hg as discussed in section 6.3.3, having the closest-packed plane and direction. Modes 3 and 4 are the twinning mode and its conjugate of α-Hg which involve the smallest possible shear

strain and indeed is the same as the well-established mode in the other rhombohedral metals (Hall 1954) where the axial angles are just less than 90°, like this γ-structure. Mode 5 is the observed twinning mode of α-mercury. Mode 6 is the observed high temperature slip mode. Although these modes have mainly been referred to in terms of the α-structure, the simple nature of the correspondences implies that they could equally well be operative modes in the γ-structure used in this work.

6.6. The Stereographic Analysis

6.6.1 Introduction

The simple nature of the first correspondence relating the parent and product structures lends itself to the stereographic analysis of the crystallography of martensitic transformations (Liebermann 1958). One of the principal distortion axes in this case is the $[111]_{\alpha}$ direction, the one usually chosen for the standard stereographic projection for α-mercury. Thus all lines left undistorted by the pure strain associated with the correspondence lie on a right circular cone around this $[111]_{\alpha}$ direction. The final cone is shown as B in Fig. 6.6 Now for a given shear mode the problem is to find, stereographically, vectors which are unchanged in length due to a critical amount of shear and the lattice deformation. The critical amount of shear is established by trial and error (Liebermann 1958) but in some cases possible habit planes will not exist, since no such vectors can be found. If a solution exists, there are four possible habit planes corresponding to two values of shear. The conditions for solution have been

given by Liebermann (1958).

6.6.2 Results

Using the stereographic analysis outlined above, together with the lattice invariant shears of Table 6.1 and the first correspondence, no solutions for the habit planes were found arising from modes 1, 2, 3 and 6. In these cases one or more of the conditions for solution were violated. Mode 4, whose shear plane and direction are plotted as K_4 and d_4 in Fig. 6.6, predicts two pairs of crystallographically equivalent habit planes indicated by poles 4_{a-d} in this figure. These pairs are 24° and 19° respectively from the nearest experimentally observed $\{\bar{1}13\}$ planes and are thus most unsatisfactory. Mode 5 provides and illustrative example as the shear plane is irrational, the indices being given by $(-1-5c, -1-c, 1-3c)$ where c is the cosine of the rhombohedral angle. Thus, the plane has different indices when referred to the α - and γ - bases. For the two structures, c is given by approximately $-1/7$ and $+1/7$ so that the indices become $\{\bar{1}\bar{3}5\}$ and $\{\bar{3}\bar{2}1\}$ respectively. The relevant twinning plane and direction in the γ -structure when referred, by means of the correspondence, to the α -basis are plotted as K_5 and d_5 in Fig. 6.6. The two possible associated habit plane predictions are labelled 5_a and 5_b which are at 16° and 24° respectively from the nearest observed $\{\bar{1}13\}$ habit plane. These predictions are thus again unsatisfactory. The reciprocal of mode 5 involves a $\{11\bar{1}\}$ type composition plane and like mode 1 will yield no solution.

A possible explanation is that the 82° axial angle of the γ unit cell, which is not accurately predicted by the pseudo-potential treatment, is incorrect. In particular, the larger the product axial angle, the less the distortion along $[111]_{\alpha}$ implying smaller principal strains, and the more likely that this correspondence is applicable. Thus for modes 4 and 5 this angle was varied by $\pm 5^{\circ}$. The effect of this variation manifests itself as a change in the semi-apex angle of the final cone of unextended lines and, in the case of mode 5, in the position of the shear plane. The effect on the final cone is shown by the dotted circles B' and B" in Fig. 6.6 corresponding to axial angles less than and greater than 82° respectively. Modes 1, 2, 3 and 6 again yield no solution. The variation of the predicted habit plane poles using mode 4 is shown by the solid lines passing through 4_a and 4_c in Fig. 6.6. For mode 5, the variation of the shear plane position is shown in a similar manner, but this variation together with the change in the cones leaves the habit plane predictions almost unaffected by this variation of axial angle. In no case did these predictions come within 10° of the experimentally observed plane.

With reference to the second correspondence, it was observed in section 6.4 that with a γ-phase axial angle the exact supplement to that of the α-phase, this correspondence was equivalent to a simple shear on a $\{100\}_{\alpha}$ plane. Assuming this representation for this one particular case, the observed habit plane should be either $\{100\}_{\alpha}$ with a shear direction given by $\underline{y}$ in Fig. 6.3, or the reciprocal of this

mode. The reciprocal has been found stereographically and its habit plane was found to lie 25° from $\{\bar{1}13\}$, and is thus unsatisfactory.

Therefore no significance can be attached to these predictions. In the next section the results of a full numerical analysis based on the Bullough and Bilby approach will be presented using both correspondences and including a variation of the product axial angle. The first correspondence acted as a check on the stereographic analysis just discussed, and the second was considered in more detail since it involves smaller principal strains, as shown in section 6.4.

6.7 The Bullough and Bilby Theory

6.7.1 Introduction

The graphical analysis discussed in the preceeding section is extremely valuable from an illustrative point of view, but lacks the numerical accuracy of the matrix algebra calculations. The approach of Bullough and Bilby (1956) to the algebraic versions of the theories lends itself to computer application and is based on the dislocation structure of the interface between the two phases. The transformation is regarded as proceeding by the motion of a two-dimensional array of dislocation lines, referred to as a surface dislocation, in the interface separating the two phases. The parent structure is consumed as the dislocation sweeps out regions beyond the interface, with a resultant shape change due to the shear and the concurrent lattice deformation.

In common with the other treatments the total shape deformation is regarded as an invariant plane strain and is expressed in the form

$$F = RPS$$

where F is the total shape deformation, S the simple shear, P the lattice deformation, and R a rigid body rotation. All these elements can be expressed as matrices, P being diagonal and R orthogonal. The habit plane determination again involve finding vectors unchanged in length by the combination of the two deformations, the subsequent application of a rigid body rotation ensuring a total shape deformation that is an invariant plane strain. The theory was programmed for the Elliott 503 computer by Mr.N.D.H. Ross and the habit plane determinations performed initially to see if there was any correspondence between the predictions and the observed habit.

6.7.2 Results

Using the first correspondence, this analysis confirmed the results of the previous section; no satisfactory predictionswere found. With the second correspondence, involving smaller principal strains, various predictions arose using the modes 1 - 6 of Table 6.1. In this case, the lattice deformation associated with the correspondence was not symmetrical with respect to $[111]_\alpha$ as for the first case, and different variants of these shear modes gave rise to distinct solutions. The axial angle of the product cell was varied in 1° steps from 78° to 98°. Of all the predictions of possible habit planes only one gave a pole near $\{113\}$.

Using mode 5 and a product axial angle of 82°, theindices were (0.277, 0.899, -0.341) which is 3° from (13$\bar{1}$). However, the corresponding shear direction was found to be [0.531, 0.166, 0.883] which is 20° from [101] , the observed macroscopic shear direction. Variation of the axial angle only made the prediction worse. Thus, for both correspondences, this analysis produced no acceptable predictions.

6.8 Discussion

Possible explanations of this failure to account for the observed features associated with this transformation are that the predicted product structure is incorrect or that the assumed correspondence and lattice invariant shears are unsatisfactory. The correspondences used here are the ones involving the smallest principal strains, a criterion usually found to apply on many transformations. Thus it is not likely that ones implying higher strains will suffice. The shear modes used are the ones thought most likely to occur based on previous results and consideration of the nature of the product structure, even though the criteria given for the production of a twinned product (Mackenzie and Boules 1954, Ross and Crocker 1968) are not necessarily satisfied. The results presented in this chapter constitute a fairly exhuastive application of the theories of martensite crystallography to this transformation. This has been performed assuming a product crystal structure not verified by experiment, and the failure of the application of the theories seems to be readily explained by the suggestion that this structure is in fact incorrect. Consequently, an experimental investigation, using

an X-ray diffractometer technique, aimed at determining the actual product structure was initiated and a full description of these experiments is given in the next chapter.

Finally, it may be that the theories of martensite crystallography are themselves inadequate for treating this mercury transformation and in this connection it was felt that, due to the low symmetry of both parent and product structures, this phase change could provide a challenging test to the theories. Thus, despite the experimental difficulties involved described in full in the next chapter, the attempt to determine the product crystal structure of γ-Hg appeared to be an essential part of the work conducted at these low temperatures.

Mode	1	2	3	4	5	6
Plane	$11\bar{1}$	111	011	100	-	$11\bar{1}$
Direction	$1\bar{1}0$	$1\bar{1}0$	100	011	$\bar{1}21$	101

Table 6.1 Possible shear modes of γ-Hg. Indices of mode 5 are irrational being given by (-1-5c, -1-c, 1-3c) where c is the cosine of the rhombohedral angle. For γ-Hg c is approximately + 1/7 giving indices $\{\bar{3}2\bar{1}\}$

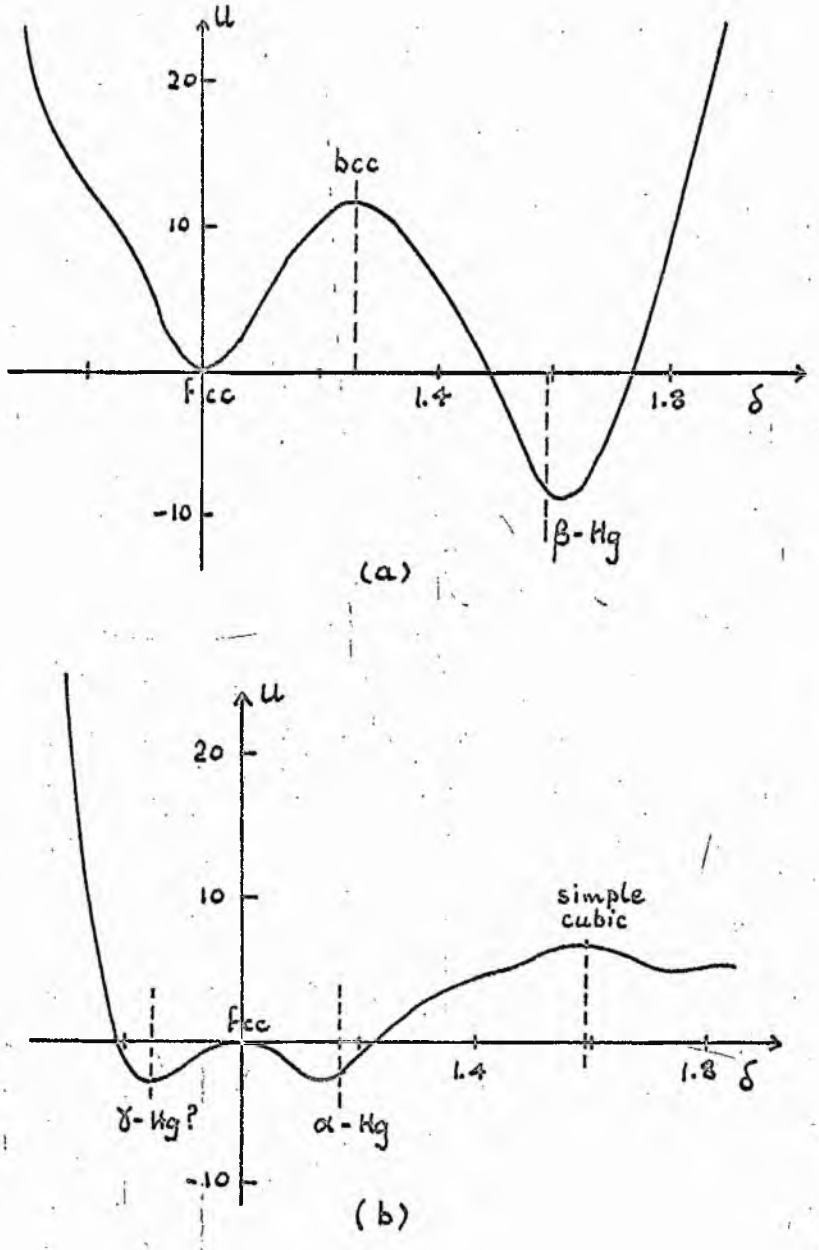

Fig. 6.1 Variation of energy (in 10^{-3}ryd /ion) with (a) tetragonal and (b) rhombohedral distortion.

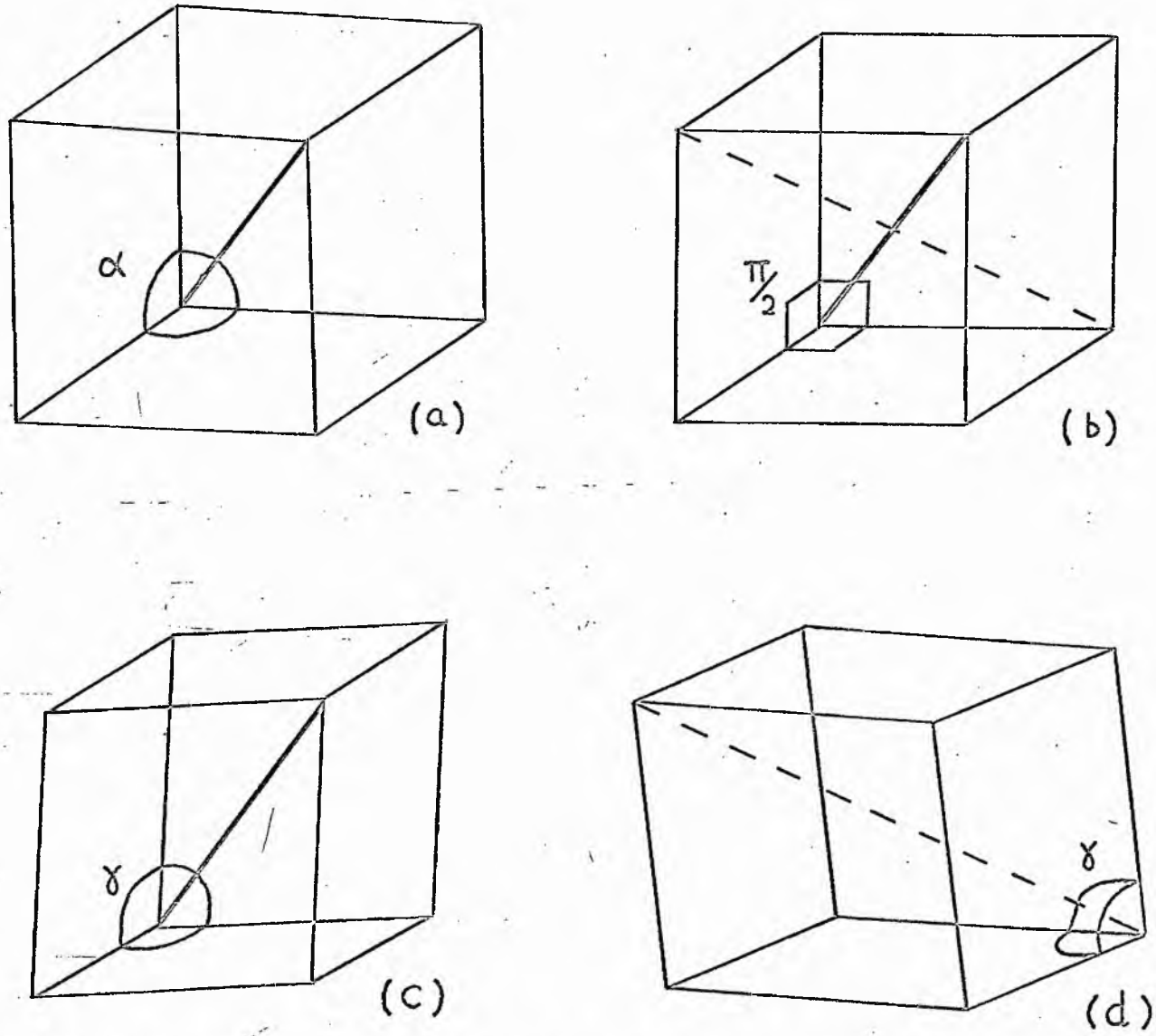

Fig. 6.2 Two correspondences relating α-Hg and the predicted structure of γ-Hg.

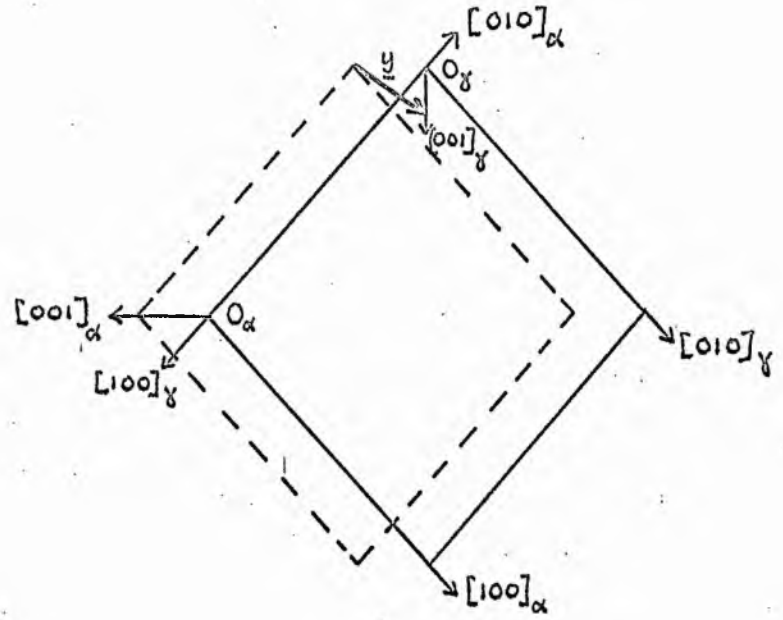

Fig. 6.3 Shearing of two $\{100\}_\alpha$ planes in direction y to produce the γ-cell having the supplementary axial angle.

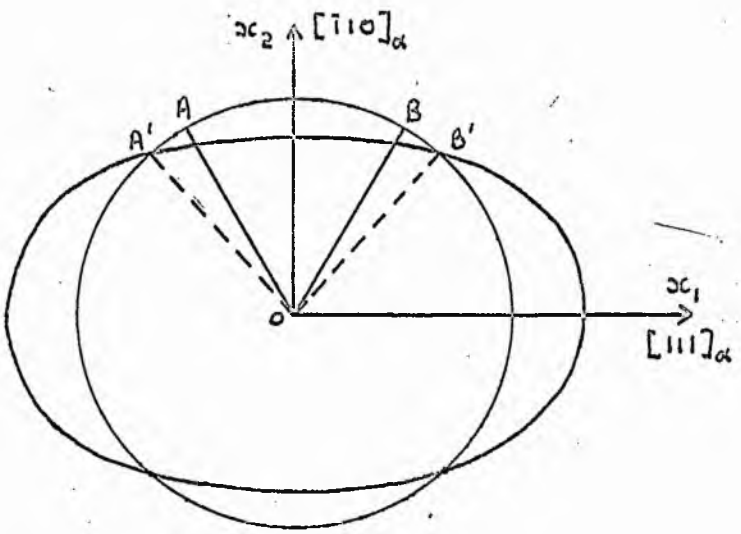

Fig. 6.4 Sphere and ellipsoid corresponding to the initial and final lattices. Cones of unextended lines are indicated.

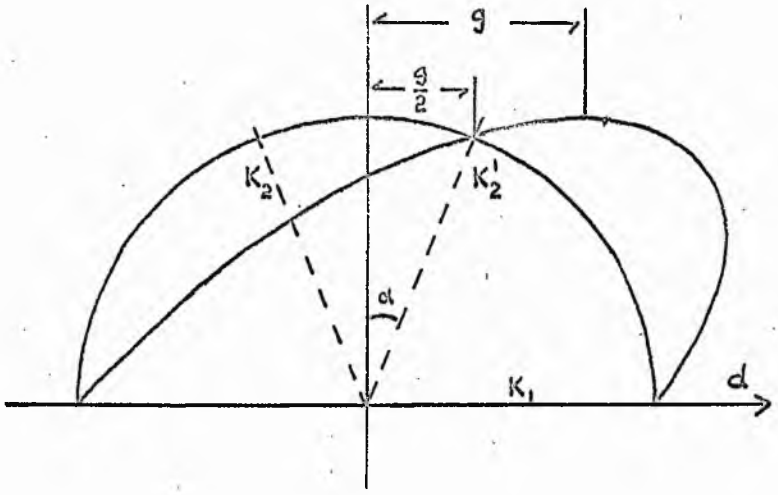

Fig.6.5 Simple shear on K_1. K_2 is undistorted after shear being rotated to K'_2.

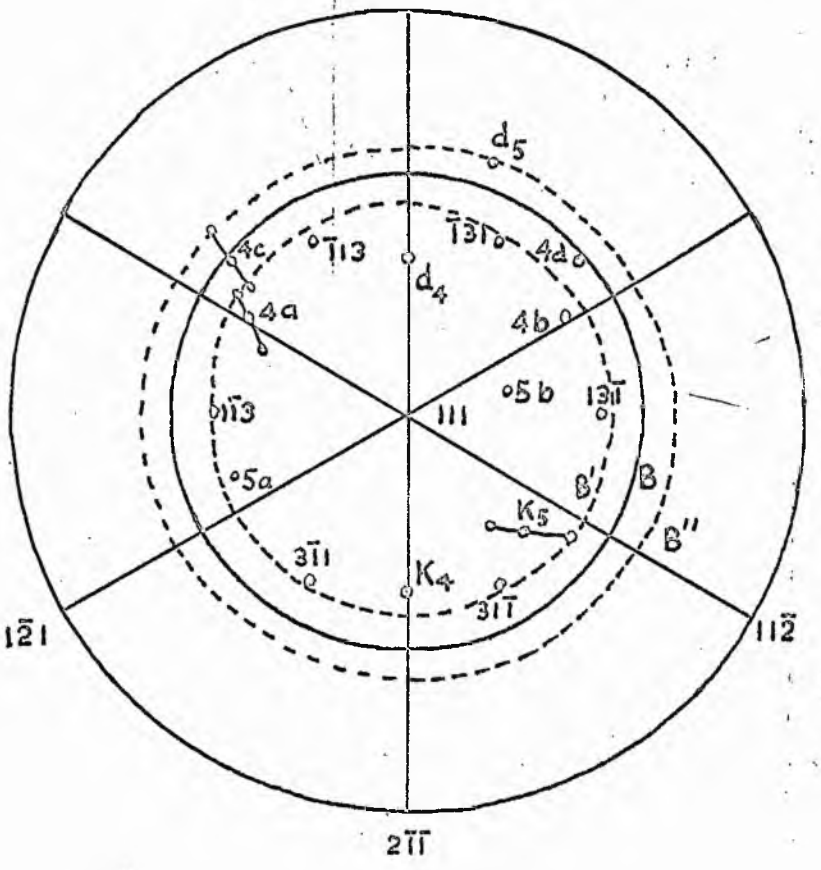

Fig. 6.6 Standard α-mercury stereogram showing habit plane predictions.

CHAPTER VII - STRUCTURE DETERMINATION OF THE γ - PHASE

7.1 Introduction

This chapter is concerned with experiments performed in an attempt to determine the crystal structure of the product γ-phase of the martensitic transformation in mercury, which has been the subject of the previous three chapters. The results presented in the last of these have clearly demonstrated that a knowledge of this structure is required before a full understanding of the transformation can be achieved. In particular, it was considered necessary to check whether the γ-Hg structure predicted using the pseudo-potential theory of metals (Weaire 1968) did in fact correspond to the actual product structure of this transformation. At the same time, these experiments would serve to establish whether the product structure is the same as that for β-mercury even though the results presented in Chapters 4 and 5 do not appear to indicate this. In order to give a complete picture of the low temperature structure studies of mercury, a short summary of the work to date will be included.

The possibility of a transformation at low temperatures was strongly suggested by Bridgman's work (1935) at high pressure. This has now been confirmed by the work of Schirber and Swenson (1963), as summarised in Chapter 4, the product phase being termed β-Hg. Using a low temperature X-ray power camera in experiments conducted at 77°K β-Hg has been found to crystallise on a b.c.t. lattice (Atoji et al. 1959).

In these experiments the sample of β -Hg was produced outside the cryostat by high pressure extrusion and subsequently inserted at 77°K prior to recording the diffraction patterns. This proved possible since the experimental temperature of 77°K was well below the reversion temperature (90°K) for the α-β transformation. Extrapolation of Bridgman's results indicated that this transformation should occur under atmospheric pressure near - 200°C. Barrett (1957) has reported a series of experiments on the structure of mercury at low temperatures involving metallographic and X-ray powder pattern studies, designed to look for a low temperature transformation at ordinary pressures. The metallographic observations involved simple cooling to 1.2°K and subsequent warming for examination, while the X-ray experiments were conducted at 5°K and included the cold-working of the surface of some samples. None of the experiments yielded results which could be interpreted in terms of the occurence of a transformation. In this respect, Barrett's work confirmed the X-ray work previously carried out on mercury, a summary of which is contained in his paper.

However, the results so far presented in this thesis show that a transformation can occur at low temperatures and atmospheric pressure under the influence of an applied tensile stress. As already discussed in Chapter 4, the product structure reported here is believed to be of a different form than β -Hg and consequently for convenience the product phase will be referred to as γ -Hg even though the results of these experiments might show that this is unjustifiable. The observed reversion temperature of this transformation of 50°K

makes the procedure of Atoji et al. impossible, and so an experimental investigation using a modified X-ray diffraction technique, to determine the product structure is reported. Suitable X-ray diffraction equipment having a low temperature cryostat attachment was not available in this department. Consequently, with the kind permission of Professor J.G. Ball, the low temperature diffractometer developed by King and Preece (1967) in the Department of Metallurgy at Imperial College has been adapted for this use. The investigation has entailed a unique modification (Abell and King 1969) of existing techniques to enable a liquid specimen to be mounted at room temperature and subsequently to apply a tensile strain at low temperatures to the cast specimen while under direct observation in the crystal. These modifications will be described in the next section, and the experimental procedure and results obtained appear in subsequent sections followed by a discussion of the results.

7.2 Experimental Technique

7.2.1 Diffraction Equipment

The low temperature diffraction equipment consisted of a Siemen's diffractometer and X-ray tube placed on an Elliot 315/Gx8 Type X-ray Generator with the cryostat mounted on the diffractometer in place of the standard specimen holder. The cryostat stands on a cylindrical frame with sections cut out to allow the removal of a tail-piece at an O-ring vacuum seal. Thus, direct access to the specimen is possible permitting it to be mounted or removed without misaligning the cryostat with respect to the diffractometer. Precision rotation and translation mechanisms in the base of the support frame enables the specimen surface to be aligned at all temperatures, and the

cutaway shape of this frame allows scanning of the Bragg angles from zero up to 163°, 2θ, on the normal side of the beam. For precise lattice parameter measurements both sides of scanning are used and angles from 30° to 163° are possible on the reverse side. Only the normal side was used in these experiments and because of the necessary modifications, described later, the effective range of Bragg angles was reduced to 10° - 125°, 2θ.

Filtered Cu K_α radiation was used for all the experiments the diffracted beam being detected by a Xe proportional counter and recorded graphically. Two main scanning speeds of 2° min^{-1} and $\frac{1}{4}$° min^{-1} were employed, these two being referred to as the fast and slow scans respectively throughout this chapter. Appropriate chart speeds were chosen so that 1 cm of chart paper represents 1° or $\frac{1}{4}$° according to which scanning speed was being used. A $\frac{1}{2}$° divergent slit with a 0.4 mm receiving slit were most often used but these varied according to specimen conditions.

7.2.2 The Cryostat

The low temperature attachment was designed by H.W. King and C.M. Preece of Imperial College and constructed by Oxford Instrument Company. A schematic representation is shown in Fig. 7.1 The outer case is made of bright nickel plated brass and is supported by the cylindrical frame at its base. Suspended inside from the top is a liquid helium reservoir made of thin-walled stainless steel labelled (1) in Fig. 7.1. Round the base of this reservoir is an annular section liquid nitrogen vessel (3) made of copper with which the helium reservoir maintains thermal contact at joint (2). Specimens for X-ray examination are attached to the copper block (4), in thermal contact with the helium reservoir, which is surrounded by a copper radiation shield (5) cooled

by the liquid nitrogen in (3). A 180° X-ray window (6) cut in the outer case tail-piece and in the radiation shield are covered in 175μ Mylar which has aluminium evaporated on it to reduce thermal radiation. These two radiation shields have been modified in the present experiments, the alterations being described in the next section.

Liquid helium temperatures can be maintained for up to 6 hours in the cryostat and higher specimen temperatures can be obtained using the electrical heater (7) in conjunction with a thermal spacer (8). In the experiments described here, (8) was replaced by a copper block as the lowest temperatures possible were required. The temperatures were measured by a Au-0.03% Fe/chromel thermocouple. The selection of specimen mount for use in the cryostat depends on the type of information required but must be designed such that the specimen surface contains the axis of the diffractometer.

7.2.3 Modifications and Specimen Preparation

The modifications necessary for use with mercury arise from the following three points:

1. In normal use a specimen is mounted in the cryostat in a vertical plane; further, it has to be mounted at room temperature in order that a high enough vacuum can be obtained to ensure thermal insulation during the subsequent functioning at low temperatures. These two facts present obvious difficulties in this case, and special consideration had to be given to the design of the specimen mount to overcome the problems arising from mercury being a liquid at room temperature.

2. The X-ray diffractometer method depends on the ability of a small grain sample, usually in the form of a powder, to give strong diffraction rings. Since the mercury sample will be loaded in the liquid form and subsequently cooled, provision must be made for ensuring the occurence of a small grain size when it solidifies.

3. Since the transformation product is not produced by simple cooling but needs the application of a tensile stress, it was considered necessary for the specimen mount to have a miniature tensile jig incorporated in it, together with a suitable attachment to the cryostat so that a measured amount of strain can be imparted to the specimen while under direct observation in the cryostat. This attachment needs to be operative from outside the cryostat and must not strain one part of the cryostat relative to another for fear of misalignment.

A prototype specimen holder was designed to test the first two of these points since these had to be overcome before the most involved design problems, necessary for the construction of the straining jig, were considered. A diagram of this prototype appears in Fig. 7.2. The mount, made of copper, is in two pieces which are screwed together before inserting on the tail of the cryostat (4) shown in Fig. 7.1. The sample of liquid Hg in the form of a small pool is located in the rectangular recess in component A which is held horizontally. The recess and its surrounds have previously been coated with silicone grease to prevent amalgamation. A small piece of Mylar is then placed over the surface of the pool of mercury pressing the liquid level flat

so that the surface lies in the plane of the surface of component A and the mercury occupies as much of the recess as possible. The Mylar adheres sufficiently to the silicone grease to maintain the mercury surface flat. The amount of liquid mercury to be placed in the recess is found largely by experience. The components A and B are then screwed together, securing the Mylar sheet and thus the mercury sample, and upon turning the whole mount vertical, the mercury is found to stay in position. The mount was so designed that when the whole assembly was located by means of three dowel pins and allen screws in the tail of the cryostat, the plane of contact of components A and B lay in the reference plane of the diffractometer circle. Thus the specimen surface was automatically aligned, upon the location on the cryostat tail, in the correct position for subsequent diffractomer runs. The size of the specimen was approximately 10 x 5 x 2 mm. The access to the window in component B was shamferred to permit low angles of incidence of the X-ray beam to be used.

The method used to ensure a small grain size specimen, which could not be achieved upon subsequent cooling, was to cold work the surface of the mercury after it had solidified with a subsequent anneal if necessary. The alternative method of using a suspension of small droplets of mercury was not considered suitable since, in this case, the applied tensile stress necessary to produce the transformation would not be transmitted to the whole of the specimen under X-ray observation. Provision for this cold working necessitated re-designing the cryostat outer tail piece and copper radiation shield. The outer case was fitted with a probe, sliding on

an O-ring seal, which in turn passed through a clearence hole in the inner radiation shield and could locate on the specimen surface. This sliding O-ring vacuum seal system was much simpler to construct than the bellows system Barrett (1957) used to cold-work his specimens and, as the results presented later will show, proved just as effective. The end of the probe, which is called the cold-work probe, was lathed to leave an eccentric chiselled edge on the end as shown in Fig. 7.3. By rotating the probe, the whole specimen surface could be cold worked since the axis of rotation was positioned to be perpendicular to the centre of the specimen area. The probe could be withdrawn to the outer shield when not in use to preserve the thermal insulation and so not to obscure the path of the X-ray beam. The windows in the shields secured with Araldite AY111, were 175μ thick and coated with a thin layer of aluminium to minimise thermal radiation to the cold specimen.

It now becomes clear how critical is the choice of the material used to cover the mercury specimen when it is initially mounted at room temperature. It has to be sufficiently strong to prevent the mercury bulging in the liquid state when the assembly is mounted vertically. It must be as thin as possible, and have low X-ray absorptivity to ensure no loss of intensity when the sample is irradiated. It must be non-crystalline or spurious reflections would be obtained. Further it must be durable enough to withstand cooling to extremely low temperatures and the subsequent warming. Above all it should be of such a composition that

the cold-working using the probe described above is transmitted through it to the mercury, but that this working does not break it at the working temperature. If it did break on the subsequent heating up to room temperature at the end of the experiment, the mercury would not only fall out of the specimen mount but proceed to evaporate under the high vacuum and contaminate the whole cryostat.

Several plastic films and sheets were tested for suitability and it was found that 50 μ thick Mylar polyester film satisfied all these conditions. This Mylar film was observed to give one strong broad X-ray reflection, similar to that from the liquid state, which occurred at a 2θ value of approximately 28.5° with the Cu characteristic radiation used in these experiments. It, therefore, did not interfere with the reflections from the α-structure but could concievably, however, mask a reflection from the product γ-Hg. This possibility could not be avoided since no alternative material was available which could satisfy the above conditions as well as Mylar and have a reflection at a lower 2θ value.

Using the first part of the procedure described in section 7.3, preliminary runs at 77°K with this specimen assembly showed that the principle involved in this arrangement were adequate to overcome the first two problems set out previously. The criterion employed for the satisfaction of the second of these points, that is the small enough grain size, was the the diffraction peaks obtained at 77°K corresponding to the α-Hg structure, should be of an intensity not less than 1×10^4 cps. This figure will be discussed in section 7.4.

7.2.4 Final Design

The success of the prototype in overcoming some of the technical problems described have enabled the consideration of the design of the final specimen mount which would incorporate the tensile jig necessary for the eventual production of the χ-phase. The final design consisted of three parts, photographs of which are shown in Fig. 7.3 (a) and (b), the first showing the three components and the second the completed assembly. A line diagram of the specimen mount, radiation shield and outer tail piece in position on the cryostat is shown as Fig. 7.4 (a). The overall specimen assembly has much the same form as the prototype. However, in this case the specimen recess (9) was in the form of a tensile-shaped cast, the lower half of which could move with respect to the upper. This movement is controlled by the brass screw (10) on the back of the assembly, the head of which points downwards when the mount is in position in the reference plane (11) on the cryostat tail. The groove in thehead of this screw is purposely widened in order that a second probe (12), built in to the bottom of the outer case of the cryostat again through a sliding O-ring seal, having a corresponding screwdriver tip, can locate when the applied stress is required. Simple rotations of this probe are again adequate, in this case the strain all being taken within the specimen mount resulting in no misalignment. This probe, termed the tensile probe, may be withdrawn in a similar manner to the cold-work probe when not in use. However, because the tensile probe is likely to be in contact with the specimen mounting for longer periods while the stress is being applied, it was made from nylon to

minimise the thermal path, a precaution not found necessary for the cold-work probe. A photograph of the final outer tail piece assembly showing the two probes and the inner radiation shield appear as Fig. 7.4(b). The size of the gauge length of the specimen was 8 x 2 x 2 mm and the component containing the specimen recess was Ni-plated to prevent amalgamation.

In the preliminary tests of this assembly, it was found to be advantageous to line the specimen recess with Mylar film to facilitate the movement of the specimen gauge length during the tensile test. Similarly it was found that 25μ thick Mylar film could be used to retain the liquid in the recess on locating the jig in the cryostat. This had the effect of cutting down the X-ray absorption, but more important of making the cold-working of the specimen surface more effective. For this specimen assembly the cold-work probe, when in use, locates on the gauge length of the tensile-shaped specimen. Thus the small grain size was produced precisely in the region where the γ-phase would be produced upon application of the tensile stress.

7.3 Experimental Procedure

The evidence of the previous three chapters indicates that a total transition to the γ-phase is not usually achieved. Consequently at low temperatures the diffractometer traces which will be recorded after the applied tensile stress will correspond to a superimposition of two patterns, one due to the remaining α-structure the other associated with new γ-phase. Thus the procedure to be adopted will involve an effective subtraction of traces, one before the tensile stress has been applied, being that of the virgin α-phase, the other after

the stress which will record both the α and γ patterns.

After locating the specimen assembly on the cryostat tail and securing it there, and attaching the radiation shields the whole inner space is evacuated to less than 10^{-6} cm Hg. Liquid nitrogen is added to the outer refrigerant container, followed by a small amount to the inner container until the specimen temperature reaches 77°K. A quick scan through the expected α-Hg diffraction peaks at this stage invariably indicates that a small enough grain size has not been achieved. The surface of the specimen is then cold-worked using the appropriate probe, being careful not to leave the probe in contact with the specimen too long. A subsequent scan usually reveals the peaks corresponding to the α-structure.

The description so far corresponds to the procedure necessary to ensure that a satisfactory specimen has been prepared. The remainder of the experimental technique involves the initiation of the transformation, having cooled down to a suitable temperature, and the attempted detection of the structure of the new phase. Liquid helium is transferred to the inner dewar and the diffractometer scan repeated to ensure no change in the condition of the specimen. A series of scans is then performed, incremental amounts of tensile strain being applied before recording each set of traces. It was found possible to impart large strains to the specimens (100%) and as shown in the next section these strains were invariably absorbed by the gauge length under observation.

Having recorded the traces at low temperatures corresponding to the effect of increments of strain on the diffracting

properties of the specimen, the temperature was allowed to rise either by the use of the heater in the cryostat tail or by allowing all the liquid helium to boil off. Scans through 2θ values were recorded as often as possible during this period until the temperature reached approximately 77°K where it usually reamined for long periods because of the liquid N_2 in the outer space.

7.4 Results

Cold working of the specimen surface at 77°K prior to initiating the transformation at liquid He temperatures invariably produced well-defined diffraction peaks corresponding to the α-mercury structure. A subsequent anneal at higher temperatures was therefore not considered necessary. Part of a set of such peaks is reproduced as Fig. 7.5(a) which shows two α-mercury reflections having the lowest 2θ values. The corresponding planes are also indicated in the figure. A list for the 2θ range 0° - 100° of the α-mercury diffraction peaks with the corresponding 2θ values calculated for the Cu K_α radiation used in these experiments is presented in Table 7.1. This table also includes the possible reflections from a structure based on the predictions of the pseudopotential theory presented in Chapter 6. It will be recalled that according to this theory the product γ-structure would have the same symmetry as the parent but with an axial angle of approximately 82°. These values presented in Table 7.1 have been found assuming an axial angle equal to the supplement of the parent α-cell.

The intensities of the γ -peaks it was hoped to detect would be smaller than those corresponding to the α -structure, and would be directly related to the intensities of these α -peaks, their size depending on the amount of transformation achieved. Consequently, it was necessary to set a minimum intensity for the initial α -peaks in order that the subsequently produced γ -peaks would be of sufficient intensity to be readily detectable. With the experience gained in examining these mercury samples a minimum intensity of 1×10^4 cps with the usual slit systems was decided upon. On cooling the specimens by the addition of liquid helium, temperatures of below $20^{\circ}K$ were obtained, the form of the diffractometer traces as a result of this simple cooling being the same as at $77^{\circ}K$ as shown in Fig. 7.5(b).

The effect of applied tensile strains at low temperatures on the diffracting properties of the specimens is indicated in Fig. 7.5(c). This represents a scan taken after a 25% tensile strain on one typical speciment. It is observed that the intensities of the α -peaks have decreased with the increase of applied strain. This clearly demonstrates that the applied strain is being successfully imparted to the specimen gauge length, that is the part of the specimen under X-ray observation. Seven specimens which exhibited this effect were examined in detail to find evidence of a transformation product in the form of the appearance of additional diffraction peaks. For three of these a new peak has been observed as can be seen in Fig. 7.5(c) where the additional peak occurs at a slightly greater 2θ value than the $(11\bar{1})_{\alpha}$

reflection. Further, on one specimen a second additional peak has been observed at a higher 2θ value, removed from such close proximity to a parent α-peak. Traces in this higher 2θ region corresponding to the as-grown specimen at 77°K and 20°K and to the same specimen after approximately 75% strain appeared as Fig. 7.6(a), (b) and (c) respectively. Traces (d) of both Figs 7.5 and 7.6 represent scans through the same regions after the temperature had been allowed to rise to approximately 77°K, where it can be seen that the additional peaks observed at 20°K no longer appear.

Slow scans through the 2θ region containing these additional peaks revealed the profiles shown in Fig. 7.7, where (a) shows the $(11\bar{1})_\alpha$ peak with the first new peak close to it, and (b) the second additional peak at higher 2θ. The values of 2θ for these new reflections measured from similar slow scan appear in Table 7.2 with the corresponding values of interplanar spacing. The new reflections have been termed $(h_1k_1l_1)_\gamma$ and $(h_2k_2l_2)_\gamma$ since it is felt that they correspond to crystallographic reflections from the transformation product structure, which has already been termed γ-mercury.

Similar scans through the same 2θ regions were performed as the temperature of the specimens was allowed to rise, and for temperatures about 50°K, the profiles shown in (c) and (d) of Fig. 7.7 were obtained. Again it is apparent that the new peaks disappear as the temperature rises, the observed critical temperature for this transition being approximately 50°K. Careful inspection of the remaining 2θ range available on these traces has unfortunately revealed no further additional diffraction peaks.

The structure of the profiles of the α -diffraction peaks at different strains has been used to construct the graphs of peak intensity and peak area as a function of strain. Graphs corresponding to the behaviour of two of these peaks, the $(11\bar{1})_\alpha$ and the composite $(111, 100)_\alpha$, are shown in Fig. 7.8(a) and (b). Also plotted here are similar curves for the $(h_1k_1l_1)\gamma$ diffraction peak; it should be noted that the α- and γ -peaks have been plotted with reference to different scales and in the case of Fig. 7.5(b), the scale for the γ -peak area is approximately an order of magnitude less than that for the α-peaks. However, qualitative deductions are possible, and for the α -peaks both the intensity and area decrease with strain whereas for the γ -peak there is an initial increase followed by a decrease with increasing strain. However, the ratio of the area of the γ -peak to that of the $(11\bar{1})_\alpha$ peak when plotted as a function of strain is found to increase as is clear from Fig. 7.9.

7.5 Discussion

The appearance, clearly indicated in Fig. 7.7(a) and (b), of the two new reflections after straining at low temperatures cannot be explained in terms of a possible Cu or Ni reflection, corresponding to the specimen holder; nor is it attributable to Cu K_β reflections from the α -Hg structure, since in neither case do the 2θ values agree. They remain reproducible over a period of time and thus spurious X-ray source fluctuations are not responsible. Consequently the only possible interpretation is that they correspond to reflections from the product structure as a result of a partial transformation induced by the tensile strain at low temperature. This explanation is

consistent with the results presented in previous chapters where it was found that simple applied tensile stress at 4.2°K produced the transformation, the detection of the product phase in that case being achieved through superconductivity and electrical resistance measurements. The disappearance of the peaks for temperatures above 50°K indicating a full reversion back to the parent α-structure is again in agreement with the previous observations of this temperature presented in Chapter 4.

Further support in terms of evidence of a shear transformation can be found by considering the curves in Fig. 7.8. For α-reflections, both the peak intensity and the peak area fall off in a similar manner with increasing strain. If, as a result of the tensile strain, the α-structure had been deforming by conventional slip the peak would have been broadened, with an associated fall in peak intensity, but the area would have remained approximately constant. However, in this case the energy of the α-reflection is being directly transferred into the $(h_1 k_1 l_1)_\gamma$ reflection with no significant broadening and with a resultant fall in α-peak intensity and area. Further, Fig. 7.9 shows that the proportion transformed increases with strain as one would expect even though in absolute terms the size of the $(h_1 k_1 l_1)_\gamma$ peak above background level decreases at high strains. The rate of increase of the proportion of $(h_1 k_1 l_1)_\gamma$ to $(11\bar{1})_\alpha$ with strain appears to level off at high strains as the amount of γ produced reaches a maximum, this level indicating that over a 2/5ths transformation is usually achieved. Further observation of the

diffractometer traces showed that the two new peaks appear broad when compared with the α -reflections. This can be explained by regarding most of the internal strain to be in the product phase and not in the parent material, this interpretation being consistent with the occurrence of an internally strained martensite product phase. However, at higher strains the α -peaks begin to broaden as the rate of production of the new phase levels off and inevitably some of the strain is imparted to the α -lattice causing slip and resultant broadening.

Having interpreted the results in terms of a shear transformation, it remains to infer as much as possible about the product structure to which the reflections correspond, since a full structure determination is obviously not possible using these results. It should be noted first of all that the reflections are not attributable to the body-centred tetragonal structure. This is clearly indicated in Table 7.2 where the last two columns give the β -Hg body-centred tetragonal reflections and corresponding d-spacings lying nearest the observed values. It can thus be inferred that the product structure being observed in these experiments is distinct from that of the β -phase, thus demonstrating the unique nature of the transformation product under discussion.

As mentioned in Chapter 4 some of the observations on this transformation have led Barrett (1968) to suggest an explanation in terms of the $\alpha - \beta$ transformation. It was pointed out at that stage that in particular the critical temperature observations were inconsistent with this suggestion. It is felt that the evidence reported in this

chapter is even more indicative of the fact that such an interpretation is not feasible. It is therefore proposed that the product phase being observed is that of the $\alpha - \gamma$ transformation in mercury as was the proposal following the results obtained in Chapter 4.

Comparison of the 2θ values of the γ-structure predicted on the basis of the pseudopotential theory and the observed 2θ values in Tables 7.1 and 7.2 respectively, shows that there is no agreement for either new reflection. Thus, this predicted structure, having the supplementary axial angle to the parent α -cell does not coincide with the observed structure. Variation of the axial angle of the product cell, a parameter not accurately predicted by the pseudopotential treatment, while retaining the rhombohedral symmetry, indicates, as shown in Fig. 7.10, that the axial angle would need to be either 94° or 89° for a crystallographic reflection of the predicted structure to correspond closely with the observed $(h_1k_1l_1)_\gamma$ peak. This situation is considered most unlikely since both the resultant structures would be too closely allied to f.c.c., a structure not acceptable to pseudopotential theory (Weaire 1968). Another possibility considered by Weaire is an h.c.p. structure with c/a about 2.0. An interpretation in terms of this structure with this axial ratio has also proved unsatisfactory.

The $(h_2k_2l_2)_\gamma$ reflection appears much broader than the $(h_1k_1l_1)_\gamma$ peak; this is to be expected since the effect of broadening increases with the Bragg angle. However, the possibility of $(h_2k_2l_2)_\gamma$ being composed of more than one

crystallographic reflection was investigated. In particular, the second order reflection from $(h_1k_1l_1)\gamma$ does not contribute to this higher angle peak, since this second order reflection would occur at a 2θ of 69.75°, but in these experiments was not detectable above the background radiation. The dependence of the broadening of peaks on the Bragg angle makes it possible to deduce the expected breadth of a high angle peak assuming the breadth of a low angle peak. This has been done for the two observed peaks and it was found that the broadening of the $(h_2k_2l_2)\gamma$ was consistent with that of the $(h_1k_1l_1)\gamma$ reflection. Thus it may be assumed that the $(h_2k_2l_2)\gamma$ reflection corresponds to a unique crystallographic reflection of the γ -mercury structure.

We therefore have observed two reflections from the product structure of the $\alpha - \gamma$ transformation, and while it is unfortunate that a full structure determination has not proved possible, it is encouraging that the results obtained so far do confirm the observations of the previous three chapters. The lack of observation of further γ-Hg reflections and the failure rate in the performance of these experiments indicates the importance of the condition of the specimen examined. The remaining reflections of the γ-Hg structure in these experiments are presumably not strong enough to be detectable above the background level. The implication is that more intense reflections from the initial α-structure at $77^{\circ}K$ should be sought since, as mentioned before, the eventual intensity of the γ-reflections is inevitably related to that of the α-peaks.

In addition it is worth noting that the lowest temperature as yet achieved using the cryostat is approximately 18°K which is well above the temperatures at which the transformation was first observed to occur readily. It may well be that at this higher temperature the transformation is more difficult to initiate, thus acting as a contributing factor to the failure rate. By addition of a further radiation shield cooled by liquid helium, temperatures down to approximately 6°K would be obtainable. Although this temperature effect was not a significant factor in Barrett's (1957) work, the high observed failure rate associated with the production of this transformation, due largely to specimen condition, may serve to explain why his results indicated no evidence of a transformation. It is true that a different form of working the specimen at low temperatures was used in the experiments reported here, but it is felt that no significant difference in the conditions necessary for the transformation to occur would result from this.

In conclusion the results presented in this chapter indicate very strongly that the product structure observed in these experiments corresponds to a unique phase of crystalline mercury and should not be confused with the β-phase. It is reasonable to assume that the product phase in these experiments is in no way different from that whose properties have been observed in the superconductivity and electrical resistance experiments reported in Chapters 4 and 5, and which was termed γ-Hg. On the basis of results presented here and in Chapter 4 it can thus be implied that both the properties of the product phase and the nature of its production serve to

distinguish the α - γ transformation from the previously reported α - β transition. However, this cannot be considered to be rigorously established until a full structure determination has been performed.

α - Hg		γ - Hg	
hkl	2θ	hkl	2θ
$11\bar{1}$	32.69	111	29.86
100	40.38	$11\bar{1}$	36.03
111	40.49	100	40.06
$1\bar{1}0$	52.79	011	54.03
$11\bar{3}$	63.51	$01\bar{1}$	61.98
011	63.75	222	62.03
$22\bar{2}$	68.51	113	62.96
$1\bar{1}3$	68.58	$1\bar{1}3$	70.30
113	78.30	$11\bar{3}$	73.85
$13\bar{3}$	87.10	$22\bar{2}$	86.75
200	87.32	$\bar{1}33$	94.37
222	87.51		
$0\bar{1}2$	91.67		

Table 7.1 2Θ values for parent structure and predicted product structure

Refln.	$2\Theta_{obs.}$	$d_{obs.}$ Å	d_β Å	$(hkl)_\beta$
$(h_1k_1l_1)_\gamma$	33.24 33.29 33.19	2.6935	2.824	110
			2.303	101
$(h_2k_2l_2)_\gamma$	72.70	1.3000	1.414	220, 002
			1.263	112, 130

Table 7.2 Comparison of observed 2Θ and d values with those for beta - mercury.

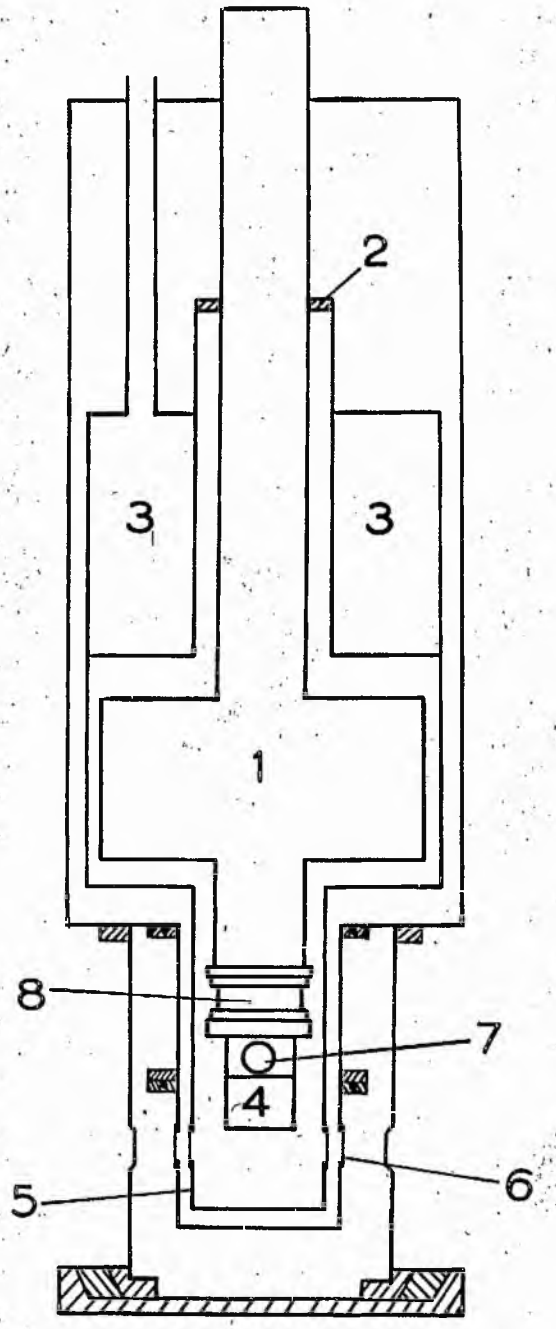

Fig. 7.I Cryostat attachment for X-ray diffractometer

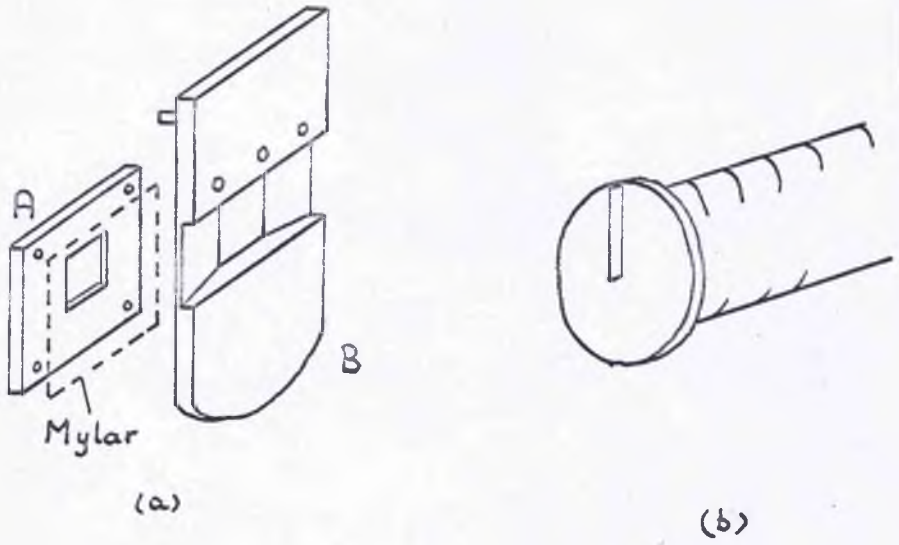

Fig. 7.2 (a) Components of initial specimen holder
(b) Chiselled end of cold - work probe

Fig. 7.3 Final specimen jig : (a) the three components
(b) the complete assembly

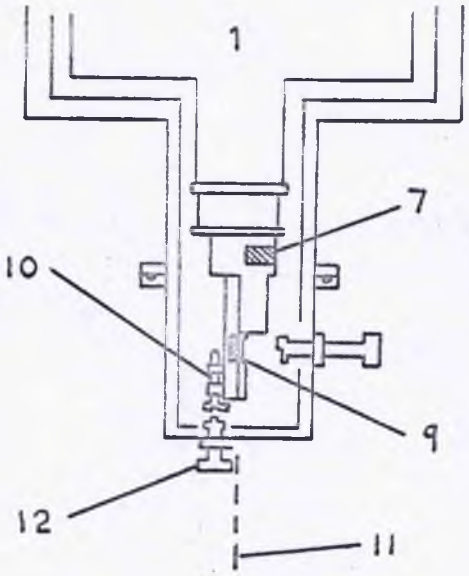

Fig. 7.4 (a) Lower end of cryostat showing modifications

Fig. 7.4 (b) Outer vacuum shield with its two probes, and the inner radiation shield.

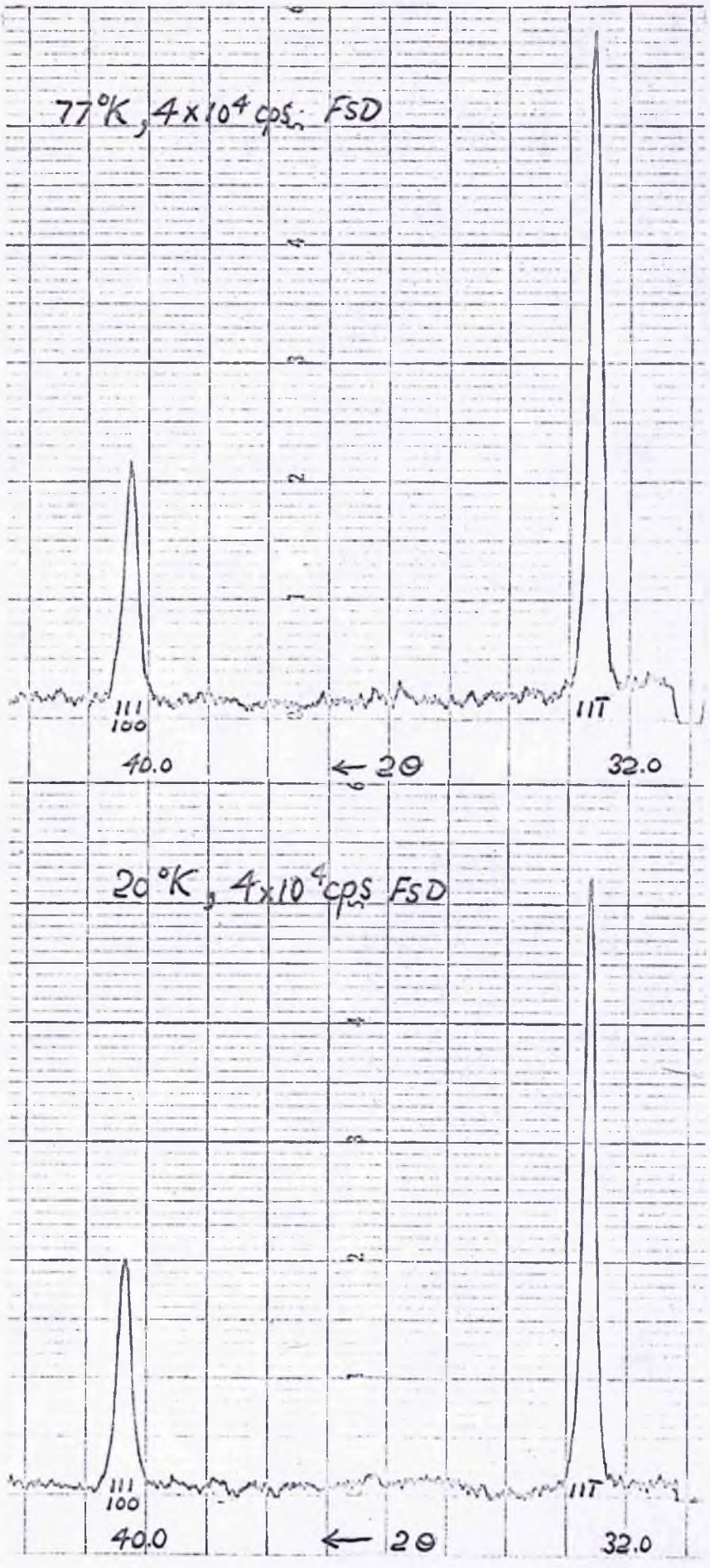

Fig. 7.5 Scan through the first two low angle reflections of α-mercury at (a) 77°K, (b) 20°K.

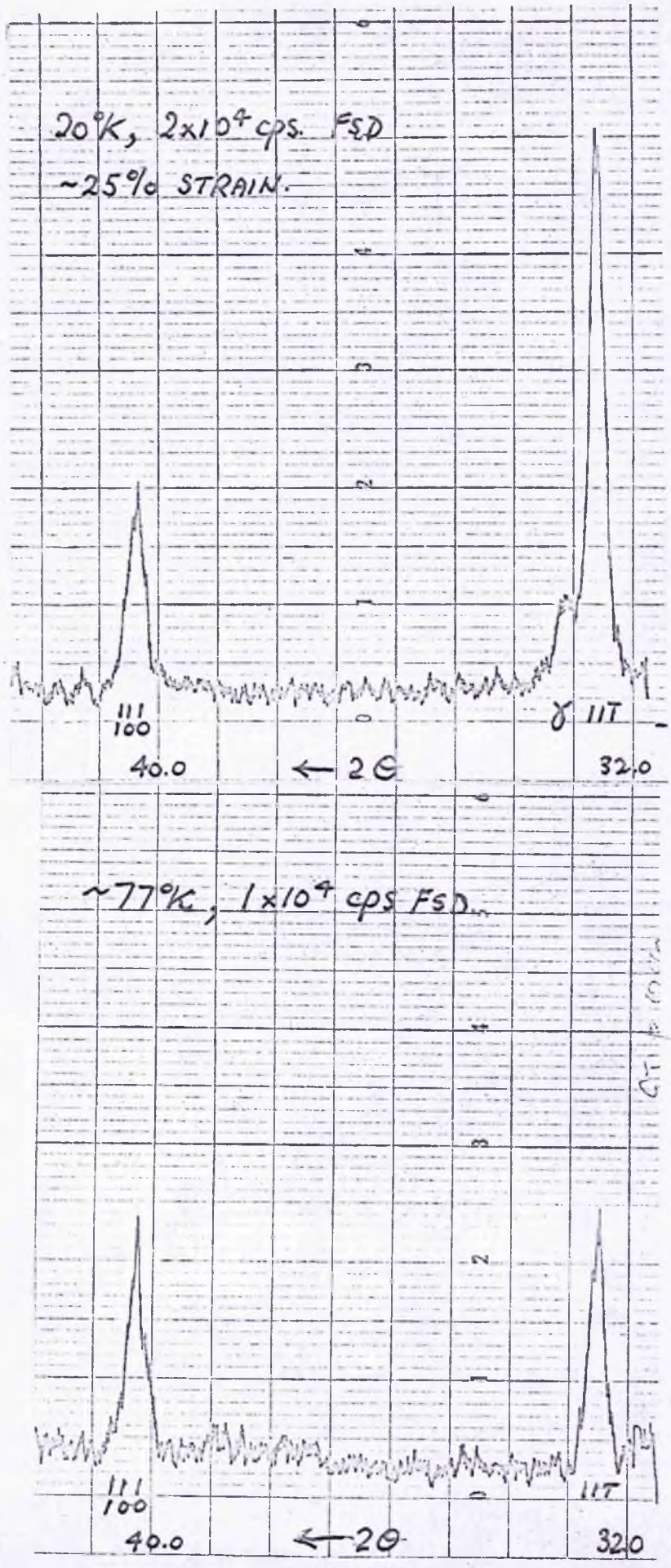

Fig. 7.5(contd.) Similar scans (a) after strain at 20°K, showing additional peak; and (b) after warming up to 77°K - the new peak has disappeared

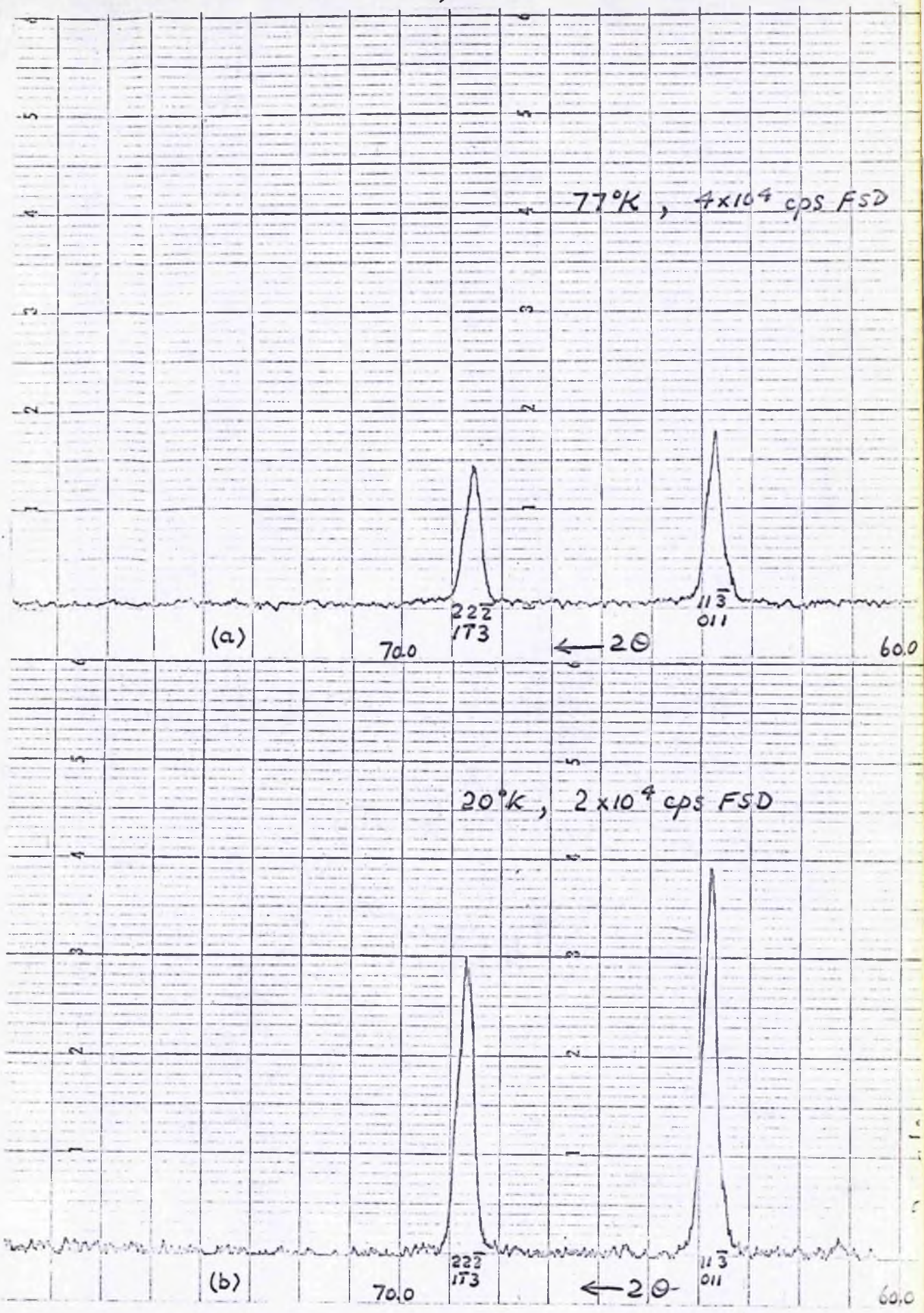

Fig. 7.6 Scan of 2θ from 60° to 79° showing two α-Hg reflections at (a) 77°K and (b) 20°K

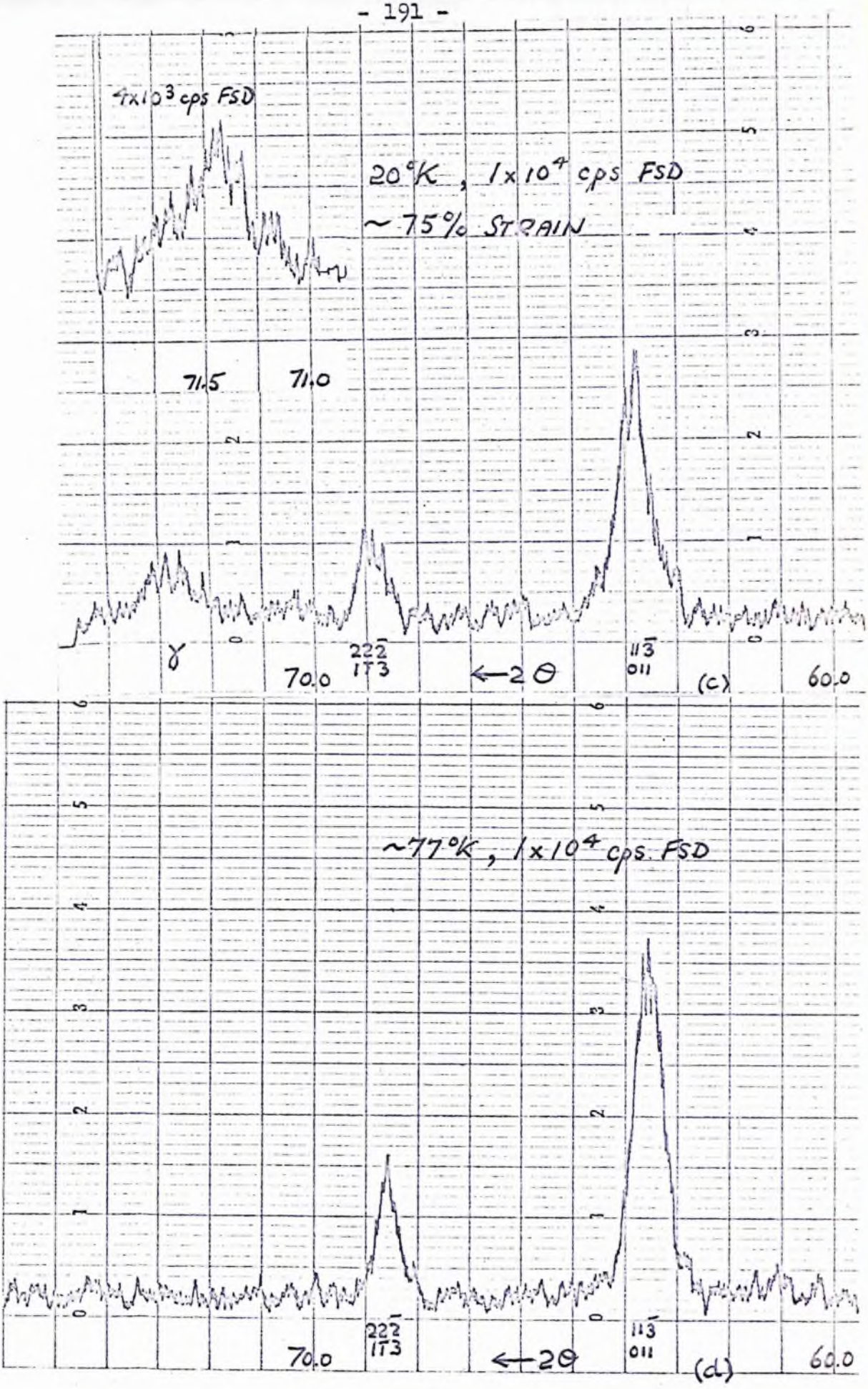

Fig. 7.6(contd.) (c) second additional peak after strain at 20°K

(d) same scan after warming up to 77°K

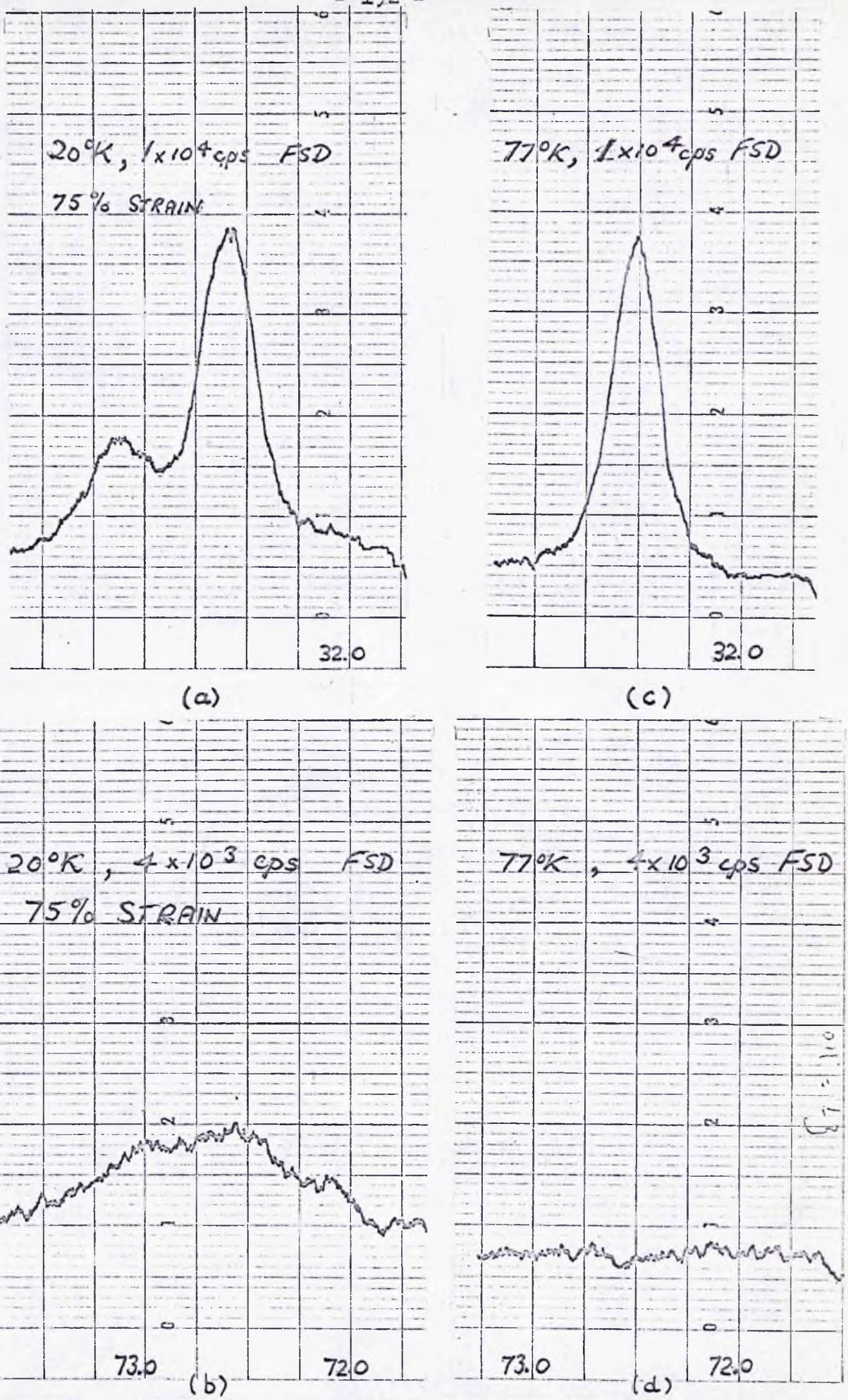

Fig. 7.7 Slow scans: (a),(b) the new peaks; (c),(d) same regions, 77°K

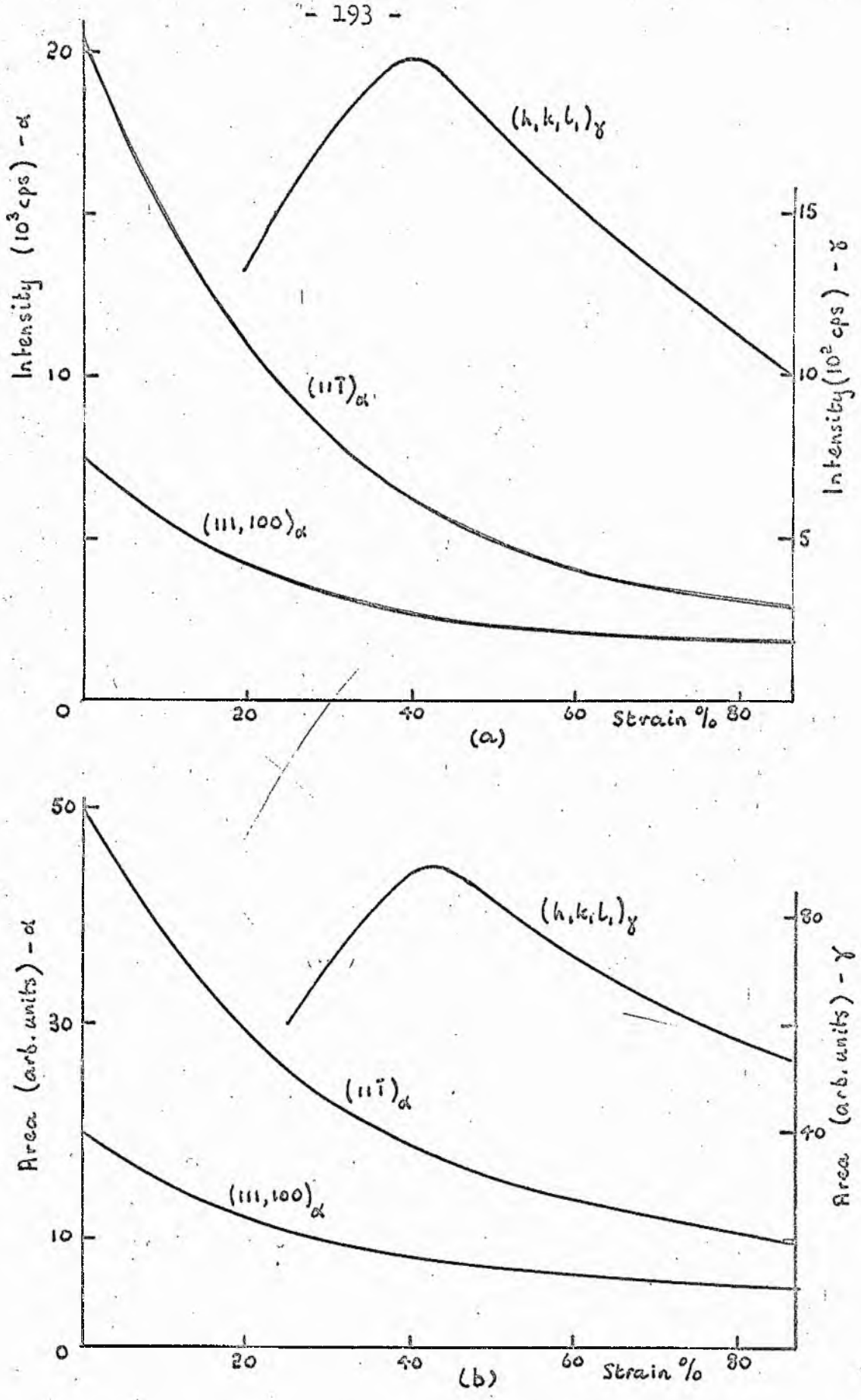

Fig. 7.8 (a) Intensity, and (b) area vs. strain for α - and γ - peaks

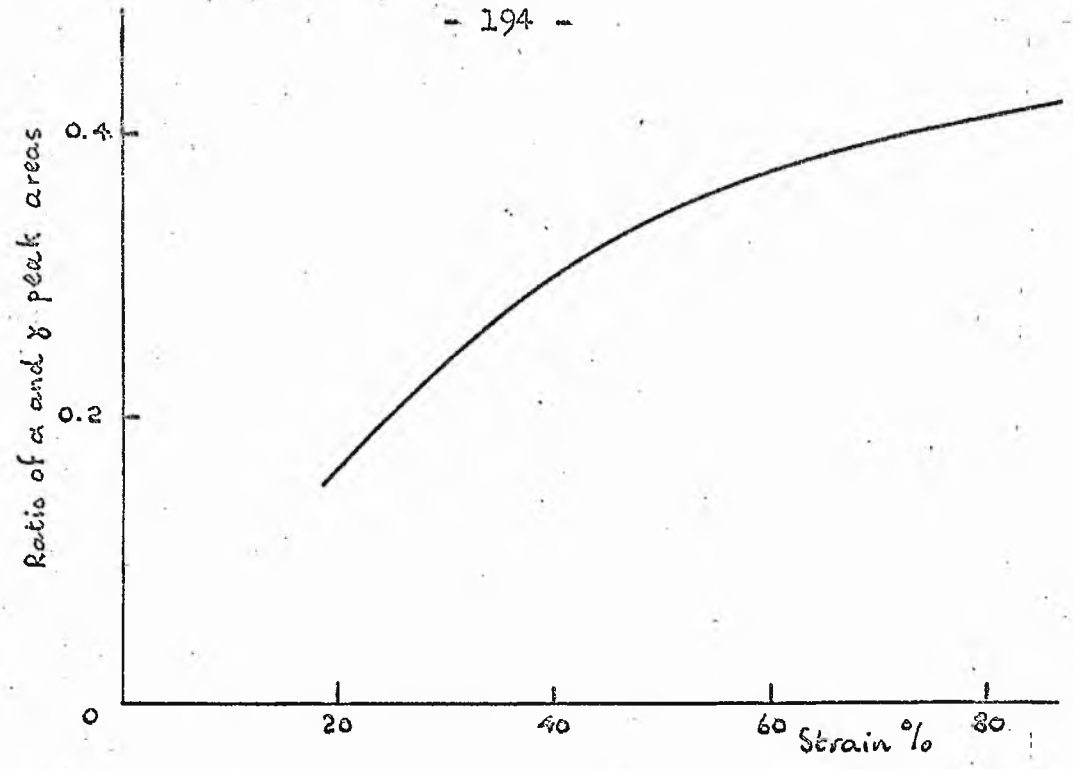

Fig. 7.9 Ratio of areas of α - and γ - peaks vs. strain.

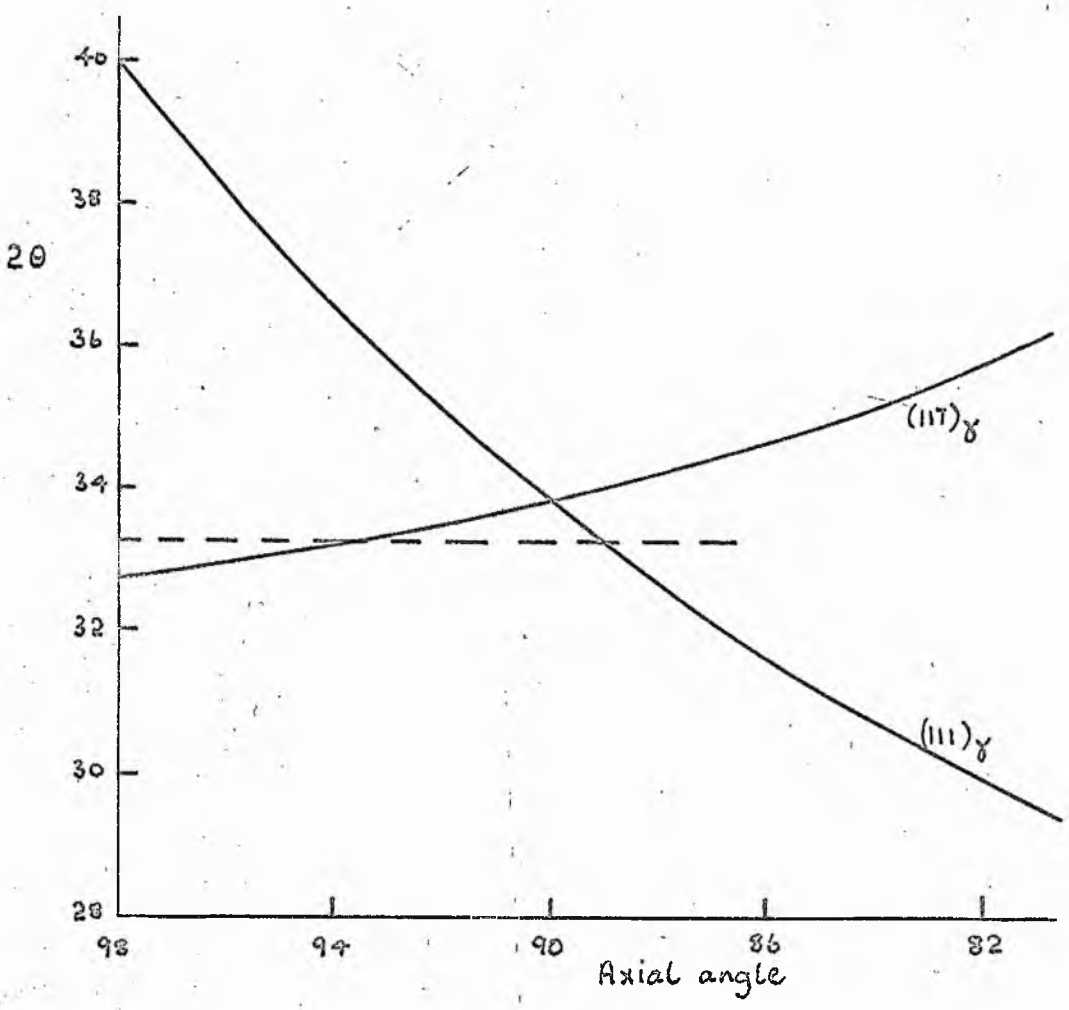

Fig. 7.10 Variation of Bragg angle with axial angle for predicted γ - structure.

CHAPTER V111 - CONCLUSION

8.1 Summary

The work described in this thesis has clearly demonstrated how the deformation characteristics of single crystals in mercury are dependent on the orientation with respect to the applied stress; and, further, how striking is the variation in behaviour at different temperatures. At 77°K three deformation mechanisms are observed, slip on the close-packed $\{ 11\bar{1} \}$ planes in the second closest-packed $< 1\bar{1}0 >$ direction, Type II twinning on the irrational '$\{ \bar{1}35 \}$' habit plane and kink formation defining the $\{ 1\bar{1}0 \}$ planes. The occurrence of twinning is confined to orientations where the resolved shear stress on $\{ 11\bar{1} \}\langle 1\bar{1}0 \rangle$ is low. The stress-strain curves of crystals tested in tension together with the metallographic observations show that the large regions of primary glide expected as a result of the large unit triangle for mercury are in general realised. Three variants of the $\{ 11\bar{1} \}\langle 1\bar{1}0 \rangle$ slip mode can be found to operate in one triangle. The c.r.s.s. for slip on this mode is not constant with crystal orientation but varies with the Schmidt factor in an inverse manner.

These deformation modes are also found to be operative at low temperatures, long diagonal slip being the only observed slip mode. Cross twinning observed at 77°K also occurs at 4.2°K, the two operative variants being the complementary modes having the special crystallographic relationship involving an accommodation slip plane. The most interesting

result of the deformation behaviour at 4.2°K is the observation of the stress-induced martensitic $\alpha - \gamma$ transformation. Evidence for this reaction arises out of four different types of observation.

(a) The occurrence of a new superconducting - normal state transition not corresponding to the α or β phases of mercury.

(b) The observation of a discontinuity in the electrical resistance as a function of temperature curves following plastic deformation at 4.2.°K.

(c) The observation of a well-defined surface shape change and audible clicks on testing, which cannot be interpreted in terms of a mechanical twinning process.

(d) The most conclusive evidence of all: the appearance of additional X-ray diffraction peaks after the application of a tensile stress to a fine grain polycrystalline sample maintained at low temperature.

The properties observed during the course of these four techniques have demonstrated the distinct nature of the product phase and indicate that it should not be confused with the other low temperature modification β-Hg. The habit plane of the $\alpha - \gamma$ transformation has been identified to be approximately $\{\bar{1}13\}$ and the associated macroscopic shear direction is $\langle \bar{1}\bar{1}0 \rangle$. The morphology of the plates of

γ -mercury is determined by the accommodation of the plates in the parent matrix, and consequently two plates usually occur together intersecting in the common $\langle \bar{1}\bar{1}0 \rangle$ shear direction. The high shear strain magnitude of 0.47 necessitates this ease of accommodation and the analogy of twins in mercury, where g = 0.63, is clear, the accommodation in this case being supplied by slip dislocations.

Experiment has shown that the occurrence of the transformation is dependent on the orientation of the applied stress as, indeed, has been found for all the operative deformation modes of crystalline mercury. For slowly applied stresses, the transformation occurs in tension preferentially to slip provided the resolved shear stress is greater than half that on the slip mode. For orientations near $[110]$ when the resolved shear stress for the transformation mode and for slip become low, twinning is predominant. The indications are that in compression the transformation will not occur. The behaviour for orientations near $[111]$ is again surprising as it was at 200°K (the $\{11\bar{1}\}\langle 011 \rangle$ slip mode) and 77°K ($\{100\}$ composite slip with $\langle 011 \rangle$ direction). At 4.2 °K a deformation process on $\{\bar{1}13\}\langle 110 \rangle$ appears to operate, the mechanism behind it being somewhat obscure. The positive sense of the shear direction and the shear strain magnitude of 0.24 serve to distinguish it from the shear elements associated with the α - γ transformation.

The failure of the theories of martensite crystallography in dealing with this transformation is most likely due to the predicted product structure being incorrect.

However, inadequacies in the theories in treating other systems have been observed and it is possible that a similar situation exists in this case. In this respect, it is felt that the low symmetry of both the parent and consequently the product structures make this transition a challenging test to the theories. The possibility of transforming one lattice into another purely by a combination of shears is being investigated in this department. It is hoped to base a theory on this concept which will eliminate the need to determine a lattice correspondence between the two phases, which can present problems. Crocker and Ross (1968) pointed out that it was such a problem that has prevented the successful application of the theories to the $\beta - \alpha$ transformation in uranium.

8.2 Proposals for further work

The most immediate experimental work to arise out of the results presented in this thesis is a full determination of the crystal structure of γ-mercury. This will enable a full assessment of crystallographic features associated with the transformation to be performed. Further work on low-temperature metallography of the transition is desirable to yield direct information on the growth behaviour of the martensite plates.

The direct observation of dislocations in the α-mercury structure would be extremely valuable in interpreting the anomalous deformation behaviour of mercury but the technological problems to be overcome before this can be

realised are quite considerable. Investigation of stacking faults from X-ray line-broadening and peak shifts as a result of cold-work using a low-temperature diffractometer would also help in explaining this anomalous behaviour.

Finally, as already mentioned in Chapters 1 and 3, the possibility of an assymmetry in the slip behaviour of mercury provides an interesting experimental study involving four-point bending tests on square cross-section crystals, enabling the tensile and compressive behaviour to be examined on one crystal.

APPENDIX I

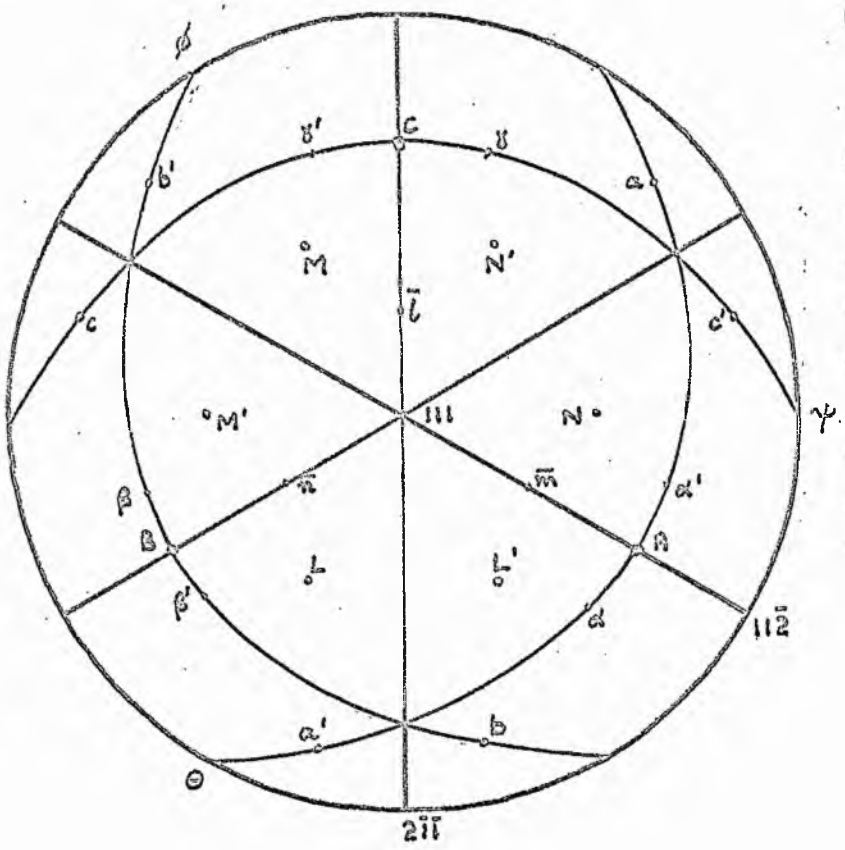

A, B, C	:	$\{11\bar{1}\}$ slip planes
θ, ϕ, ψ	:	$\langle 1\bar{1}0\rangle$ slip directions
a, a', b, b', c, c'	:	$'\{\bar{1}\bar{3}5\}'$ twin habit planes
α, α', β, β', γ, γ'	:	$\langle\bar{1}21\rangle$ twin shear directions
L, L', M, M', N, N'	:	$\{\bar{1}13\}$ transformation habit planes
$\bar{l}$ $\bar{m}$ $\bar{n}$	:	$\langle\bar{1}\bar{1}0\rangle$ transformation shear directions (and high temperature slip directions)

Appendix II

On many of the Laue back reflection plates of single crystals diffuse scattering rings were observed. A typical example is shown in Fig. A1. The rings vary in position on the plate depending on the orientation of the crystal. They also vary in intensity as a function of rotation round the ring and the ring always appears to avoid Bragg reflections from low index planes. When plotted out on the indexed stereogram of the crystal to which they relate it is found that the rings are indeed approximately circular and are always centred about the close-packed $\langle 011 \rangle$ direction. The diameter of the rings not constant but does not vary dramatically.

It is thought that the rings correspond to thermal scattering of the incident X-ray beam. The effect of thermal vibration of the lattice will be most marked in the close-packed direction and the diameter of the ring indicates the magnitude of the vibration and hence the temperature. The small spread of diameters suggests that the temperature of the specimens while in the X-ray camera does not change too markedly.

APPENDIX III

Obvious difficulties surround the observation of dislocations in mercury using electron microscopy, and X-ray topography constituted a more feasible approach. The transmission technique developed by Lang (1959) allows specimens of far greater thickness to be used than in the electron microscopy case. In this method, the crystal is positioned to Bragg - reflect the incident monochromatic beam and the image recorded on a fine-grained nuclear emulsion plate. The specimen and plate are traversed together to bring the whole crystal in the incident beam. A topograph of the interval structure of the crystal is thus built up on the plate. A Jarrell-Ash camera was used with a Hilger microfocus X-ray generator. The camera was aligned and tested using a silicon crystal of high perfection and low dislocation content.

The optimum dislocation contrast is obtained when the criteron $\mu t = 1$ is satisfied, where μ is the mass absorption co-efficient of the material and t the thickness of the sample. For mercury this relation implies that $t \sim 10$ μm for AgK_α, the most penetrating radiation available. When one considers that for silicon, the first material to be investigated using this technique, the specimen thickness can be up to 1 or 2 mm, preparation of mercury crystals with this dimension does raise problems. When the thickness of sample involved becomes this thin, another criterion involving the nature of the radiation has to be taken into account. Lang has found that when the X-rays penetrate the specimen, no information is transmitted

from a region just below the incident surface. The thickness of this region has been found empiracally to be one-third of the so-called extinction distance and is dependent on the set of reflecting planes, g, being used and is given by $\xi_g = {}^1/D$ where $D = \left(\frac{e^2}{mc^2}\right) \frac{\lambda F}{\pi V \cos\Theta}$. F is the structure factor and Θ the Bragg angle of the set of reflecting planes, and V the volume of the unit cell. F is dependent on the atomic scattering factor, f, and for a face-centred cell is zero or equal to 4f (Cullity 1956). f depends on the Bragg angle but for silver radiation does not vary much for the strongest reflecting planes of mercury. Consequently, the extinction distance is approximately constant for mercury and for the $\{11\bar{1}\}$ reflection is equal to 6.6 μm. Thus, no information will be transmitted from the first 2 μm of the specimen. It is therefore desirable to turn the specimen through 180° and take a second topograph to obtain a complete picture of the dislocation structure within a specimen. This criterion is particularly vital when using the technique to determine the Burgers vector of dislocations. Such a determination relies on the disappearance of a dislocation image between subsequent topographs using two different sets of reflecting planes. In the mercury case this effect would not be too great since, as we have seen, the extinction is approximately constant for the most usable reflecting planes. A method of producing suitable specimens which has been attempted, is to grow flat discs of mercury in the device shown in Fig. A2. The sampe is grown in the spoked copper wheel between two sheets of thin Mylar. The copper pins in the wheel are designed to fit into the cold stage built for the goniometer of the Lang camera, and

allow all possible orientations of the sample to be used. The thickness of the specimen is determined by the radius of the globule of mercury inserted between the Mylar sheets prior to flattening it out to the size of the copper wheel with the centre plunger of the device. The specially built evacuated cold stage was found to be inadequate in maintaining the specimen over long enough time for the exposure, and a more sophisticated cryostat is required. By attaching a temperature controller into the cryostat a temperature investigation could be undertaken. Preliminary work on growth of platelets from the vapour following the method of Sears (1956) are encouraging and further attempts are envisaged.

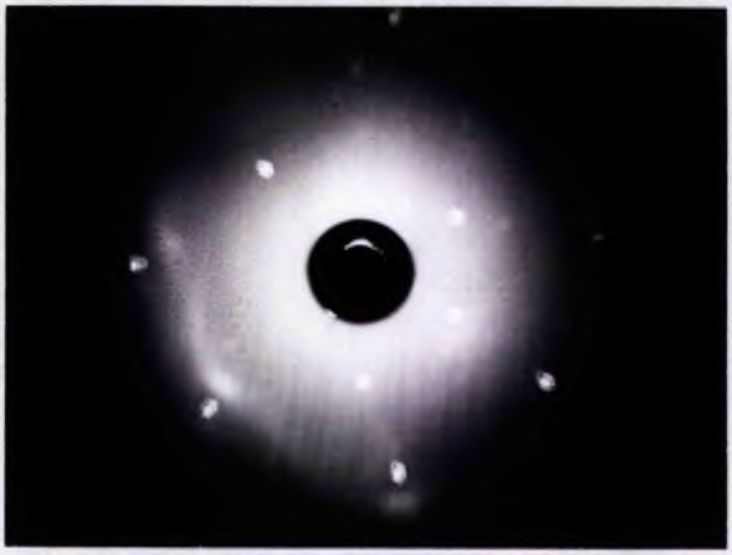

Fig. A1 Diffuse scattering on Laue X - ray plate.

Fig. A2 Device for producing flat discs of mercury.

REFERENCES

Abell J.S. and Crocker A.G. (1968a), Scripta Met. 2, 419.

Abell J.S. and Crocker A.G. (1968b), Proc. Int.Conf. on the Mechanisms of Phase Transformations in Crystalline Solids, July 1968, Institute of Metals, in the press.

Abell J.S. and King H.W., to be published.

Andrade E.N. and Hutchings P.J. (1935), Proc.Roy.Soc. A 148, 120

Andrew E.R. (1949), Proc.Phys.Soc. A 62, 77.

Animalu A.O.E. and Heine V. (1965), Phil.Mag. 12, 1249.

Alecksandrov B.N., Lomonos O.I., Tsivinskii S.V., Antonova, N.N. (1967), J.E.T.P. 26, 53.

Atoji M., Schirber J.E., Swenson C.A. (1959), J.Chem.Phys. 31, 1628

Bacon D.J. (1963), 'Crystallographic Angles for Mercury Bismuth Antimony and Arsenic.' Deposited at University of Surrey Library.

Barrett C.S. (1955-56), J. Inst. Metals, 84, 43; (1957), Acta Cryst., 10, 58, (1968), private communication.

Basinski Z.S. (1960), J. Aust.Inst.Met. 13, 284.

Bell R.L. and Cahn R.W. (1957), Proc.Roy.Soc. A 239, 494.

Bevis M. (1966), Ph.D. Thesis, University of London

Bevis M., Heckscher F. and Crocker A.G. (1964), Phys.Stat.Sol. 6, 355.

Bilby B.A. and Christain J.W. (1956), Inst.Met.Monogr. No. 18, 121; (1961), J.Iron Stl.Inst. 197, 122.

Bilby B.A. and Frank F.C. (1960), Acta Met. 8, 239.

Bowles J.S. and Mackenzie J.K. (1954a), Acta Met. 2, 129; (1954b), Acta Met. 2, 224.

Bridgman P.W. (1935), Phys, Rev. 48, 893.

Bullough R. and Bilby B.A. (1956), Proc.Phys.Soc.B 69, 1276.

Burkart M.W. and Read T.A. (1953), Trans. AIME 197, 1516.

Cahn R.W. (1953), Acta Met. 1, 49.

Christian J.W. (1965a), Theory of Transformations in Metals and Alloys. Pergamon; (1965b), ISI Special Report 93, 1; (1968), Proc.Int.Conf.Mech.Phase Transformation in Crystalline Solids, July 1968, Institute of Metals, in the press.

Cohen M.H. (1962), J. Phys.Radium 23, 643.

Crocker A.G., Heckscher F. and Bevis M. (1963), Phil.Mag. 8, 1863

Crocker A.G., Heckscher,F., Bevis M. and Guyoncourt D.M.M. (1966) Phil. Mag. 13, 1191.

Crocker A.G. and Ross N.D.H. (1968), Proc.Int.Conf.Mech. Phase Transformations in Crystalline Solids, July 1968, Inst. of Meta Metals, in the press.

Cullity B.D. (1956) Elements of X-ray Diffraction. Addison - Wesley.

Doidge P.R. and Eastham A.R. (1968a), Phil.Mag. 18, 655. (1968b) private communication.

Dove D.B. (1956), Ph.D. Thesis, University of London.

Fisher A. (1943), Nature, Lond. 152, 567.

Foxall R.A., Duesbery M.S., Hirsch P.B. (1966), Can.J.Phys. 45, 607.

Foxon T. (1965), Ph.D. Thesis, University of London.

Foxon T. and Selway B. (1966), unpublished work.

Gmelin (1965), Handbuch der Anorganischen Chemie 34.

Goss A.J. (1953), J. Sci. Instr. 30, 283.

Greenland K.M. (1937), Proc.Roy.Soc. A 163, 28.

Greninger A and Troiano A.R. (1949), Trans.AIME 185, 590.

Gruneisen E. and Sckell O. (1934), Ann.Phys. 19, 389.

Guyoncourt D.M.M. (1967), Ph.D. Thesis, University of London.

Guyoncourt D.M.M. and Crocker A.G. (1968), Acta Met. 16, 523.

Hall E.O. (1954), Twinning, Butterworths.

Harrison W.A. (1963), Phys.Rev. 129, 2503; (1966), Pseudo-potentials and the Theory of Metals, Benjamin, New York.

Heckscher F. and Crocker A.G. (1965), Phys.Stat.Sol. 10, 141.

Heine V. and Weaire D. (1966), Phys.Rev. 152, 152.

Honeycombe R.K. (1950), Proc.Phys.Soc. A 63, 673.

Jaswon M.A. and Dove D.B. (1956), Acta.Cryst. 9, 621.

Kiho H. (1954), J.Phys.Soc.Japan 9, 739.

King H.W. and Preece C.M. (1967), Adv. X-ray Analysis 10, 354.

Lang A.R. (1959), Acta.Cryst. 12, 249.

Liebermann D.S. (1958), Acta Met. 6, 680.

Machlin E.S. and Cohen M (1951), Trans. AIME, 191, 746.

Mackenzie J.K. and Bowles J.S. (1954), Acta Met. 2, 138.

Mitchell T.E., Foxall R.A. and Hirsch P.B. (1963), Phil.Mag 8, 1895.

Pomeroy C.D. (1952), M.Sc. Thesis, University of London.

Price D.B. (1960), Proc.Roy.Soc. A 260, 251.

Reed R.P. and Breedis J.F. (1966), Behaviour of Metals at Cryogenic Temperatures, ASTM STP 387, 60.

Reynolds J.E. and Bever M.B. (1952), Trans. AIME 194, 1065.

Rider J.G. and Hecksher F. (1966), Phil.Mag. 13, 687.

Roberts E. and Partridge P.G. (1966), Acta Met. 14, 513.

Ross N.D.H. and Crocker A.G. (1969) Scripta Met., in the press.

Schirber J.E. and Swenson C.A. (1959), Phys.Rev.Lett. 2, 296; (1961), Phys.Rev. 123, 1115; (1962), Acta Met. 10, 511.

Schmidt E. and Boas W. (1950), Plasticity of Crystals, Hughes, London.

Sckell O. (1930), Ann.Phys. 25, 637.

Sestak B. and Zarubova N. (1965), Phys.Stat.Sol.10, 239.

Swenson C.A. (1958), Phys.Rev. 111, 82.

Tanner L.E. and Maddin R. (1959), Acta Met. 7, 76.

Taylor G. and Christain J.W. (1967), Phil.Mag. 15, 873.

Thompson N. (1953), Proc.Phys.Soc. 66, 481.

Thompson N. and Hingely M. (1955), Acta Met. 3, 289.

Thompson N. and Millard D.J. (1952), Phil.Mag. 43, 421.

Wayman C.M. (1964), Introduction to the Crystallography of Martensitic Transformations, Macmillam.

Tucker M.O. (1966), to be published.

Weaire D. (1968a), J.Phys.C. 1, 210; (1968b), Phil.Mag. 18, 213, (1968c), private communication.

Wechsler M.S., Liebermann D.S. and Read T.A. (1953), Trans. AIME, 197, 1503.

ACKNOWLEDGEMENTS

I would like to express my gratitude to Dr. A.G. Crocker for his valuable guidance and encouragement during this research.

I wish to thank Dr. H.W. King for his help in the work conducted at Imperial College and Professor J.G. Ball for providing the facilities; also Denis Weaire of the University of Cambridge for several useful discussions.

I am grateful to David Guyoncourt for guidance with experimental work; the Department workshop for making apparatus; Mr. Scobie, Dick Leong and the A.V.A. unit for the photographic prints; Lesley Small for typing the thesis and Horice for help with proof reading and encouragement during most of the research; and also the University of Surrey for providing a grant and facilities for this work.